Analysis of cyclic deformation under non-proportional tension and torsion loading

Tennekoon Mudiyanselage Devika Nimali Medagedara
B.Sc.Eng(Hons)

A thesis submitted in partial fulfilment of the requirements of
Sheffield Hallam University
for the degree of Master of Philosophy

August 2003

Collaborating Organisation: Asian Development Bank

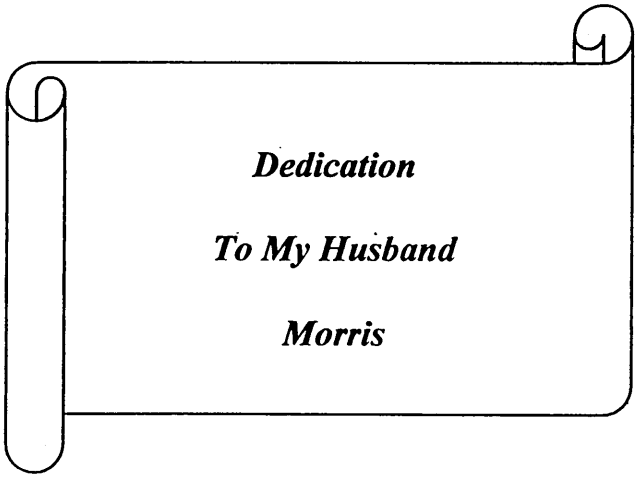
Dedication
To My Husband
Morris

Preface

I declare that this thesis based on the findings of research carried out in the school of Engineering, Sheffield Hallam University.

The content of the thesis is original except where specific references are made to other work.

No part of this thesis has been submitted to any other University.

T.M.D.N. Medagedara

Acknowledgement

I would like to express my gratitude to Sheffield Hallam University for the opportunity granted to me to under-take the postgraduate studies, and also to the Sri Lankan government for the financial support given to me.

I am particularly indebted to my director of studies Mr. David Eaton for his guidance, support and continuous assistance for my research. In addition, particular thanks are reserved for Dr. U. S. Fernando, for his superb supervision, continuous assistance and for keeping me focused on the critical issues of the research work.

I also would like to express my sincere thanks to Mr. K. Wright, Mr. S. Brandon and Mr. J. Stanley for their assistance with the manufacturing of test equipment and the technical assistance provided for computer work.

I too owe sincere thanks for Mr. P.D. Sarath Chandra, Head of Department/Mechanical Engineering, Mr. W.R.G.A. Wijesundara, Senior Lecturer and Mr. R. Perera Lecturer in OUSL for their unstinted support, guidance, timely advice and support during the course of my work.

Lastly but not leastly I would like to thank my husband, daughter Hansika, son Ovindu and parents for their support, patience and encouragement during the course of my work.

CONTENTS

Appendices

Appendix - 1

Input-programmes for ABAQUS package

Appendix – 2

Calculations for stress concentration factor

Abstract

The knowledge of cyclic deformation behaviour is essential for fatigue analysis of industrial components. However such knowledge is difficult to obtain for non-proportional loading situation. Although notch deformation can be analysed by methods such as Neuber, but these methods are not suitable for critical non-proportional loading paths encounted in industrial components.

The aim of this research was to study the cyclic deformation of a medium carbon steel EN 8. It is essential to find the plastic strain ranges under cyclic loads as it is used for fatigue life prediction under variable amplitude tension-torsion multiaxial, proportional and non-proportional loops. Hysteresis loops were obtained experimentally for different loading conditions of uniaxial, torsional, proportional and non-proportional loads. Finite element analyses were also performed. Experiment and the FEA results obtained using ABAQUS code were compared. Neuber predictions were performed for uniaxial load and torsion loads. Comparisons of analytical and finite element results show good correlation.

The specimens used for the testing programme were solid cylindrical with a notch and made from EN8 medium carbon steel. A series of tests were conducted under various axial-torsion loading conditions. For the testing, a computer controlled biaxial ESH machine was used. Rosette strain gauges attached at the notch root were used to measure the three strain components.

The hysteresis loops obtained from the experiment were compared with the Finite Element results for uniaxial, torsion, in-phase, out of phase and three other non-proportional paths. Considering the results obtained from different non-proportional multiaxial loading paths, Path-C non-proportional loading was found to be more damaging and Path-A was least damaging in both FEA and experiment cases.

Notations

b = fatigue strength exponent

c = fatigue ductility exponent

C,m,n = material constant

E = modulus of elasticity

N_f = cycles to failure

σ_y = yield strength

σ_u = ultimate strength

$\Delta\sigma$ = normal stress range

$\Delta\sigma_{eq}$ = equivalent normal stress range

σ'_f = fatigue strength coefficient

$\Delta\tau$ = shear stress range

$\Delta\tau_{eq}$ = equivalent shear stress range

ΔT = torque range

k = strength coefficient

n = strain hardening exponent

n' = cyclic strain hardening exponent

K_{short} = stress intensity factor for the short crack

S = nominal stress

K_t = elastic stress concentration factor

l = free surface crack length

f(g) = free surface or edge correction factor

$\varepsilon,\Delta\varepsilon$ = axial strain and axial strain range

$\Delta\varepsilon_p$= plastic strain range

ε'_f= fatigue ductility coefficient

$\Delta\varepsilon_n$ = the tensile strain normal to the maximum shear strain plane

γ_{max},$\Delta\gamma_{max}$=maximum shear strain, maximum shear strain range

$\Delta\gamma/2$ = the shear strain amplitude on the maximum shear strain plane

Chapter 1

Introduction

Structural components with complicated geometries are frequently subjected to alternating loads, which produce multiaxial stresses. In most cases, the loading is non-proportional. The alternating loads tend to initiate fatigue cracks at notches and at other regions of high stresses. Some obvious areas in which fatigue can occur are the repeated expansions and contractions of a pressurised aircraft, a car suspension unit absorbing the undulations of a normal road surface and the rhythmic crashing of waves against a ship hull. However, fatigue is a problem that occurs in almost every engineering component and most of the failures are directly related to fatigue.

Fatigue is produced by the repeated application of cyclic loading. The first method for understanding and assessing fatigue in the 1870's used the relationship between the magnitude of nominal stress cycles and the number of cycles to failure [1]. This is the S-N method and it still has applications for components that are designed to survive very large numbers of cycles such as engine connecting rods.

Fatigue testing is recognised as one of the most critical, time consuming and costly activities in product development. Any reduction in the time spent for fatigue testing will reduce the time taken to market the product as well as to cut the cost of the development process. For this reason, the ability to shorten fatigue tests has always been a much sought after goal.

Many engineering components are subjected to multiaxial variable amplitude loads that vary either proportionally or non-proportionally. Therefore accurate fatigue life assessment is an essential requirement in the durability prediction of real design components. Therefore knowledge of cyclic deformation is essential to find the plastic strain ranges, which is used for fatigue life prediction.

There are a number of software tools to assist design engineers where conceptual designs can be fatigue analysed at the design stage. A majority of these software tools require the actual stress-strain history at the critical location in order to predict fatigue life. In practice, the elastic-plastic stress strain history at the critical location is unknown (unless it was measured from a prototype) and there by requires to be predicted from the knowledge of external load histories. However, the stress-strain prediction procedure

and the accuracy of the life prediction of current software tools have not been verified for a wide range of multiaxial loading cases.

Historically the field of fatigue has been classified into a number of specific areas such as high cycle and low cycle fatigue; fatigue of notched members; the initiation and propagation of cracks and fatigue life extension techniques. Fatigue initiation and crack growth programs require an accurate knowledge of the local notch tip stresses and strains. These quantities can be determined in several ways, that is direct strain gauge measurements, using finite element analysis or by using approximate methods, such as Neuber approach, that relate local stresses and strains to their remote values.

The overall aim of the work of this project is to study the cyclic deformation that is essential to find the plastic strain ranges, which are used for fatigue life prediction under variable amplitude tension-torsion multiaxial axial proportional and non-proportional paths. The hysteresis loops were obtained for different load sets of proportional and non-proportional loads and the experimental notch root strains were compared with Finite Element Analysis data obtained using ABAQUS code. The shapes of the hysteresis loops (axial and torsional) also were compared for different proportional and non-proportional loading paths. Neuber rule is used to evaluate the notch tip behaviour under cyclic loading (tension and torsion). Figure 1.1 shows the flow chart of the experimental and theoretical study of this work.

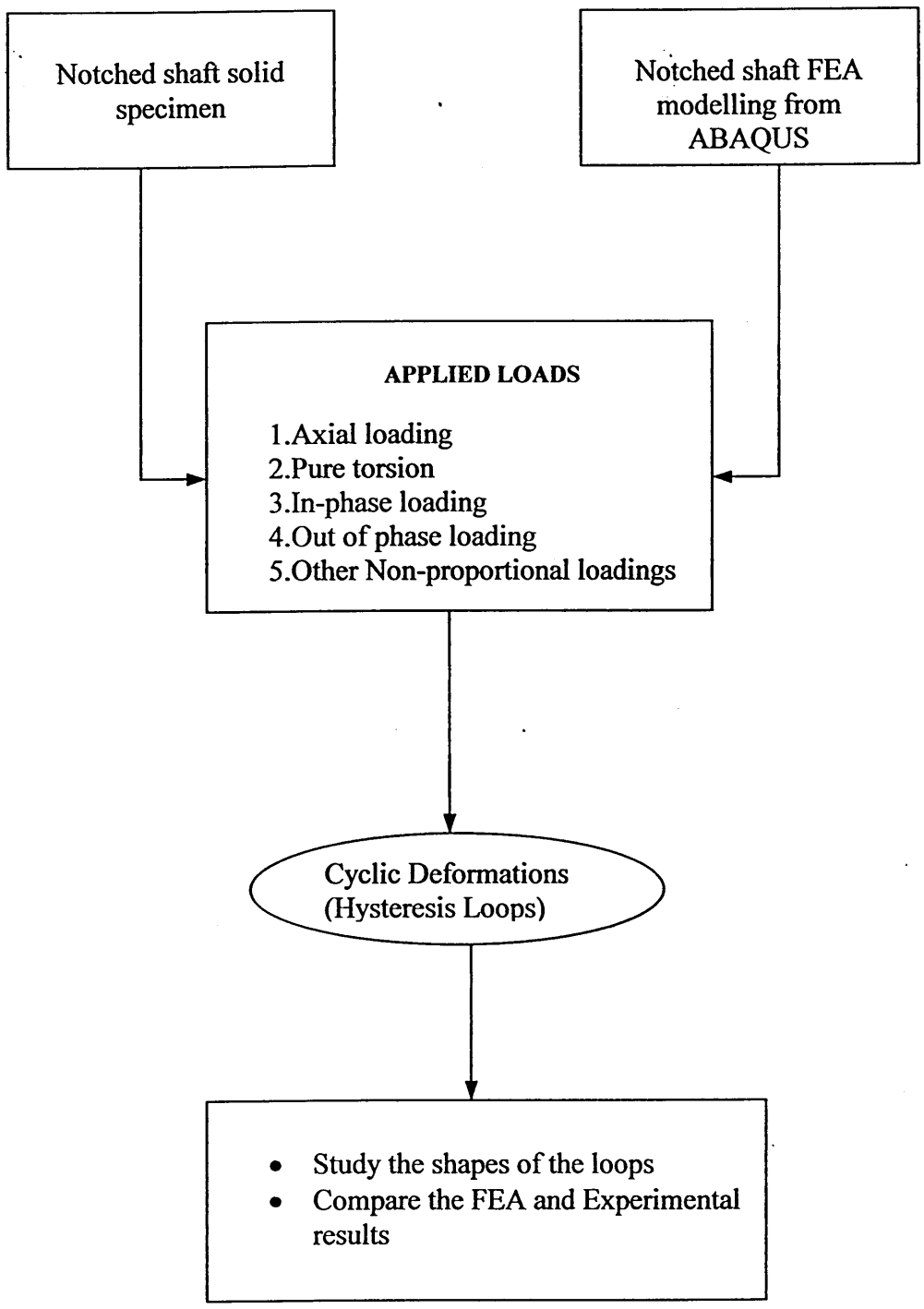

Figure 1.1: The flow chart of the study programme

Chapter 2

Literature Review

2.1 Introduction

Fatigue has been the cause of many engineering problems since the earliest of components were manufactured. It manifests itself by the initiation of cracks, which may cause a sudden catastrophic failure of the component. However, there are cases where the crack may be allowed to exist or be controlled.

Metal fatigue may cause premature damage or indeed failure in a component subjected to repeated loading. The source of the failure will usually be attributed to a defect in the component material, which, when subjected to stress fluctuations, will gradually propagate until failure occurs. Often fatigue failure takes place when components are subjected to nominal cyclic stresses well below their tensile strength [1-2].

Fatigue analysis techniques, whether based on the conventional stress life parameter or the more recent strain-life parameter, are based on the premise that the fatigue damage can be accounted for by a single stress or strain variable without regard to the simultaneous presence of other stresses and strains. Essentially the stress-strain field is regarded as uniaxial. Such an assumption simplifies the calculation procedure and may give answers of sufficient accuracy under loading conditions, predominantly uniaxial. However, such an assumption cannot be made about many components, which undergo complex multiaxial loading. A method is therefore required which takes into account the interaction between coexisting stresses and strains [3].

Fatigue analysis has become a widely accepted engineering tool and with the introduction of computers the use of the technique for the design and development of components has become increasingly more wide spread [4].

It's common for most components to be subjected to different states of cyclic stress with loading of various magnitudes. Therefore, it is necessary to have some form of accountability of the loading to give confidence in the working life of the engineering component. In certain complex fatigue patterns, the question of quantifying fatigue damage sustained during each cycle and the necessary summation is still unanswered. However there appears to be no universally accepted definition of fatigue damage,

although there have been many attempts to provide suitable explanations and all are attempting to apply different criteria and approaches to account for fatigue damage. The conventional approach to fatigue analysis uses the *stress* range as the primary fatigue parameter. The components have a characteristic stress life curve, which describes how many cycles of a given stress range the component would endure before failing. This S-N curve has a threshold stress range (Failure Limit) below which no fatigue damage is believed to occur. Fatigue life under random stress excursions is calculated by reducing the stress-time history to a histogram of cycle counts, which is subsequently used to calculate, in conjunction with the above S-N curve, the fractional damage due to each stress cycle. The cumulative damage is obtained by a linear sum (Miner's summation) of the fractional damages. A cycle counting procedure called the 'Rain flow Algorithm' is widely used because of its ability to identify complete stress-strain loops as individual cycles.

The advantage of this method includes the simplicity of the calculation procedure and the availability of a vast quantity of fatigue data for many metals in a variety of metallurgical states. Furthermore, simple 'rules of thumb' are available to predict the S-N curve from other mechanical properties. The limitations of this method includes its inability to model adequately the notch behaviour and the effects of manufacturing processes like welds, residual stresses etc.

The modern approach the fatigue under uniaxial loading is based on *strain* rather than *stress*, the former being more appropriate for modelling the plasticity which the component undergoes at the critical site of failure. The local stress strain approach brings together three sets of information, namely the material fatigue properties in terms of a strain-life curve, a nominal service history defining the endurance duty and the geometry details responsible for stress concentrations. The stress-strain response at the local site of failure is calculated with due regard for the plastic-elastic behaviour of the material. The fatigue damage for individual excursion, as identified by the Rain flow algorithm, is calculated and the cumulative damage obtained via the linear summation rule [5].

This method offers some distinct advantages over the S-N method because of its ability to model more comprehensively the notch effects as well as the fatigue effects of non-reversed loadings, that is cycles with non zero mean stress. It is particularly suited for computer based fatigue life prediction procedures because large amounts of information

can be held on database covering material properties, service life histories and geometric stress concentration factors.

The limitations of this method include the fact that the predictions are to the onset of crack initiation and hence it cannot be applied in situations where significant cracks are already present. Under these situations the rate of crack growth governs the fatigue life [6].

The fatigue life assessment based on the crack growth philosophies usually relies on the use of Linear Elastic Fracture Mechanics (LEFM). The life estimation under this approach is made by integrating an exponential crack growth function between the limits set by the initial crack or flaw size and the final crack length above which the component fractures catastrophically. The crack may propagate under the application of cyclic loading in any of three modes (Crack Opening Mode, In-plane Shear Mode and Out-of –plane Shear Mode) each of which is characterised by a different crack growth function [7].

Currently there are three major approaches to estimate fatigue life, namely, the stress life approach, the strain life approach and the fracture mechanics approach [8].

The stress-based approach has been widely used in high-cycle fatigue (HCF) design applications where the applied stress is primarily well within the elastic range of the materials. However, for low-cycle fatigue (LCF) applications where the local plastic strains can be quite large, the strain-based approach is more appropriate [8]. Therefore to study the cyclic deformation that is essential to find the plastic strain ranges which is used for fatigue life prediction.

When selecting an approach the points are considered such as the relative economics, the level of acceptance and the accuracy of the method compared to input variables such as the load history.

2.1.1 The stress life approach

The stress life approach was the first and the quickest and cheapest of the approaches. It is widely used in design applications where the applied stress is primarily in the elastic range of the material and only requires an understanding of elastic stress analysis techniques. This method may be used in almost any situation to get a rough estimate of

life. The method works very well in situations involving constant amplitude loading and long fatigue lives [5].

The advantages of the stress life approach include:

- The analysis and estimation of material constants necessary for this method are quite simple;
- Calculations are quick and result in reasonable estimates of life;
- This method works well for designs involving long life, constant amplitude histories;
- A substantial amount of data is available concerning almost any variation of surface finish, load configuration and environment.

In contrast, the disadvantages of the stress life approach include:

- The method is completely empirical in nature;
- The true stress-strain response of materials is ignored in favour of fictitious fully elastic strains;
- The approach does not distinguish between initiation and propagation, which gives limited insight into the concept of damage.

2.1.2 The strain life approach

The strain life approach estimates fatigue life utilising the total strain amplitude, incorporating both the elastic and plastic strain contributions. This method is applied where significant plastic strains are present. The response of material in critical locations is strain or deformation dependent. Fatigue studies depend on prototypes being available to provide a service load history [9].

The advantages of the strain life approach include:

- Plastic strain, the mechanism that leads to crack initiation, is accurately modelled;
- This method can be used in high strain, low cycle situations;
- This method allows for accurate accounting of cumulative damage under variable amplitude loading;
- This method can be easily extrapolated to situations involving complicated geometries.

In contrast, the disadvantages of the strain life approach include:

- Technique is important when determining notch root strains;
- The life calculation involves numerical iterations which are best handled with computers;
- This method only accounts for initiation life and cannot be used to predict propagation life.

The strain life approach frequently makes use of Neuber's rule to compute the local (notch) stresses and strains. In this approach the theoretical stress concentration is taken as the geometric mean of the stress and strain concentration factors. Problems associated with this and other related approximations are the notch stress-strain response root must be in phase with the global load and no account is taken for time dependent process such as creep and mean stress relaxation [10-11].

2.1.2.1 The strain life curve

The strain-life approach is most generally used for low cycle fatigue where the fatigue life is highly dependent on the plastic strain. The total strain amplitude is the sum of the elastic and plastic terms such that

$$\frac{\Delta\varepsilon}{2} = \frac{\Delta\varepsilon_e}{2} + \frac{\Delta\varepsilon_p}{2} \quad \text{---------- (1)}$$

where,

$\Delta\varepsilon_e$ - elastic strain range

$\Delta\varepsilon_p$ - plastic strain range

In 1910, Basquin observed that the stress-life (S-N) data can plot linearly on a log-log scale and can be expressed as:

$$\frac{\Delta\sigma}{2} = \sigma_f'(2N_f)^b \quad \text{---------- (2)}$$

where,

$\Delta\sigma$ - stress range

σ_f' - fatigue strength coefficient

N_f - cycles to failure

b - fatigue strength exponent

The elastic strain can be written as,

$$\frac{\Delta\varepsilon_e}{2} = \frac{\Delta\sigma}{2E} \text{ ---------- (3)}$$

We can obtain,

$$\frac{\Delta\varepsilon_e}{2} = \frac{\sigma_f'}{E}(2N_f)^b \text{ ---------- (4)}$$

Coffin (1954) and Manson (1954), working independently on thermal fatigue problems, proposed a characterization of fatigue life based on the plastic strain amplitude.

Strain-life data can also be linearly developed on log-log co-ordinates. Plastic strain can be related by the power law function:

$$\frac{\Delta\varepsilon_p}{2} = \varepsilon_f'(2N_f)^c \text{ ---------- (5)}$$

where,

$\Delta\varepsilon_p$ - plastic strain range

ε'_f - fatigue ductility coefficient

c - fatigue ductility exponent

From these statements, an expression relating the total strain range to life to failure was developed. This is the basis of the strain-life method and is termed the strain-life relation.

$$\frac{\Delta\varepsilon_e}{2} = \frac{\sigma_f'}{E}(2N_f)^b + \varepsilon_f'(2N_f)^c \text{ ---------- (6)}$$

Similar to the S-N diagram, the E-N diagram was generated from empirical data for fully reversed cycles. For a realistic loading history it is important to take account of residual stresses or mean stresses at the area of interest since they will have an effect on the fatigue life estimation [10].

- **Mean stress effects**

Cyclic fatigue properties of a material are combined from completely reversed constant amplitude strain-controlled tests. Components seldom experience this type of loading, as mean stress or mean strain is usually present. The effect of mean strain is, for the most part, negligible on the fatigue life of a component. Mean stresses, on the other hand, may have a significant effect on the fatigue life.

Mean stress effects are seen predominantly at longer lives. They can either increase the fatigue life with a nominally compressive load, or decrease it with nominally tensile value [5-11].

- **Morrow's law**

Modifications to the strain-life equation have been made to account for mean stress effects. Morrow suggested that the mean stress effect could be taken into account by modifying the elastic term in the strain-life equation, as below.

$$\frac{\Delta\varepsilon}{2} = \frac{(\sigma_f' - \sigma_0)(2N_f)^b}{E} + \varepsilon_f'(2N_f)^c \text{ ---------- (7)}$$

This equation has taken mean stress effect, to modify the elastic term. Therefore this equation is good to analyse high cycle fatigue where the applied stress is primarily in the elastic range.

- **Manson and Halford equation**

Manson and Halford modified both the elastic and plastic terms of the strain-life equation to maintain the independence of the elastic-plastic strain ratio from mean stress. In this form the strain-life equation becomes

$$\frac{\Delta\varepsilon}{2} = \frac{(\sigma_f' - \sigma_0)(2N_f)^b}{E} + \varepsilon_f'\left[(\sigma_f' - \sigma_0)/\sigma_f'\right]^{c/b}(2N_f)^c \text{ ---------- (8)}$$

Hence this equation has modified both elastic and plastic terms, this is good for analysing low cycle fatigue.

- **Smith Watson Topper parameter**

Smith Watson Topper parameter offers an alternative solution to accounting for mean stress effects. The strain-life equation in this case is then

$$\frac{\sigma_{\max}\Delta\varepsilon_t}{2} = \frac{(\sigma_f')^2(2N_f)^{2b}}{E} + \sigma_f'\varepsilon_f'(2N_f)^{b+c} \text{ ---------- (9)}$$

where

$$\sigma_{\max} = \frac{\Delta\sigma}{2} + \sigma_m$$

The above tensile based damage model proposed by Smith et al.[10] has been found to be superior in correlating fatigue lives for materials whose damage development was tensile dominated.

- **Fatemi and Socie equation**

The following shear based damage model proposed by Fatemi and Socie has been found far superior for materials whose damage development was shear dominated.

$$\gamma_{ac}\left[1+k\left(\sigma_{\max}/\sigma_{ys}\right)\right]=\frac{\tau_f'}{G}\left(2N_f\right)^b+\gamma_f'\left(2N_f\right)^c \text{ ---------- (10)}$$

The critical plane of this model is identified as the plane experiencing the maximum shear strain amplitude and the fatigue life is estimated based on the accumulated damage on this plane. This equation is used for analysing fatigue life for multiaxial loading [13].

2.1.3 Fracture mechanics approach

Fracture mechanics approaches may also be used in the fatigue analysis of notched components. In the application of this method to notched component, the near notch stress-strain field must be considered. Important aspects of the analysis include the determination of the size of the region over which this field is effective and the stress intensity factor in this region [5].

The advantages of the fracture mechanics approach include:

- This is the only method that deals directly with the propagation of fatigue cracks;
- Crack growth rate must be incorporated with non-destructive inspection techniques;
- This method gives a good insight into the actual mechanisms of fatigue.

In contrast, the disadvantages of the fracture mechanics approach include:

- This method has problems when used to deal with crack initiation;
- In certain situations the assumptions of linear elastic fracture mechanics are not valid and elastic-plastic fracture mechanics concepts must be used;

- This method requires an estimate of stress intensity factors, which may be difficult to determine for complicated geometries.

2.2 Multiaxial fatigue

In many applications, engineering components are subjected to complicated states of stress and strain. In complex stress states the three principal stresses are non-proportional or their directions change during a loading cycle. Fatigue under these conditions, termed multiaxial fatigue, is an important design consideration for reliable operation and optimisation of many engineering components.

Many engineering components and structures are subjected to multiaxial stresses and strains under service conditions. Most of the engineering components contain stress concentration features or notches. For such notched components, even when the remotely applied load is uniaxial, the local stress-strain state developed at the critical locations or notches (where fatigue failures are likely to occur) is usually multiaxial because of the constraint effect at the notch. In recent years, a number of investigations have shown that the local state of stress or strain does indeed influence the fatigue strength of a component and uniaxial based life predictions are very non conservative [12]. Various multiaxial fatigue life prediction methods based on effective stress/strain, plastic work/energy, critical plane approaches, etc., have been proposed, but as yet there is no universally accepted approach. In general, better correlations of multiaxial fatigue data have been obtained using critical plane approaches [13-14].

Machine components can experience a complex state of stress because generally they are not of simple geometry or as a result of multiaxial stress field that develops due to the application of two or more loads, which can be applied either simultaneously or in sequence. Such a circumstance is still a cause for concern for designers who are confronted by 'real' life problems on industrial components. Since multiaxial stress fields can result from some particular design feature that may include the presence and shape of notches on the component [12].

In the case of uniaxial loading, the directions of the principal stress and strain remain constant. Therefore in the past, a majority of fatigue research has been conducted under uniaxial loading conditions. This was partly due to the difficulties involved in obtaining experimental multiaxial fatigue data. This area continues to be a topic of concentrated

research, with theories being developed and modified continuously. Consequently there is still no universally accepted multiaxial fatigue theory [5].

The development of multiaxial fatigue analysis methods requires an understanding of the facts such as the state of multiaxial stress and strain in a component and the cracking behaviour of a material under multiaxial fatigue loading.

Multiaxial fatigue is concerned with the effect of biaxial and triaxial stresses or strains on the orientation and growth rate of cracks on the lifetime of a component. Under multiaxial loading conditions fatigue endurance is governed by the maximum shear strain and the tensile strain normal to the plane of maximum shear [15].

Most fatigue cracks start at free surfaces where the normal stress is zero. Consequently, the study of multiaxial fatigue needs only to concern itself with biaxial stress state. The conventional techniques developed to deal with a multiaxial stress field take their lead from the conventional theories of strength under static biaxial loading. They reduce the biaxial stresses, at some critical element on the structure, to two principal stresses; the failure criterion is then defined as a single parameter function of these principal stresses. In general the same critical conditions for static yielding are adopted for dynamic loading. For random loading, the first step consists of the calculation of an equivalent stress history from the principal stress histories. This equivalent stress history is subsequently preceded with any of the above fatigue life prediction techniques. Thus, apart from the initial calculation of an equivalent stress history the methodology is exactly the same as for uniaxial fatigue.

Some of the common single parameter criteria for predicting failure under biaxial stress states are Rankine's Method [5] and this criterion defines the fatigue limit in terms of the Maximum Principal Stress; St. Venant's Method [5] which defines the fatigue limit in terms of Maximum Principal Strain; Tresca's Method [5], based on the Maximum Shear Stress. It states that the structure fails when the Maximum Shear stress reaches a critical value. Von Mises' Method is based on the use of strain energy per unit volume to determine the conditions for failure. Octahedral Shear Stress Method and the criterion for yielding under multiaxial loading, in terms of the octahedral shear stresses is very similar to the Von Mises' criterion.

In 1973 Brown and Miller developed a multiaxial fatigue theory, which arose from a physical interpretation of the mechanisms of fatigue crack growth. The theory is based on the critical plane approach to fatigue life assessment and hypothesises that cracks initiate and grow on planes and that strain normal to those planes assists in the fatigue crack growth process [15].

A form of their theory is given by: $\frac{\Delta\gamma}{2} + \Delta\varepsilon_n = C$

where,

$\Delta\gamma/2$ - The shear strain amplitude on the maximum shear strain plane

$\Delta\varepsilon_n$ - The tensile strain normal to the maximum shear strain plane

C - A material constant

2.2.1 Multiaxial fatigue: modern approach

Unlike the conventional approach, which relies on characterisation of the multiaxial fatigue process by a single parameter, the modern approach is to adopt two parameters. This theory is based on observations of the fatigue crack growth process and thus has a physical interpretation. Furthermore, it is a strain-based method, strain being judged to be a more appropriate parameter than stress when dealing with plastic deformation [7].

Conventional Strain Based Life Prediction Methods calculate equivalent uniaxial strain amplitude from a multiaxial strain history. This amplitude is then used with the uniaxial strain-life curve to predict life to crack initiation. Application of these methods is considerably more involved than the stress-based methods because even when notch strain data are available, estimates or assumptions must be made about variations in Poisson's ratio with strain level. Also, notch constraint on circumferential strain produces values, which are a fraction of notch bending strain less than those for full Poisson contraction, with the fraction also varying with strain level. Without measurement, it is difficult to estimate the fractions, except by detailed elastic-plastic finite element analysis [16].

2.2.2 Multiaxial cyclic stresses

There are many practical applications where fatigue-critical components undergo multiaxial cyclic loading. For example, the fuselage of an aircraft is subjected to hoop and longitudinal cyclic stresses due to repeated pressurerization and depressurization. Similarly, pressure vessels, tubes and pipes are subjected to biaxial stresses, which arise

from internal pressures. Transmission shafts in automobiles experience combined shear stresses arising from torque, which is superimposed on axial stresses generated by bending.

In general, different modes of imposed loads (such as tension and torsion) may occur either in a static mode (as, for example, due to a steady bending moment, mean pressure or steady torque) or they may fluctuate in phase or out of phase. The overall fatigue life under general multiaxial condition is inevitably dictated by the complex phase relations between the different modes of loading [14].

2.2.3 The cyclic stress-strain behaviour

Monotonic stress-strain curves have long been used to obtain design parameters for limiting stresses on engineering structures and components subjected to static loading. Similarly, cyclic stress-strain curves are useful for assessing the durability of structures and components subjected to repeated loading. The response of a material subjected to cyclic inelastic loading is in the form of a hysteresis loop, as shown in Figure 2.1. The total width of the loop is total strain range ($\Delta\varepsilon$). The total height of the loop is total stress range ($\Delta\sigma$). The area within the loop is the energy per unit volume dissipated during a cycle [5].

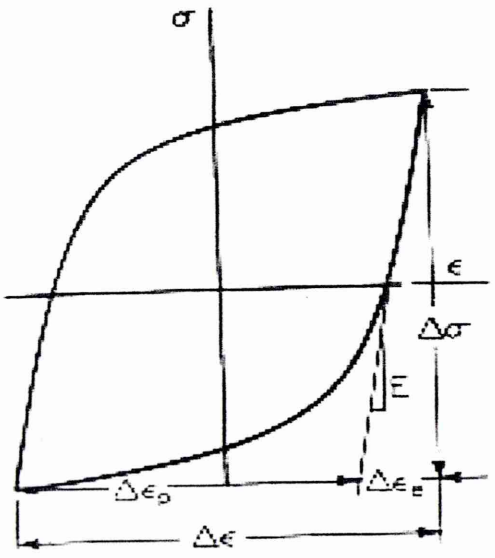

Figure 2.1: Hysteresis loop

- **Transient behaviour**

The stress-strain response of metals is often drastically altered due to repeated loading. Depending on the initial conditions of a metal and the test conditions a metal (that is quenched and tempered, or annealed) may: cyclically harden, cyclically soften, be cyclically stable or may have mixed behaviour.

Figure 2.2(a) shows the constant strain amplitude and Figure 2.2(b) shows the stress response of a material loaded in strain control. Figure 2.2(c) shows the hysteresis loops for the first two cycles. The maximum stress obtained increases with each cycle of strain. This is known as strain hardening. Conversely if the maximum stress decreases with repeated straining, strain softening occurs. This is shown in Figure 2.3 [5].

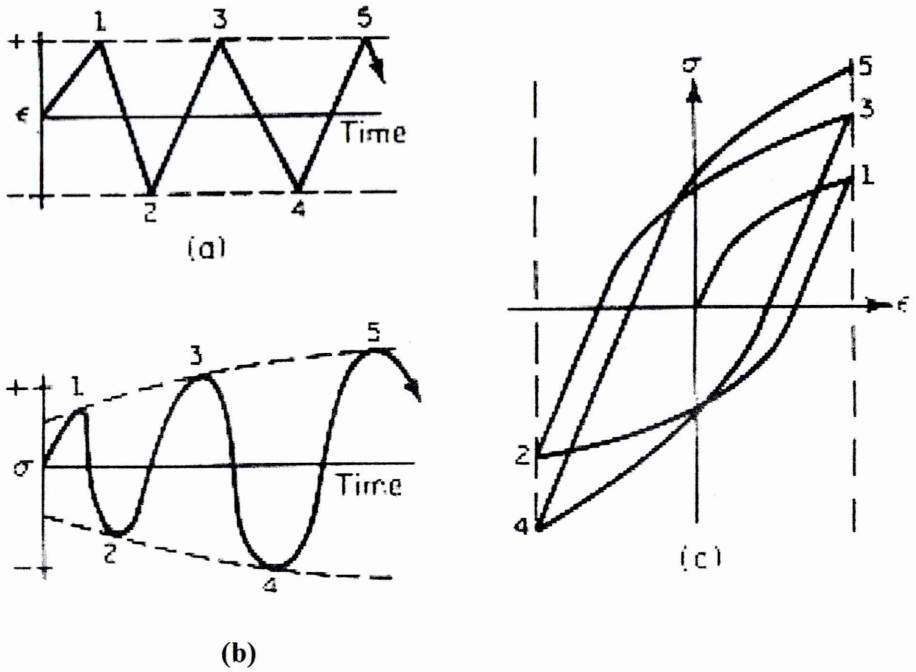

Figure 2.2: Cyclic hardening: (a) constant strain amplitude; (b) stress response (increasing stress level) ;(c) cyclic stress-strain response

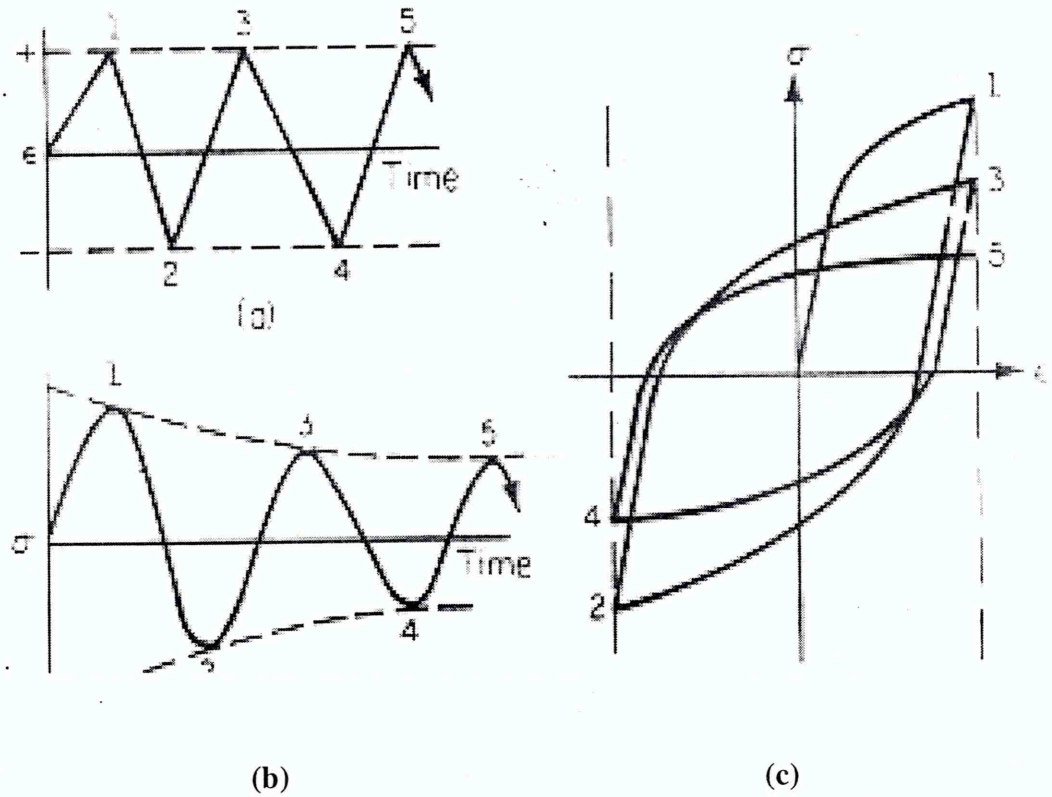

(b) (c)

Figure 2.3: Cyclic softening: (a) constant strain amplitude; (b) stress response (decreasing stress level); (c) cyclic stress-strain response

The two strain hardening rules, which are widely used in metal plasticity, are isotropic hardening and kinematics hardening. If the yield surface (which represents the yield condition in stress space) expands uniformly during plastic flow with no shape change or translation, isotropic hardening occurs.

On the other hand kinematics hardening takes place when the yield surface does not change its size or shape, but simply translates in stress space in the direction of the outward normal.

2.2.4 Fatigue life prediction under multiaxial loading

Early work into the fatigue analysis of multiaxial stress conditions attempted to reduce the multiaxial components of stress or strain to a single equivalent parameter, often based on established monotonic yield criteria, which can then be analysed using similar to the uniaxial case [7].

Fatigue life is often characterised by the cyclic plastic deformation at the notch tip and therefore, accurate calculation of stress/strain behaviour at the notch root is an essential

requirement for any fatigue life prediction procedure. Recently developed approaches for multiaxial fatigue life estimation require both stress and strain at the notch root as inputs [18].

2.2.5 Proportional and non-proportional loading

If the various cyclic stress components are in phase and change proportionally with each other (see Figure 2.4), the loading is called proportional. When the applied load causes the directions of the principal stresses and the ratio of the principal stress magnitudes to change after a load increment (see Figure 2.5), the loading is termed non-proportional [19].

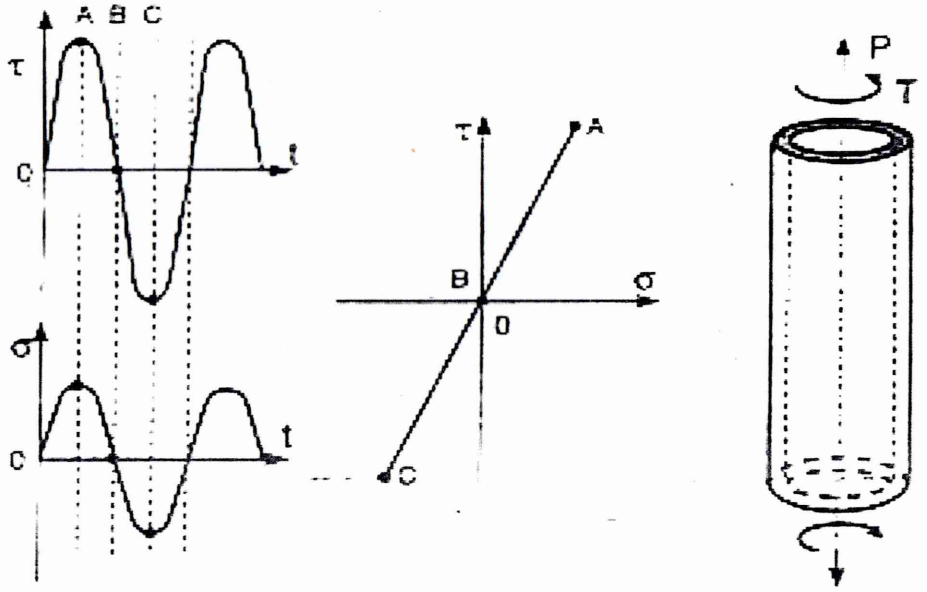

Figure 2.4: An example of proportional cyclic torsion-tension loading applied to a hollow cylinder

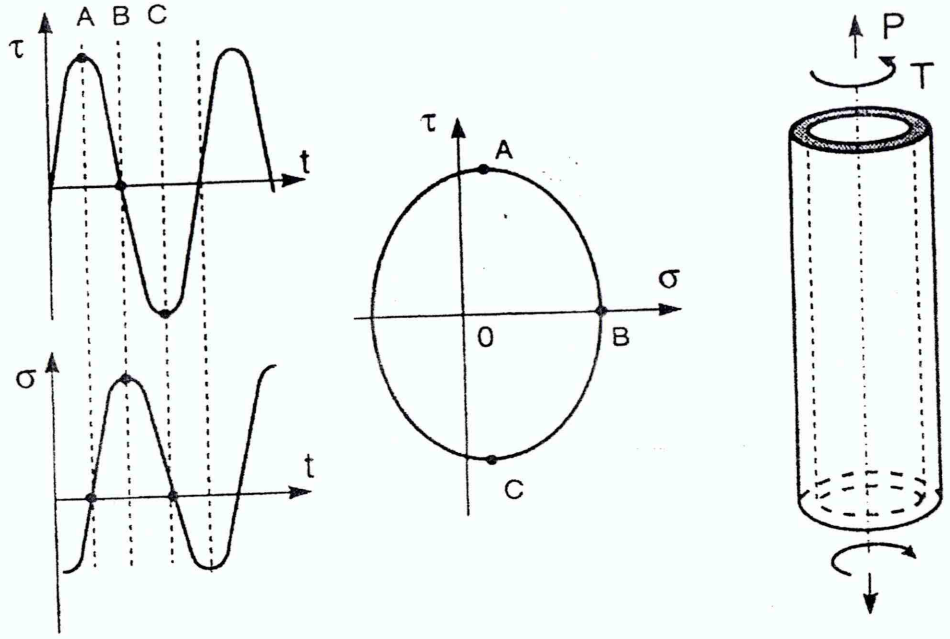

Figure 2.5: An example of non-proportional cyclic torsion-tension loading applied to a hollow cylinder

If plastic yielding takes place at the notch tip then almost always the stress path in the notch tip region is non-proportional regardless whether the remote loading is proportional or not. However, the remote proportional loading does not make the notch tip stress tensor to rotate and therefore it makes the stress analysis easier in spite of the fact that some non-proportionality of the notch tip stress history may occur [19].

The Osgood – Ramberg equation, can describe the stress relationship under uniaxial cyclic loading. In cyclic stress-strain relationship under multiaxial loading, the stress not only depends on the strain, but also relates to the loading path. The good prediction of the fatigue life under multiaxial cyclic loading strictly depends on the accuracy of the cyclic strain-life relation as well as on precise description of the stress-strain relationship under multiaxial cyclic loading. In the last two decades, multiaxial cyclic constitutive theory was widely emphasized, and many good works have been completed. Unfortunately the results, which can be directly used for the prediction of multiaxial fatigue, are very few due to the complication of the multiaxial cyclic constitutive theories that are usually developed for plasticity theory [20].

Based on Ramberg-Osgood relation and considering the material constants, the equations for cyclic stress-strain curve for first loading and hysteresis loop could be written as;

$$\varepsilon = \frac{\sigma}{E} + \left(\frac{\sigma}{K}\right)^{1/n} \quad \text{for first loading}$$

$$\Delta\varepsilon = \frac{\Delta\sigma}{E} + \left(\frac{\Delta\sigma}{2K}\right)^{1/n} \quad \text{for hysteresis loop}$$

Equation can be modified to accommodate cyclic behaviour observed during torsion loading.

$$\gamma = \frac{\tau}{G} + \left(\frac{\tau}{K}\right)^{1/n} \quad \text{for first loading}$$

$$\Delta\gamma = \frac{\Delta\tau}{G} + \left(\frac{\Delta\tau}{2K}\right)^{1/n} \quad \text{for hysteresis loop}$$

2.3 Notches

2.3.1 Introduction

The geometry of notch and the applied cyclic complex loading play an important role in the magnitude of the localised cyclic plastic deformation [21]. Fatigue life is often characterised by the cyclic plastic deformation at the notch tip and therefore, accurate calculation of stress/strain behaviour at the notch tip is an essential requirement for any fatigue life prediction procedure. Recently developed approaches for multiaxial fatigue life estimation require both stress and strain behaviour at the notch tip as inputs [18].

Inelastic analysis of stress-strain behaviour at a notch root is a complex procedure, which requires constitutive modelling based on incremental plastic theories [22]. In practice, strain gauge rosettes attached to components should provide necessary information. However where this is not possible, stresses and strains must be estimated from applied loading using notch geometry and material properties [23].

Fatigue failures usually occur at notches where high stresses occur due to stress concentration. The strain life approach was developed to account for notch root plasticity. By knowing the notch tip strain history and smooth specimen strain-life data, fatigue life evaluations may be performed for notch members. The stresses and strains at the notch root may be determined by strain gauge measurements, finite element analysis; and the relation of local stresses and strains to nominal values. The most computationally efficient method of determining these values is by relating the local stresses and strains to the nominal values [5].

Fatigue cracks most often initiate at the notch tip where the highest stress concentration occurs. Therefore most fatigue analysis is focused on the determination of fatigue life of the material, which is under the effect of the notch tip stresses and strains. They are subsequently dependent on the notch geometry, material properties and loading history applied to the notched body [19]. Fatigue initiation and crack growth programs require an accurate knowledge of the local notch tip stresses and strains. These quantities can be determined in several ways, such as direct strain gauge measurements, using finite element analysis or by using approximate methods, such as the Neuber and Glinka approaches that relate local stresses and strains to their remote values [24].

2.3.2 Neuber's rule

The stress and strain concentration factors are of the same value when only elastic deformation occurs at the tip of the notch. However, once the material yields at the notch tip, the stress and strain concentration factors take different values.

Neuber's rule states that under conditions of plastic deformation, the theoretical stress concentration is the geometric mean of the stress and strain concentration.

$$K_t = (K_\sigma K_\varepsilon)^{1/2}$$

Where,

K_t - elastic stress concentration factor

K_σ - σ/S (local stress/nominal stress)

K_ε - ε/e (local strain/nominal strain)

This approach is easily adapted for computer applications. A Neuber analysis may be used to evaluate the fatigue life of a notched component under variable amplitude loading (see Figure 2.6) [5].

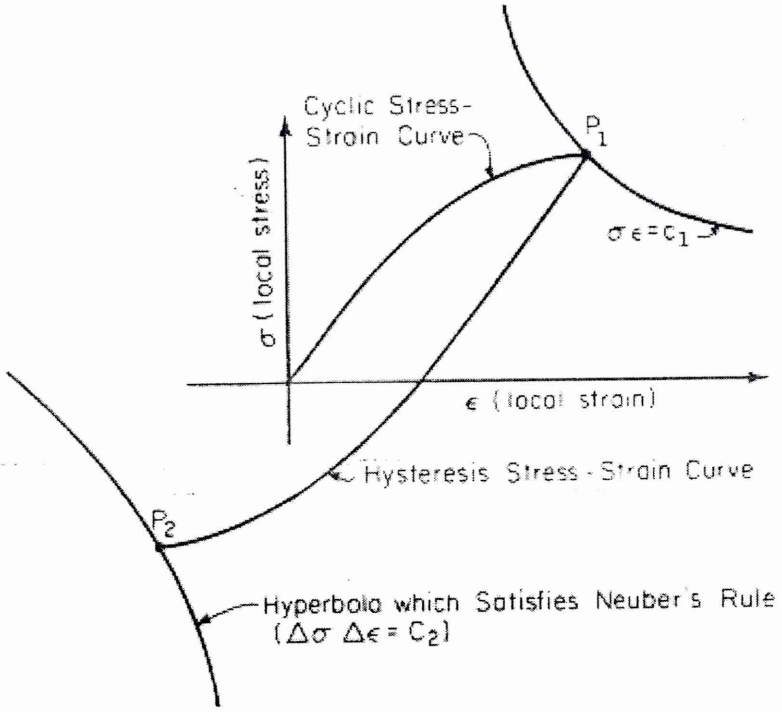

Figure 2.6: Intersection of hysteresis stress-strain curve and Neuber's hyperbola

The prediction of fatigue lives for notched members has found increasing use of local strain approaches, which are modifications and applications of the Neuber's rule to fatigue loading conditions. In these approaches, the following expressions for fatigue notch factors are found to provide satisfactory predictions of the fatigue behaviour in notched members of a wide variety of steels.

$K_t = (K_\sigma K_\varepsilon)^{1/2}$

For plastic deformation ahead of notches and

$$K_t = \frac{(\Delta\sigma\Delta\varepsilon E)^{1/2}}{S}$$

For elastic deformation S, $\Delta\sigma$ and $\Delta\varepsilon$ are the amplitudes of the fully reversed nominal stress, notch tip stress and notch tip strain, respectively. For fixed values of the imposed stress range S.

$\Delta\sigma\Delta\varepsilon = (K_t S)^2/E = \text{constant}$

There is a family of curves, with different combinations of $\Delta\sigma$ and $\Delta\varepsilon$, which satisfies this equation. K_f can be uniquely determined by simultaneously solving Neuber equation with the cyclic stress-strain constitutive equation.

2.3.3 Strain-life approach for a notched component

The strain-life method, which is commonly used to predict fatigue crack initiation, requires knowledge of notch-root stresses and strains. These quantities can be determined in several ways such as direct strain gauge measurements, using finite element analysis or by using approximate methods that relate local stresses and strains to their remote values [10]. By knowing the notch root strain history and smooth specimen strain-life data or fatigue properties, fatigue-life evaluation may be performed for notched members. An advantage of this method is that it accounts for changes in local mean and residual stresses.

2.3.4 Stress-life approach for a notched component

All machine components and structural members contain some form of geometrical or micro structural discontinuities. These discontinuities, or stress concentrations, often result in maximum local stresses, σ_{max}, at the discontinuities which are many times greater than the nominal stress of the members, S. In ideally elastic members the ratio of these stresses is designated as K_t, the theoretical stress concentration factor [5].

$$K_t = \sigma_{max} / S$$

2.3.5 Fracture mechanics approach for a notched component

Fracture mechanics approaches may also be used in the fatigue analysis of notched components. In the application of this method to a notched component, the near notch stress-strain field must be considered. Important aspects of the analysis include the determination of the size of the region over which this field is effective and the stress intensity factor in this region [5].

There are several advantages in fracture mechanics approach. This approach is the only method that deals directly with the propagation of fatigue cracks and crack growth rate must be incorporated with non-destructive inspection techniques. This method gives a good insight into the actual mechanisms of fatigue.

In contrast, the disadvantages of the fracture mechanics approach are that in certain situations the assumptions of linear elastic fracture mechanics are not valid and elastic-plastic fracture mechanics concepts must be used and this method has problems when used to deal with crack initiation. Also this method requires an estimate of stress intensity factors, which may be difficult to determine for complicated geometries.

2.3.6 Short crack growth at notches

A plastic zone often develops in the notch tip due to the stress concentrations associated with the notch (see Figure 2.7) [5]. The plastic zone is surrounded by a region of elevated elastic stresses and strains. This region is, in turn, surrounded by the bulk stress strain field.

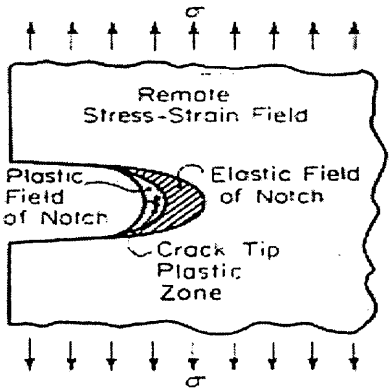

Figure 2.7: Plastic zone at notch root

There are three types of anomalous crack growth behaviour for cracks at notches. They are short crack growth only in a plastic field. Short crack growth in both plastic and elastic fields and short crack growth only in an elastic field In the notch field, a major cause of this "short crack" behaviour is the difference in residual plastic deformation in the wake of the crack [5].

For the short cracks $K_{short} = 1.12K_tS(\pi l)^{1/2}$

where,

K_{short} - stress intensity factor for the short crack

S - nominal stress

K_t -elastic stress concentration factor

l - free surface crack length

f(g) - 1.12 - free surface or edge correction factor

For long cracks $K_{long} = S (\pi a)^{1/2}$

where,

K_{long} - stress intensity factor for the long crack

a = l+D

D - radius of circular hole [5]

2.4 Fatigue damage

There are distinctly different approaches used when dealing with cumulative fatigue damage during the initiation and propagation stages. During the propagation portion of fatigue, damage can be directly related to crack length. During the initiation phase the mechanism of fatigue damage are on the microscopic level. It can be related to dislocations, slip bands, micro crack, etc. and can be only measured in a highly controlled laboratory environment [5].

There are several damage summing methods during the initiation phase of fatigue.

- **Miner's rule**

The linear damage concept is that the summation of all fractions of life equals one. The failure criterion for variable amplitude loading is thus:

$$\sum \frac{n_i}{N_i} \geq 1$$

However, the correct application of Miner's rules depends on limiting assumptions stated below.

- In each block the loading must be fully reversed.
- The rate of damage accumulation at any given level must not depend on prior loading history [25].

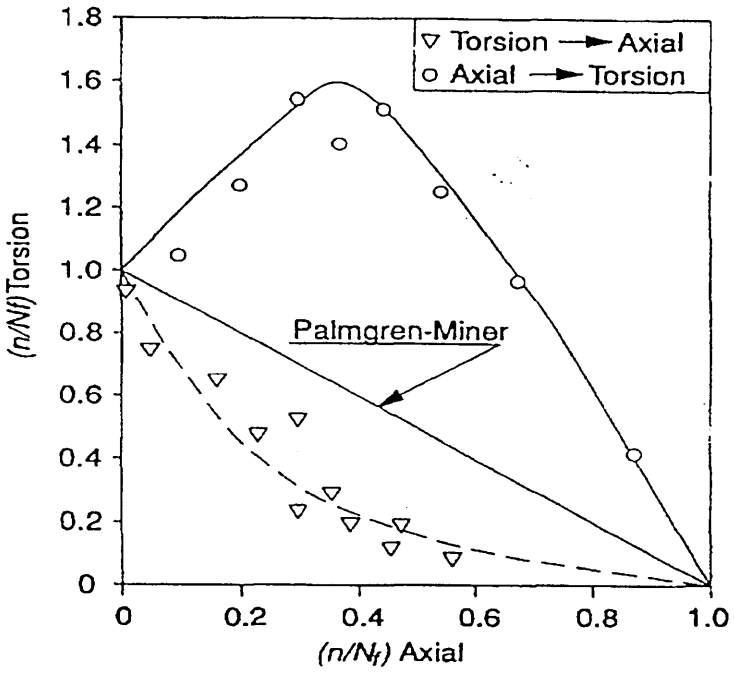

Figure 2.8: Linearly calculated damage when the mode of loading was changed from torsion to axial [17]

As seen in Figure 2.8, torsion cycling which follows blocks of axial cyclic loading is less damaging than torsion cycles applied without prior axial loading. However, axial cycles following an initial torsion load block were more damaging [17].

- **Rain flow counting**

The rain flow method of cycle counting attempts to identify closed hysteresis loops in the stress - strain response of a material subjected to a cycle loading (see Figure 2.9).

The following rules apply: [5]

- The strain time history should be plotted so that the time axis is pointing vertically downward and the lines connecting the strain peaks may be imagined as a series of roofs.
- The rain flow begins successively at the inside of each strain peak.
- The flow should initiate at the top of each peak and drip down until it comes to a maximum more positive or negative peak that from which is started.
- The flow should stop when it meets rain from a higher roof.
- The horizontal length of each rain flow is counted as one half cycle of the strain range.

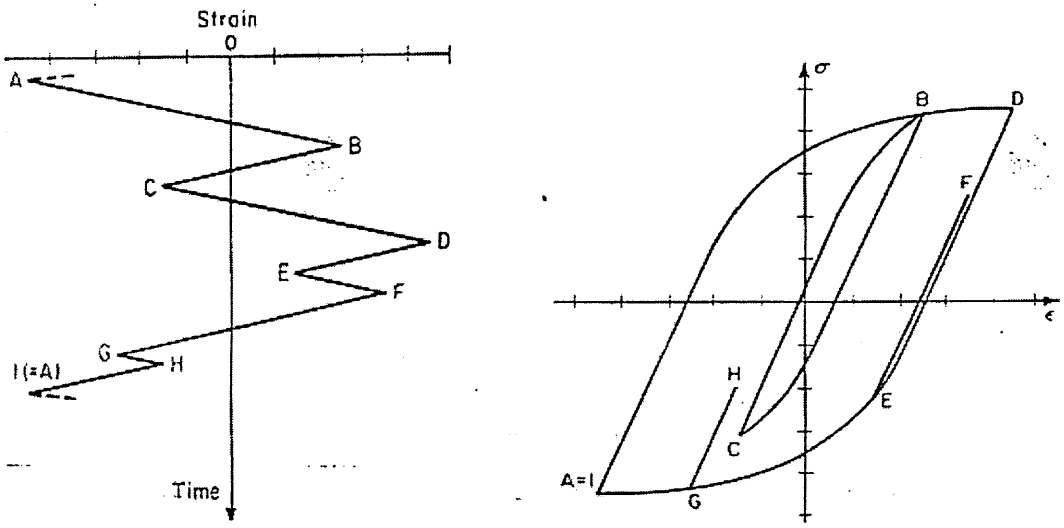

Figure 2.9: Material stress-strain response to given strain history

Chapter 3

Modern Fatigue Analysis Methods

3.1 Introduction

The extensive use of computers throughout the design process is now commonplace. As competitive pressures call for improvements in product performance, safety and quality and for reductions in development times, this role is becoming increasingly important. Computers are being used extensively to complement experimentation where it can help to identify phenomena that would be too costly and even impossible to identify by experiments alone.

Software helps manufacturers to simulate reality, which reduces the need to do physical prototype testing and allows them to consider various design alternatives, thus saving manufacturing cost. Using these, engineers can identify the design flaws earlier in their manufacturing cycles, reducing the time-to-market of their products and warranty costs, while at the same time saving on material costs without reducing the integrity of their products.

3.2 Model drafting tools and stress analysis tools

Engineering operations including the general management of projects, modelling of conceptual designs, selection of materials and the analysis of components may now be completed more quickly, efficiently and cost effectively through the use of Computer Aided Engineering (CAE) tools. The detailed design stage, traditionally involves an element of theoretical analysis, which has its limitations especially when addressing complex systems, thus extensive component testing is often favoured. However, this is a time consuming process and hence Computer Aided Design methods are being increasingly utilised in order to shorten the development cycle. The some of the model drafting tools available in the market are AutoCAD, Pro/Engineer, Solid works, I-DEAS etc. A range of analysis tools such as ABAQUS, Ansys, Cosmos, MSC.Patran, MSC.Nastran etc. may now be used to assess the integrity and durability of engineering components, minimise the time and expense associated with static testing. For the current research ABAQUS code was used for finite element analysis.

3.2.1 ABAQUS

ABAQUS is a high-performance software package developed by **Hibbitt, Karlsson & Sorensen, Inc.** for the numerical modelling of structural response. It enables to do

linear or nonlinear, and static or dynamic types of analysis for a large spectrum of engineering problems. Some of the specific capabilities of ABAQUS are: Stress analysis (both static and dynamic responses), dynamic studies (linear and non-linear problems), analyse heat transfer problems, coupled heat transfer and stress analysis and can be done element removal and replacement. ABAQUS includes a complete pre- and post- processing environment.

3.2.1.1 ABAQUS/Post

ABAQUS/Post is the interactive, graphical, post-processing module. For the finite element, it provides powerful and rapid results evaluation. ABAQUS/Post includes model plotting, deformed geometry plotting, contour plots of results, vector plots, *xy* plotting, and animation. Printed output and interactive model and results query are also provided. Post processing is done directly from the files produced by the ABAQUS analysis modules. Hence, results can be viewed rapidly, even while the analysis is running. ABAQUS/Post supports all ABAQUS capabilities.

- **View and display**

Models can be viewed from any angle. Dynamic rotate, pan and zoom by means of mouse control is available. The model can be rendered in wire frame, hidden line and filled element styles. Also whole models or partial models defined by node or element sets can be displayed.

- **Contour plots**

Contour plots can be produced for any element quantities, such as stresses and strains, or for nodal values, such as displacement components. Contours are provided on the faces of three-dimensional solid elements, for any layer of shell elements.

- ***X-Y* Plots**

Time history plots display the variation of results during the analysis. Variable versus variable plots allow the variation of one variable with respect to another to be plotted during all or part of the analysis such as stress vs strain plots [30].

3.3 Fatigue analysis software

There are a number of software tools such as Nsoft, Fatimas etc., to assist design engineers whereby the conceptual designs can be fatigue analysed at the design stage. A

majority of those software tools require the actual stress-strain history at the critical location in order to predict fatigue life.

These packages are useful to reduce the time between conceptual design and the finished product, and also to reduce fatigue-testing time. These packages can be used to select the best material and design for fatigue critical component. Also can be used to optimise the whole production process whilst satisfying operational demands on the product. Fatigue software packages are useful to analyse the effects of changing component shape, material and even vibration modes on durability performance. For accurate fatigue modelling requires high quality stress/strain records, representative materials data and geometric data [33].

3.3.1 Input requirements of fatigue software

3.3.1.1 Stress -life analysis

For stress-life analysis input is time history of stress and mainly use for 'High cycle fatigue analyses'. Stress-life approach is also known as "Nominal Stress Approach". This approach used extensively for welded joints and non-metallic. Nominal stress cycles must be elastic (hence high cycle) though local stresses at the critical location will be plastic. Stress-life (S-N) approach is not as good as strain-life (E-N) approach for general FEA use because it cannot account for the local plasticity predicted by the FE analysis. The block diagram of the stress-life approach for fatigue life prediction is shown in Figure 3.1.

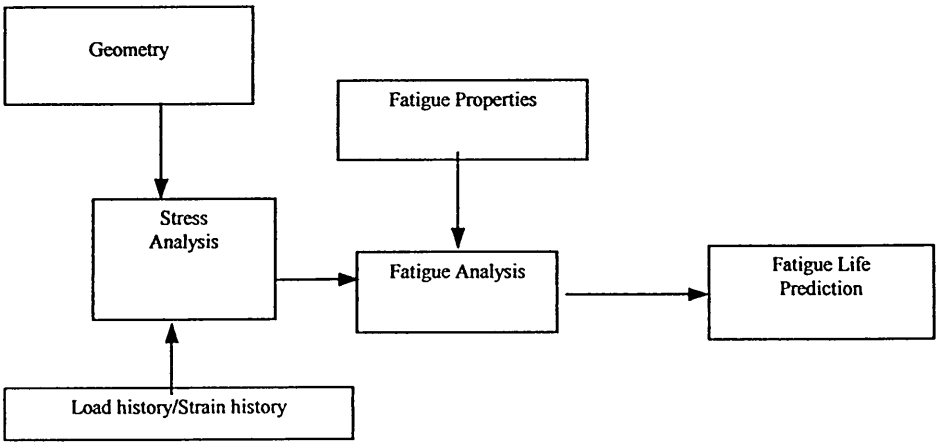

Figure 3.1: Stress life approach

3.3.1.2 Strain-life analysis

For strain-life analysis input is time history of strain. Local strains can be elastic or plastic hence its suitability for 'Low Cycle fatigue' and local plasticity predicted by FE analysis. The block diagram of the strain-life approach for fatigue life prediction is shown in figure 3.2.

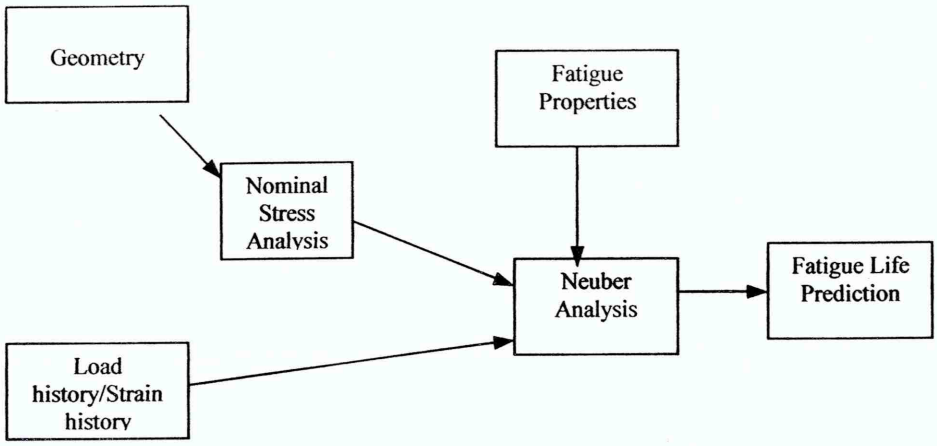

Figure 3.2: Strain- life approach

3.3.2 Using strain gauge data for fatigue analysis software

The majority of strain measurements have been made using single strain gauges located at, or close to, the known or expected position of fatigue cracking. When making measurements with a strain gauge rosette, three separate, but simultaneous, strain-time records are obtained; each relating to the strains experienced by an individual 'leg' of the rosette. Two types of rosette configuration are most commonly used: the 'rectangular' form with gauges oriented at 0, 45 and 90 degrees and the 'delta' form with gauges at 0, 60 and 120 degrees. The first step in the characterisation of a multiaxial strain field is to carry out a principal strain analysis, which calculates, point-by point, the following parameters:

- Maximum principal strain, ε_{max}
- Minimum principal strain, ε_{min}
- Maximum shear strain, γ_{max} and the angle between ε_{max} and the zero degree gauge Φ

The strain module of the software, calculates these parameters from the three component strain histories for either rectangular or delta shaped strain gauge rosettes. The fatigue life was calculated using both the Smith-Topper-Watson and Morrow procedures [33].

Chapter 4

Finite Element Analysis of a Notch Component

4.1 Introduction

Finite Element Analysis (FEA) is a computer-based numerical technique for calculating the strength and behaviour of engineering structures. It can be used to calculate deflection, stress, vibration, buckling behaviour and many other phenomena. It can be used to analyze either small or large-scale deflection under loading or applied displacement. It can analyze elastic deformation, or "permanently bent out of shape" plastic deformation. A computer is required because of the astronomical number of calculations needed to analyze a large structure. The power and low cost of modern computers has made Finite Element Analysis available to many disciplines and companies.

In the finite element method, a structure is broken down into many small simple blocks or *elements*. The behaviour of an individual element can be described with a relatively simple set of equations. Just as the set of elements would be joined together to build the whole structure, the equations describing the behaviour of the individual elements are joined into an extremely large set of equations that describe the behaviour of the whole structure. The computer can solve this large set of simultaneous equations. From the solution, the computer extracts the behaviour of the individual elements. From this, it can get the stress and deflection of all the parts of the structure. The stresses will be compared with allowed values of stress for the materials to be used, to see whether the structure is strong enough.

4.2 Usefulness of finite element analysis

Finite Element Analysis makes it possible to evaluate a detailed and complex structure, in a computer, during the planning of the structure. In the absence of Finite Element Analysis (or other numerical analysis), development of structures must be based on hand calculations only. For complex structures, the simplifying assumptions required for making any calculations possible can lead to a conservative and heavy design. A considerable factor of ignorance can remain as to whether the structure will be adequate for all design loads. Significant changes in designs involve risk. Designs will require

prototypes to be built and field-tested. The field tests may involve expensive strain gauging to evaluate strength and deformation.

Finite Element Analysis is done principally with commercially purchased software. Software at the high end of the price scale features extensive capabilities for plastic deformation, and specialized work such as metal forming or crashes and impact analysis. The FEA software includes modules to create the element mesh, to analyze the defined problem, and to review the results of the analysis. Output can be in printed form, and plotted results such as contour maps of stress, deflection plots, and graphs of output parameters.

The choice of a computer is based principally on the kind of structure to be analyzed, the details required of the model, the type of analysis (e.g. linear versus nonlinear) and the economics of the value of timely analysis, and the analyst's salary and overhead. An analysis can take minutes, hours, or days. Extremely complex models will be run on big machines.

4.3 Advantages of using the FEA

There are several advantages of using FEA. By using this method complex two and three-dimensional solids may be represented with reasonable accuracy due to the flexibility of the size and the shape of the elements and also bodies incorporating holes and corners may be modelled with ease. The size of the elements incorporated in a domain may vary; thus from FEA it may be refined at critical locations. FEA accuracy is comparable and often better than solutions achieved by means of other analytical or experimental methods. The application of computer technology to the FEA has led to the general achievement of rapid results.

The primary disadvantage of the FEA approach is the need for computer resources, vast amount of memory and the subsequent computational costs that ensue.

4.4 FE modelling of the notch specimen

The notch specimen is shown in Figure 4.1. Considering the failures of the bolts, collate and the load ring the maximum allowable notch diameter was calculated as 15.4 mm. To get the maximum plasticity area, diameter at the notch should be larger. Therefore

diameter at the notch was selected as 15 mm and the other dimensions were selected to suit the machine requirements.

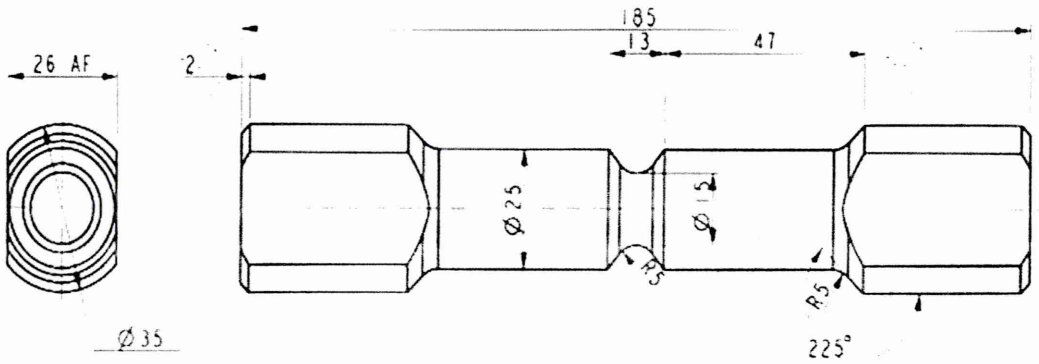

Figure 4.1: Dimensions of the specimen

As shown in Figure 4.1, opening of the notch was made wider to paste the strain gauge easily at the notch root. From Peterson's Handbook [38] stress concentration factor at the notch root K_t was found as 1.6. Other stress concentrations of the specimen also checked and the highest value was found at the notch root.

4.4.1 FEA model geometry

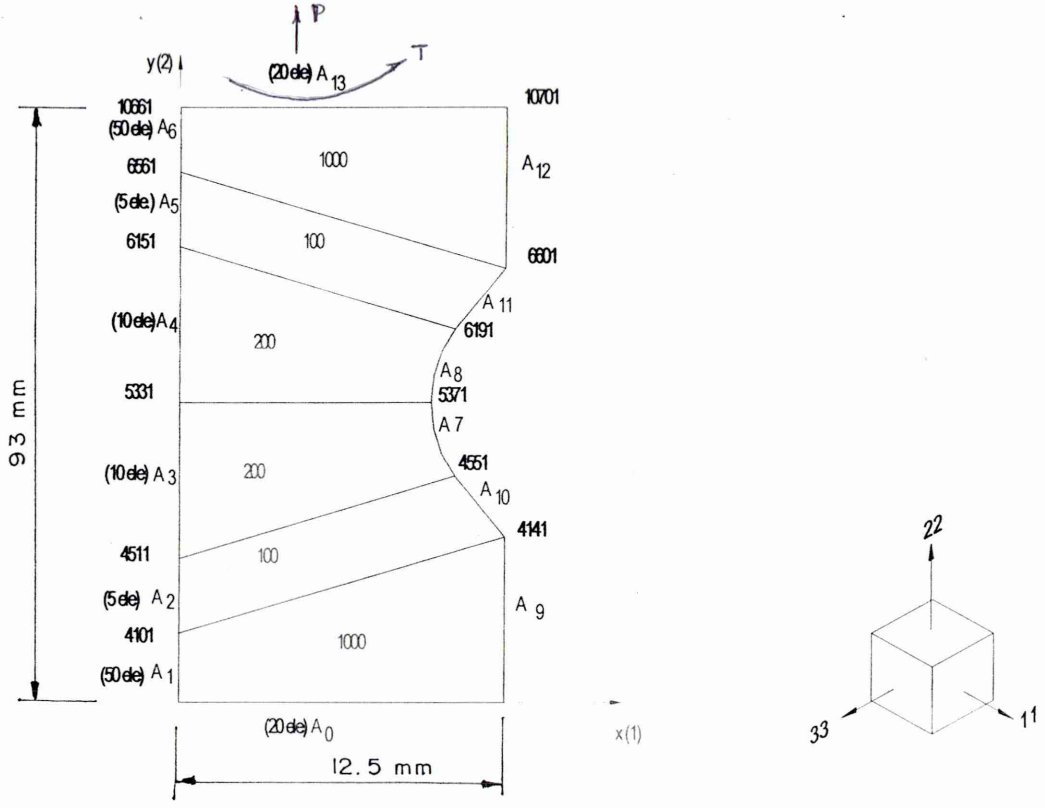

(a) **(b)**

Figure 4.2: (a) Element details (b) Stress or strain directions

Half of the specimen was modelled by using ABAQUS code, as the specimen was geometrically symmetrical. Figure 4.2 (a) shows the selected element details and Figure 4.2 (b) shows the stress or strain directions of a block at the notch root, of the model.

The total number of elements used for the model was 2600 and 600 elements were used to define the mesh in notch area as this is the main concern of the investigation. Figure 4.3 shows the element density at the notch region.

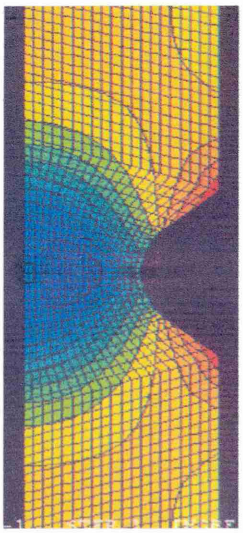

Figure 4.3: The element density of the notch area.

4.4.2 Mesh details

To model the specimen used axisymmetric elements with twist (CGAX*8* elements) in ABAQUS/Standard. This type of elements can be used for nonlinear multiaxial loadings. As the specimen is basically a solid circular bar with a notch at the middle of the specimen, these elements could be used. The main aim of the work was to study the behaviour of the stress and strain at the notch root. Standard axisymmetric elements could have used if only the axial loading was considered, but here CGAX8 elements (axisymmetric elements with twist) were used because the torsion loading was also considered in the analysis. This type of elements is recommended for studying stress/displacements.

For this CGAX8 elements co-ordinate 1 is radial (r), co-ordinate 2 is axial (z). Therefore the r-direction corresponds to the global x-direction and z-direction corresponds to the global y-direction as shown in Figure 4.2 (a). Therefore degree of freedom 1 is U_r, degree of freedom 2 is U_Z respectively. The CGAX8 elements has an additional degree

of freedom 5, corresponding to the twist angle ϕ (in radians). The total number of elements used for the model was 2600. Using 8 noded elements results in a total of 10661 nodes. Each element has eight nodes as shown in Figure 4.4 and each of the nodes has three degrees of freedom.

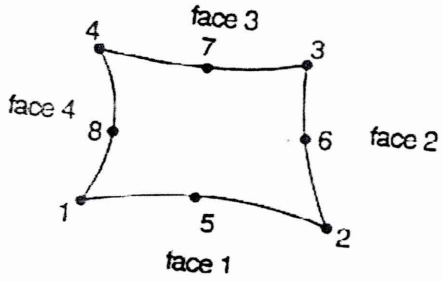

Figure 4.4: The node / face numbering of the CGAX 8 element

4.4.3 Loading and constraints

As the current research was concerned about the multiaxial loading, the axial load and torque should be applied at the same time. The selected element type was active only for rotational displacement inputs and not for torque input applications.

Therefore when analysing, displacements inputs were used instead torque. For consistency, both axial and torsion deformations were applied as displacements for every FE analysis.

Constraints

Considering Figure 4.2 (a), elements set $\mathbf{A_0}$, was constrained in axial direction (2 and Z), and transverse direction (5 and twist angle). The elements along the centre line, $\mathbf{A_1}$, $\mathbf{A_2}$, $\mathbf{A_3}$, $\mathbf{A_4}$, $\mathbf{A_5}$, $\mathbf{A_6}$ were constrained in radial direction (1 and X).

4.5 ABAQUS analysis (Input code)

For Finite Element Analysis using ABAQUS, an input file was required (all the input files are attached to the appendix-1). The input file basically consists of a number of headings of which the important headings are given below.

Mesh set-up

***HEADING (heading for the analysis)**

***NODE (coordinates of the nodes)**

***NGEN, NSET=A0 (generate node sets)**

***NFILL (fill nodes throughout the model)**

***ELEMENT, TYPE (define master element with node numbers)**

***ELGEN, ELSET=ALLEL (generate the elements throughout the model)**

***ELSET (define element sets for special regions)**

Material details

***SOLID SECTION, MATERIAL=MS (define material type)**

***MATERIAL, NAME=MS (define material properties)**

***ELASTIC (define elastic properties)**

***PLASTIC (define plastic properties)**

For the elastic plastic analysis, material yield strength and plastic strain-stress information was given for the cyclic stress-strain curve.

Analysis details

***STEP, INC=20**

***BOUNDARY (define constraints)**

***RESTART, WRITE, FREQ=1 (To run the analysis)**

***STATIC, DIRECT (define applied loading for static analysis)**

****AMPLITUDE DEFINITION**

For the cyclic, proportional and non-proportional loading, load waves amplitudes should be given under *AMPLITUDE DEFINITION command.

Results output details

***EL PRINT, POSITION=AVERAGED AT NODES (for element results)**

***NODE PRINT (for node results)**

***END STEP**

4.5.1 Accessing results

ABAQUS/Post is the post-processing module for the ABAQUS suite of general-purpose finite element software. This provides powerful and rapid results evaluation of ABAQUS analyses, and it is tightly integrated with the capabilities of the ABAQUS modules. Post processing could be done directly from the files produced by the ABAQUS analysis modules. Hence, results could be viewed rapidly, even while the analysis was running.

Contour plots could be produced for any element quantities, such as stresses and strains, or for nodal values, such as displacement components. Contours are provided on the faces of three-dimensional solid elements, for any layer of shell elements. For the current research several contour plots were used to see the stress/strain variation through the specimen. From these plots researcher could find the maximum value of stress/strain, the area of spread and also the pattern of the stress/strain distribution for elastic/plastic, proportional and non-proportional loading.

4.5.2 Typical results plots

The results for the case where the specimen was applied with 0.2 mm axial displacement (179 kN), the strain distribution (E22) throughout specimen is shown as the Figure 4.5. For the case where the specimen was applied with a 0.004 radians rotational displacement (80 Nm torque), the results are shown in the Figure 4.6. Considering both Figures the maximum strain occurred at the notch root, for both axial load and torque with elastic-plastic deformation conditions. The strains away from the notch root are found to be considerably lower, comparing with the strain at the notch root. For both loading cases the maximum strain appears within a small region, an approximately 3 mm^2 area at the notch.

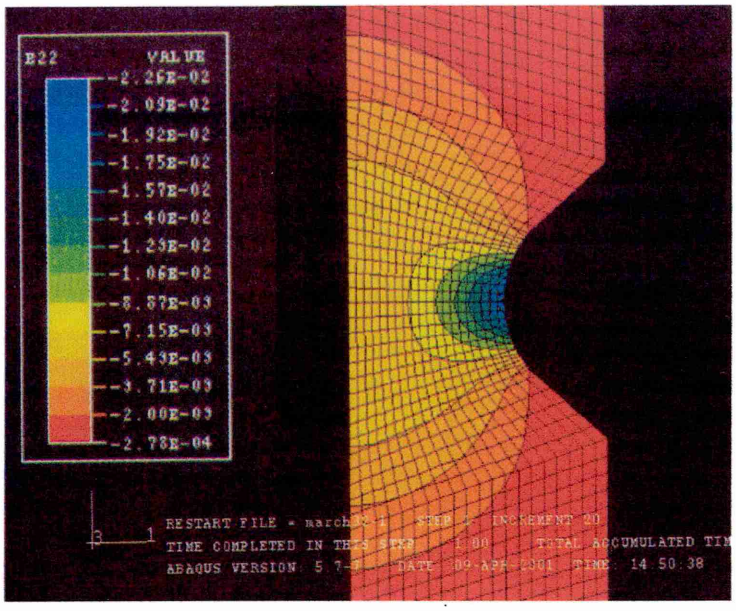

Figure 4.5: Finite element results - Axial strain (E22) distribution of the specimen for the axial load (0.2mm displacement) with elastic-plastic condition

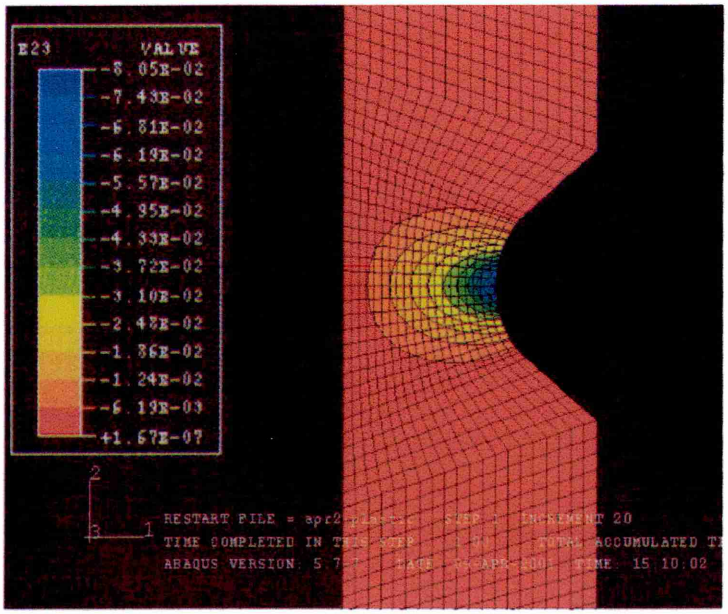

Figure 4.6: FEA results - Shear strain (E23) distribution of the specimen for the torsion load (0.004 rad rotational displacement) under plastic region

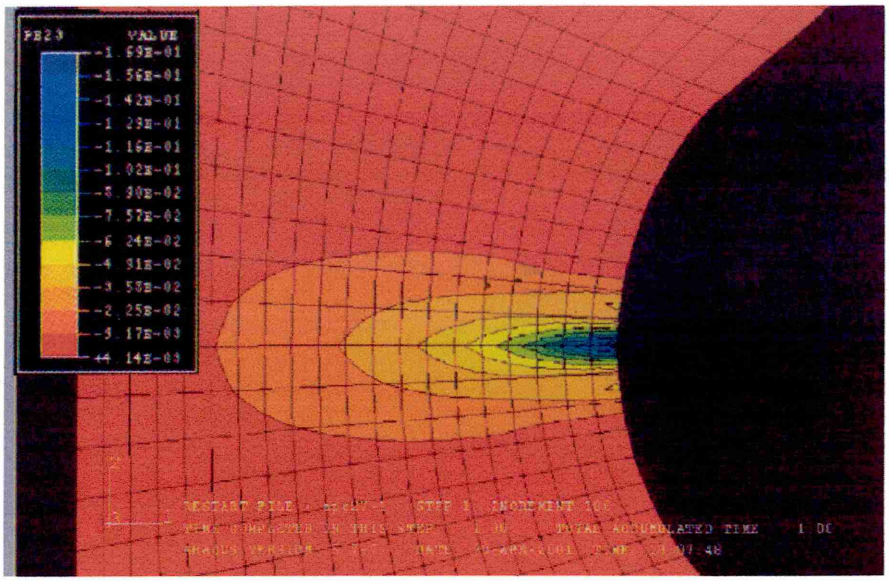

Figure 4.7: Finite element results - The principal strain distribution for out-of-phase load

For the case where the specimen was subjected to a 100 Nm torque and a 50 kN axial out-of-phase load the principal strain distribution of the notch region is shown in Figure 4.7. As shown, for non-proportional loading also the maximum strain occurred at the notch root within a small region.

4.6 Combined Axial -Torsion loading paths

During this study the cyclic deformation behaviour of the material was investigated under a number of loading paths. In addition to pure axial strain and pure torsion shear strain loadings, two types of combined axial-torsion paths were studied.

(a) Loading Paths using sinusoidal waveforms

(b) Loading Paths using non-sinusoidal waveforms

4.6.1 Loading Paths using sinusoidal waveforms

Sinusoidal loading Paths involved in-phase and out-of-phase loading.

(a) In-phase loading

For in-phase loading, the patterns of the sinusoidal waveforms of shear strain to axial strain are shown in Figure 4.8 (a) and the variations of shear strain to axial strain are shown in Figure 4.8 (b). For in-phase loading these variations should be linear and the gradient will be depended on the amplitudes of shear strain and axial strain waveforms.

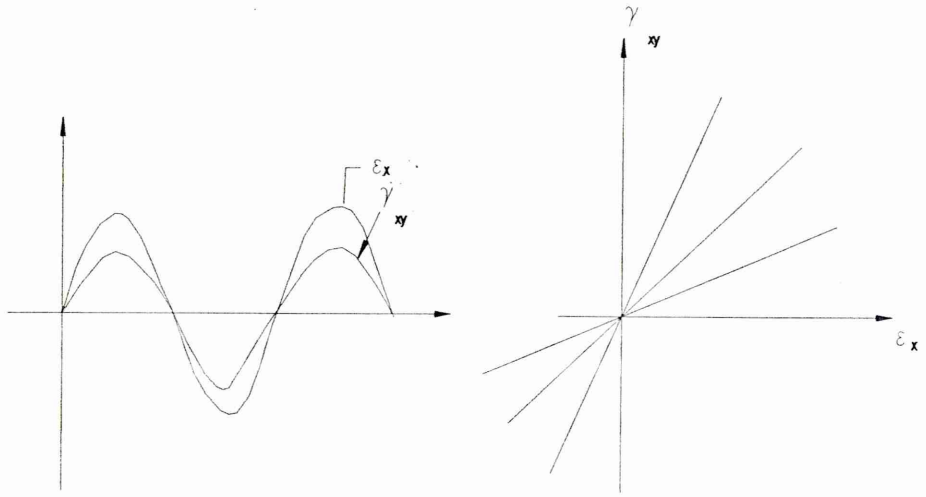

(a) (b)

Figure 4.8: (a) The wave forms of shear strain to axial strain (b) The variation of shear strain to axial strain for in phase loading

(b) Out-of phase loading

For out-of phase loading, the patterns of the sinusoidal waveforms of shear strain to axial strain are shown in Figure 4.9 (a) and the variations of shear strain to axial strain are shown in Figure 4.9 (b). For out-of phase loading these variations should be circular or elliptical and the shape will be depended on the amplitudes of shear strain and axial strain waveforms and the phase angle.

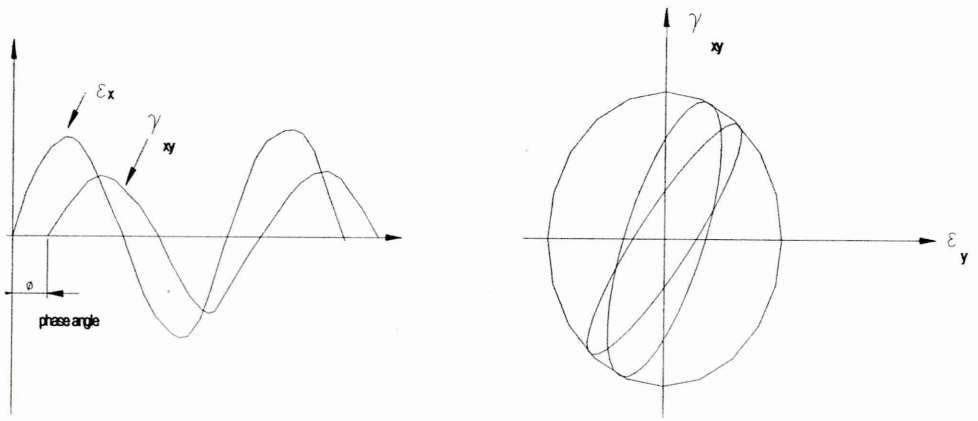

(a) (b)

Figure 4.9:(a) The wave forms of shear strain to axial strain (b) The variation of shear strain to axial strain for in phase loading

Phase angle ϕ varies from 0^0 to 90^0 for both cases amplitude of load and torque was chosen in the range of ± 35 kN to ± 70 kN and ± 85 Nm. Therefore the amplitudes of ε_x and γ_{xy} were changed relevant to the amplitudes of applied load and torque.

4.6.2 Non-sinusoidal waveforms

- **Path-B:**

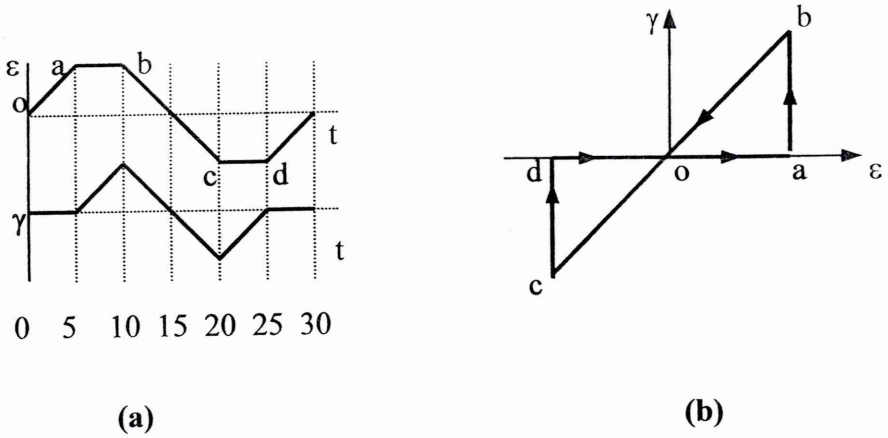

Figure 4.10: (a)The waveforms for non-proportional Path-B and (b) The variations of shear strain to axial strain for Path-B

Figure 4.10(a) shows the required waveform and (b) shows the variations of shear strain to axial strain for non-proportional Path-B. For both FEA and experiment analysis amplitude of load and torque was chosen in range ± 25 kN to ± 70 kN and ± 50 Nm to ±72 Nm respectively. Therefore the amplitudes of ε_x and γ_{xy} was changed relevant to the amplitudes of applied displacements for FEA and applied load and torque for experiment.

- **Path C:**

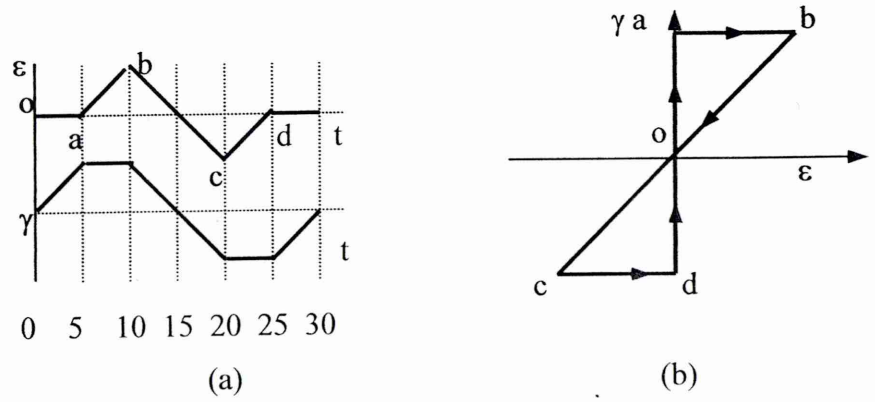

Figure 4.11: (a) The waveforms for non-proportional Path-C and (b) The variations of shear strain to axial strain for Path-C

Figure 4.11 (a) shows the required waveform and (b) shows the variations of shear strain to axial strain for non-proportional Path-C. For both FEA and experiment analysis amplitude of load and torque was chosen in range ± 25 kN to ± 70 kN and ± 50 Nm to ±85 Nm. Therefore the amplitudes of ε_x and γ_{xy} was changed relevant to the amplitudes of applied displacements for FEA and applied load and torque for experiment analysis.

- **Path D:**

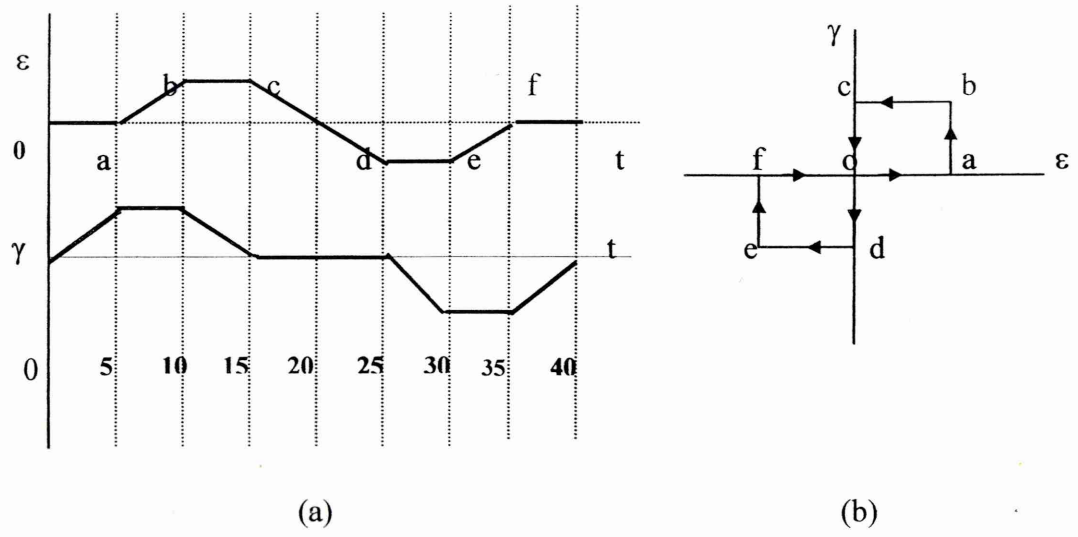

(a) (b)

Figure 4.12: (a) The waveforms for non-proportional Path-D and (b) The variations of shear strain to axial strain for Path-D

Figure 4.12 (a) shows the required waveform and (b) shows the variations of shear strain to axial strain for non-proportional Path-D. For both FEA and experiment analysis amplitude of load and torque was chosen in range ± 25 kN to ± 70 kN and ± 50 Nm to ±85 Nm. Therefore the amplitudes of ε_x and γ_{xy} was changed relevant to the amplitudes of applied displacements for FEA and applied load and torque for experiment analysis.

Chapter 5

Results of the Finite Element Analysis

5.1 Introduction

Specimen modelling and Finite Element analysis were done by using ABAQUS Code. Initially elastic analysis was done for tension and torsion separately to obtain stress and strain values. The results were also used to find a relationship between the axial load and axial displacement and the torsion load and rotational displacement. For the elastic analysis Elastic modulus (E = 2.08E05) and Poisson ratio (ν =0.3) for the material were assigned to the programme. Additional to the elastic modulus and Poisson ratio, yield strength and plastic strain were assigned for elastic plastic analysis. The stress-strain curve is given in Figure 5.8 and stress versus plastic strain is given in Figure 5.10 used in the ABAQUS file. The cyclic load, proportional loads and several non-proportional loads were applied for the same FE mesh discussed in chapter 4.

5.2 Elastic stress/strain analysis of the specimen

5.2.1 Tension loading

Figure 5.1, shows the relationship between the axial load versus axial displacement under elastic and elastic-plastic conditions. The graph under elastic condition is linearly increased while axial displacement is increased. The graph under elastic-plastic condition is linear up to 90 kN load and then shows the nonlinear elastic-plastic behaviour.

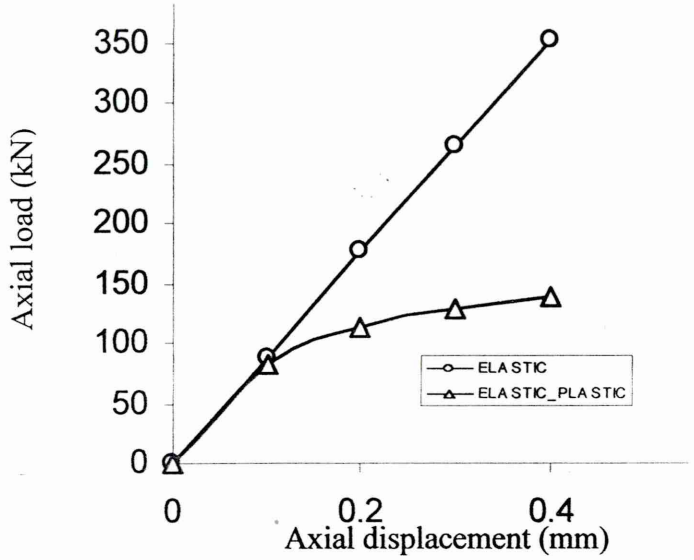

Figure 5.1: FEA results -The variation of applied load versus axial displacement

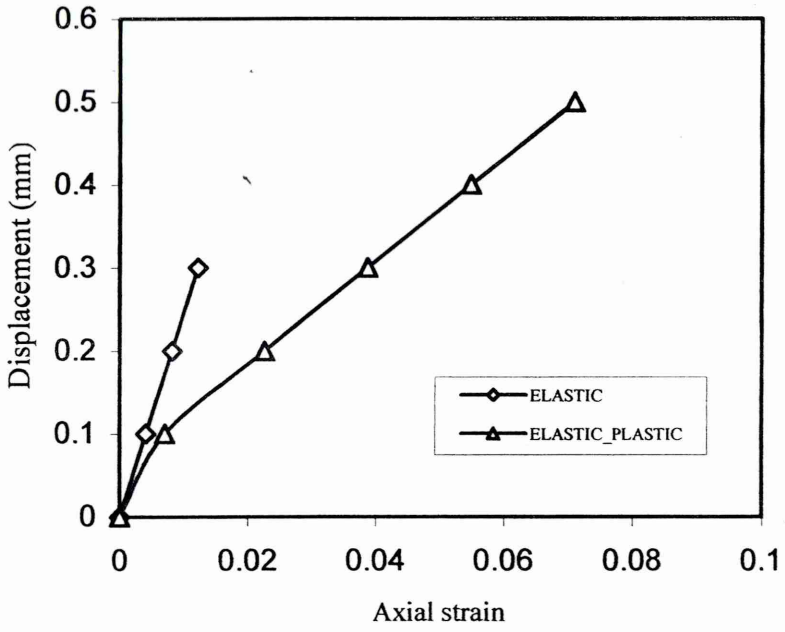

Figure 5.2: FEA results - The variation of axial displacement versus axial strain at the notch root

As shown in Figure 5.2, the variation of axial displacement versus axial strain was observed and this also linearly behaved under elastic condition and nonlinearly behaved for elastic-plastic condition. As the Figure 5.2, plastic behaviour was started when applying an approximately 0.1mm displacement.

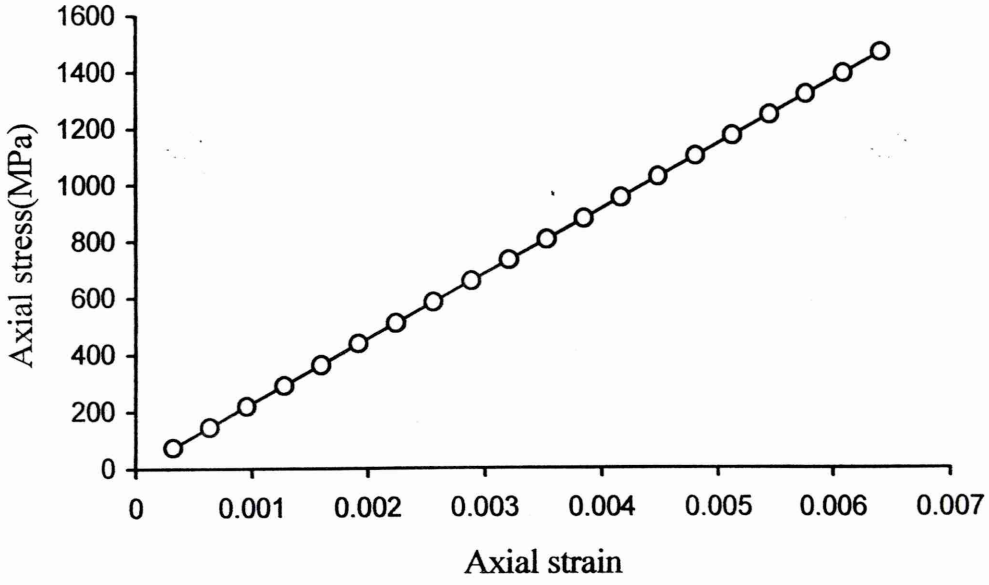

Figure 5.3: FEA results - The variation of axial stress (S22) and strain (E22) at the notch root

A relationship between the stress and the strain at the notch root was obtained by applying a 0.2 mm axial displacement to the specimen, under elastic conditions. As shown in Figure 5.3, behaviour is linear as expected in elastic region. The gradient of the graph was calculated to be 208,000 MPa, which is same as the Young's modulus of the material.

In practice, fatigue failure usually occurs at a notch or stress concentration. Stress concentrations; often result in maximum local stresses, σ_{max}, at the discontinuity, which are many times greater than the nominal stress (S) of the member. In ideally elastic members the ratio of these stresses is designated as K_t, the theoretical stress concentration factor [38].

Figure 5.4 shows the FEA results for axial stress (S22) distribution of the specimen when a 0.2 mm axial displacement is applied under the elastic condition. Maximum stress can be seen at the notch root.

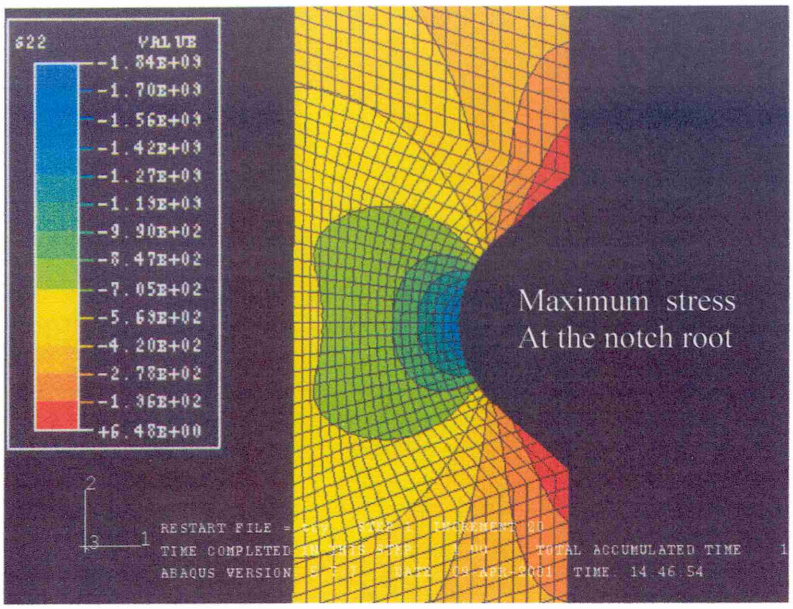

Figure 5.4: FEA results - The elastic stress distribution near the notch root

The stress distribution in the vicinity of the notch root can be seen. The first zone includes the maximum stress. Behind the third zone the stress values are quite small.

Theoretical stress concentration factor:

An estimate to the magnitude of the stress concentration factor may often be obtained by undertaking a manual analysis. Considering the Figure 5.1, from the FEA elastic results, for an applied displacement of 0.2mm, relevant axial load is 179.54 kN. Considering the Figure 5.4, maximum stress at the notch root is 1840 N/mm^2. Therefore the theoretical stress concentration factor K_t was calculated (appendix –2) and the value was 1.8. This is 12.5 % higher than K_t =1.6 which obtained from handbook [38].

5.2.2 Torsion Loading

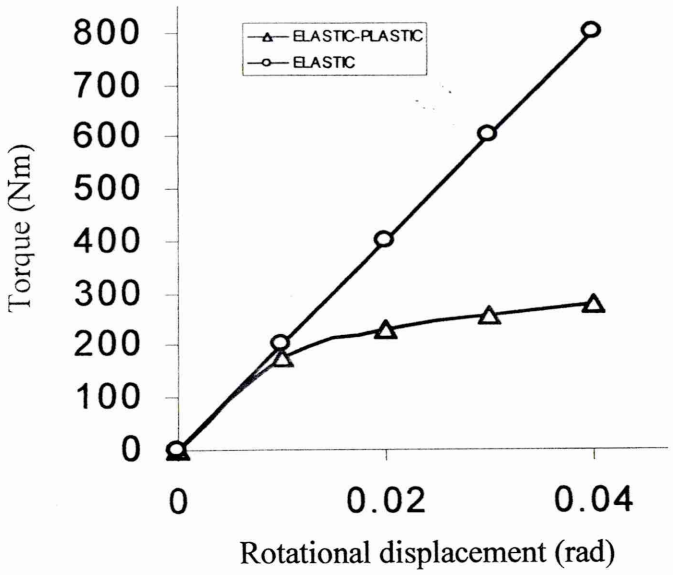

Figure 5.5: FEA results - The graph of torque versus rotational displacement

Figure 5.5, shows the relationship between the torque versus rotational displacement under elastic and elastic-plastic conditions. The graph under elastic condition is linearly increased when rotational displacement is increased. The graph under elastic-plastic condition is linear up to 180 Nm torque and then shows the nonlinear behaviour.

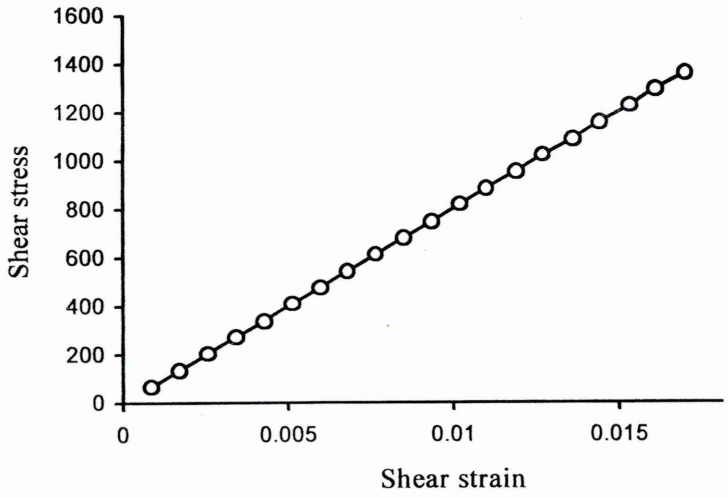

Figure 5.6: FEA results - The graph of the rotational displacements versus shear strain

Considering the Figure 5.6, shear stress versus shear strain graph under elastic condition also shows a linear graph as expected. The gradient of the graph was calculated to be 80,000 MPa, same as the rigidity modulus of the material.

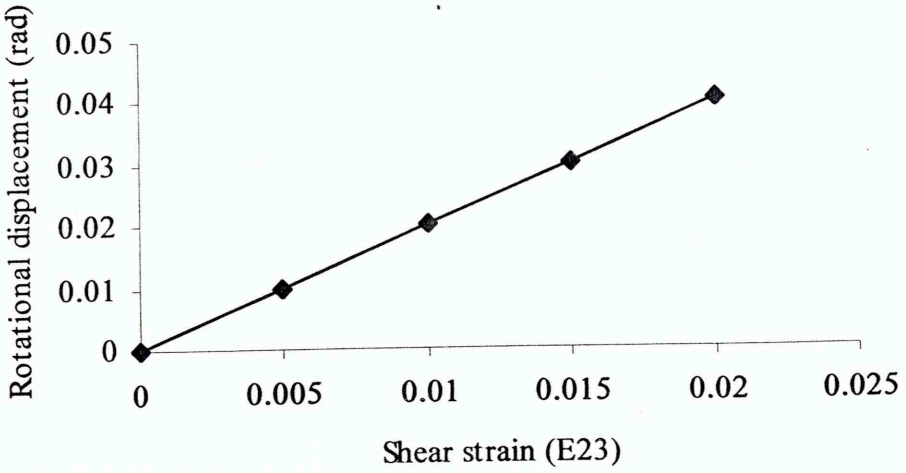

Figure 5.7: FEA results - The rotational displacement versus shear strain

Figure 5.7 shows the rotational displacement versus shear strain under elastic condition. The graph is linear as expected.

Estimation of torsion stress concentration factor:

Considering the Figure 5.5, from the FEA elastic results, for an applied rotational displacement of 0.04 rad, relevant torque is 836.6 Nmm. Considering the Figure 5.6, maximum stress at the notch root is 1650 N/mm^2. Therefore the theoretical stress concentration factor K_t was calculated (appendix –2) and the value was 1.3. This is 19% lower than K_t =1.6 which obtained from handbook [38].

5.3 Elastic/ Plastic stress analyses

Plasticity deals with the methods of calculating stresses and strains in a deformed body after part of the body has yielded. It is necessary to establish equations of equilibrium and compatibility and to determine the experimental relations between stress and increments of strain. The most difficult problem to solve in plasticity is those of constrained plastic flow [20]. Total strain within elastic-plastic range can be shown as following equation.

$$\varepsilon = \frac{\sigma}{E} + \left[\frac{\sigma}{K}\right]^{1/n}$$

Where ' K' is strength coefficient and 'n' is strain-hardening exponent. For the plastic analysis the current model was subjected to isotropic hardening behaviour. To analyse the programme material yield stress and relevant plastic strain were given as described earlier. Plastic strain is the portion which cannot be recovered on unloading. Plastic strain will produce both changes in grain shape and, on a very much smaller scale, changes in the distribution of lattice defects or dislocations. It is these changes that cause hardening. Plastic strain can produce changes in the yield point of single crystal of pure metal [32].

5.3.1 Tension loading

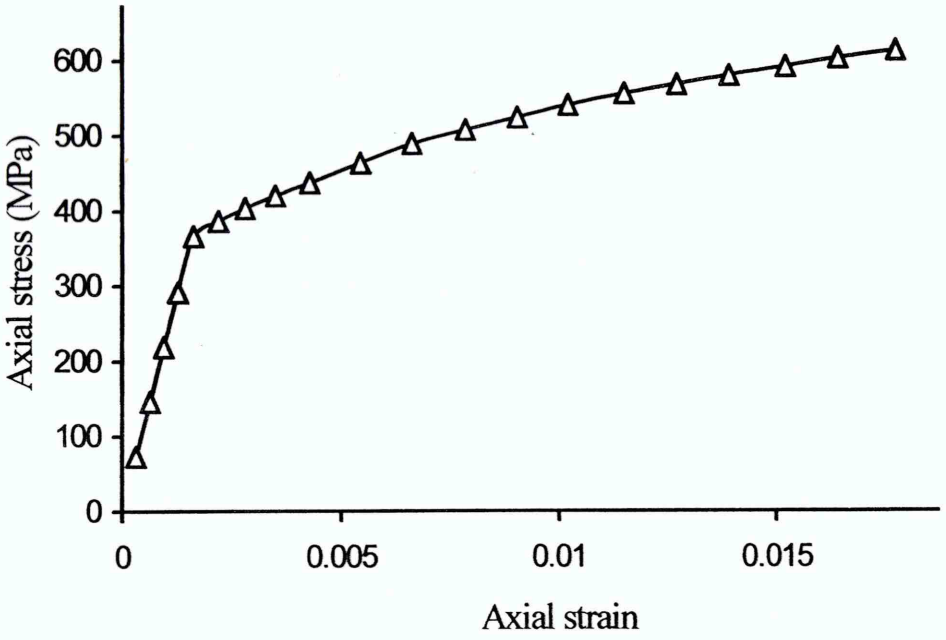

Figure 5.8: FEA results - The stress–strain response at the notch root (0.2 mm displacement)

As shown in the Figure 5.8, when applying an elastic-plastic load, the graph is linearly behaved up to 350 MPa and then started to behave plastically. Considering the elastic part, gradient of the graph was calculated to be 208000 MPa and the value is similar to the modulus of elasticity of the material.

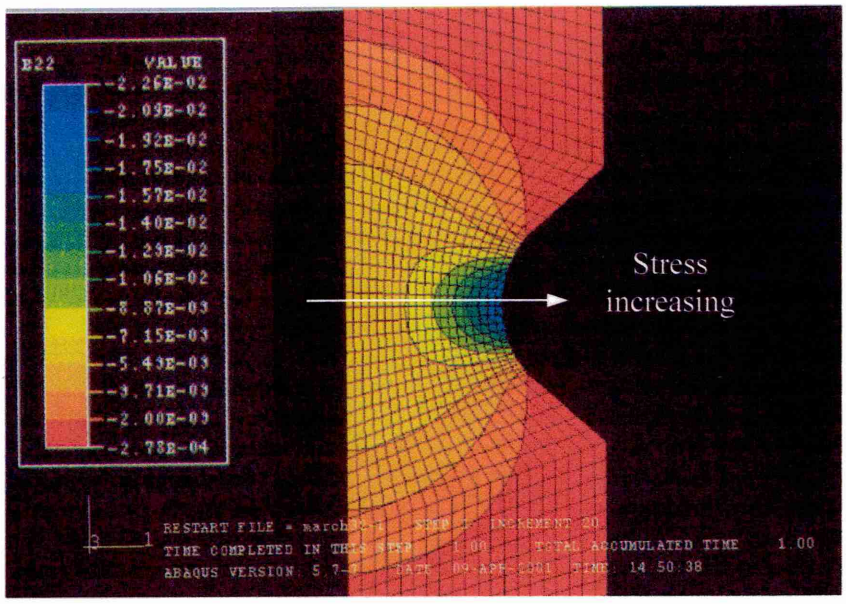

Figure 5.9: FEA results - The area of the plastic strain when applying 0.2 mm axial displacement

The elastic-plastic stress/strain distribution near the notch root exhibits first a peak point and then a decreasing dependence to the distance from the notch root. Few different stress/strain distributions in the vicinity of the notch root can be particularly distinguished as Figure 5.9.

Estimation of elastic-plastic stress concentration factor:

Elastic-Plastic stress concentration factor was estimated using FEA results and using Neuber equation $K_t^2 \, S \, e = \sigma \, \varepsilon$. Considering the Figure 5.8, from the FEA results, for an applied displacement of 0.2 mm (axial load of 115 kN), local axial stress at the notch is 600 N/mm^2 and local strain at the notch is 1.60×10^{-2} . From these values stress concentration factor was calculated (appendix – 2) and this gives the value of K_t as 1.6. This is comparable with the value K_t given in [38].

5.3.2 Elastic-Plastic torsion loading

Figure 5.5 shows the torque versus displacement for elastic-plastic condition. From 180 Nm torque the specimen was starting to behave plastically.

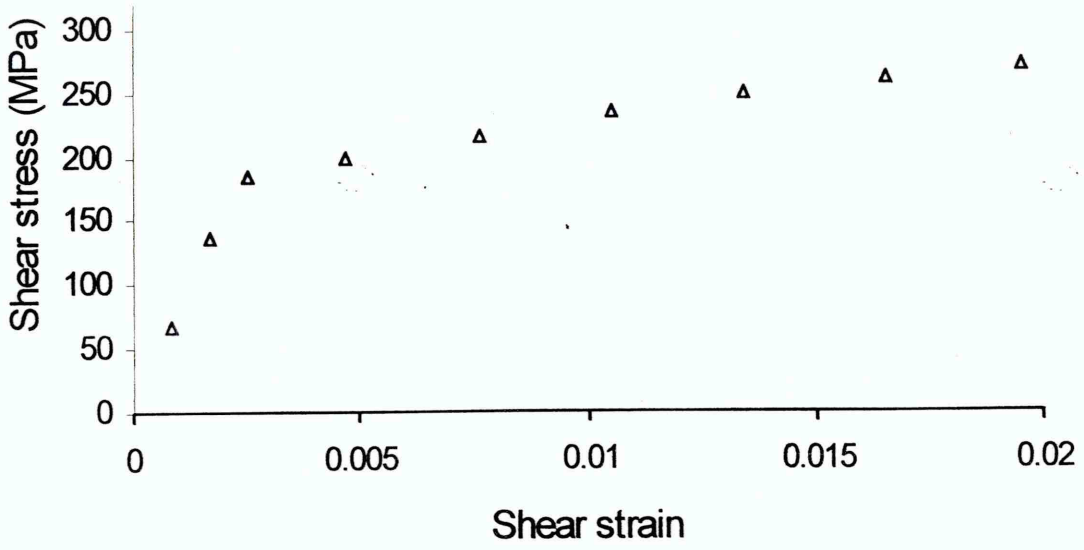

Figure 5.10: FEA results - The shear stress versus shear strain (S23-E23)

As shown in Figure 5.10, the graph is linear up to 180 MPa and then material started to behave plastically. And plastic strain is increasing by increasing applied strain amplitude.

5.4 Modelling cyclic stress-strain hysteresis behaviour

Cyclic stress-strain curves are useful for assessing the durability of structures and components subjected to repeated loading. The response of a material subjected to cyclic inelastic loading is in the form of a hysteresis loop. The area within the loop is the energy per unit volume dissipated during a cycle. It presents a measure of the plastic deformation work done on the material.

5.4.1 Cyclic axial load

For elastic plastic condition cyclic axial load was applied to the specimen model with the load (axial displacement) as shown in Figure 5.11. The details of the loads are given in Table 5.1.

Table 5.1: The details of the applied loads

Test/FEA Ref. No.	Loading path	Axial load (kN)	Torque (Nm)
	Cyclic axial load		
250	Experiment	60	
450	FE Analysis	50	
	Cyclic Torsion load		
260	Experiment		140
460	FE Analysis		140
	In-phase sine wave		
140	Experiment	80	90
240	Experiment	140	140
340	Experiment	70	140
440	FE Analysis	70	140
	Non-proportional Path-A		
200	Experiment	140	170
300	Experiment	70	170
400	FE Analysis	50	100
	Non-proportional Path-B		
110	Experiment	80	90
210	Experiment	140	170
310	Experiment	70	170
410	FE Analysis	50	100
	Non-proportional Path-C		
220	Experiment	140	170
320	Experiment	70	170
420	FE Analysis	50	100
	Non-proportional Path-D		
230	Experiment	140	170
330	Experiment	70	170
430	FE Analysis	50	100

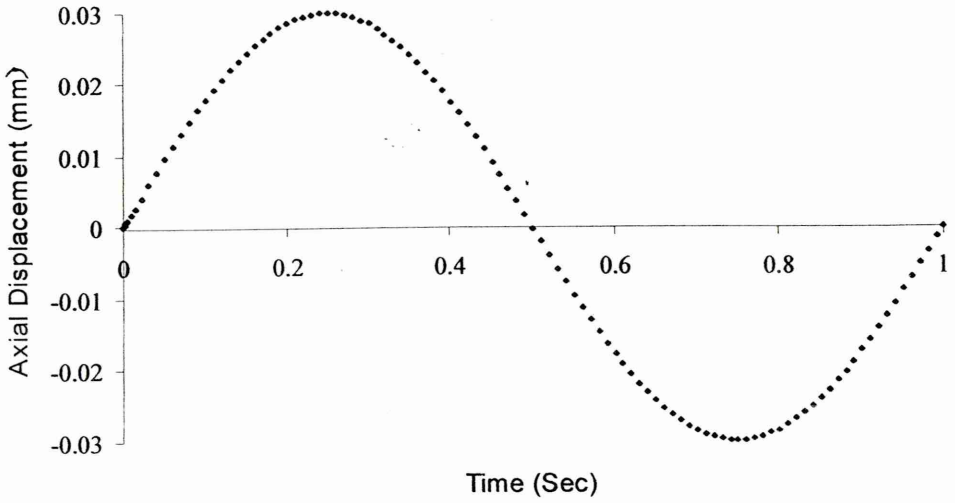

Figure 5.11: FEA results - The applied axial displacement versus time for FEA Ref No. 450 in Table 5.1

The Figure 5.11 shows the applied axial displacement versus time. And FEA analysis confirms that axial load range of 53.3 kN was required to create ± 0.03 mm axial displacement ranges.

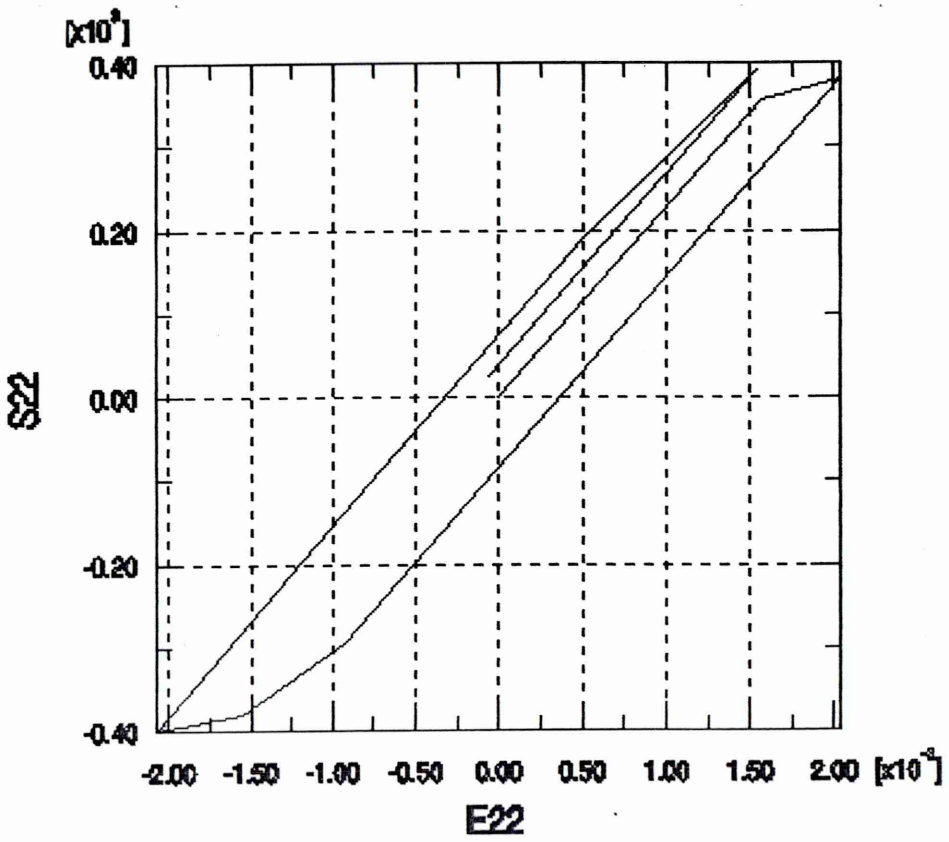

Figure 5.12: FEA results - The axial stress (S22) versus axial strain (E22) at the notch root for FEA Ref No. 450 in Table 5.1

The Figure 5.12 shows the hysteresis loop obtained from cyclic axial loading. The loop has a little plastic energy and the maximum strain range of the loop is 0.002.

Using material cyclic stress-strain curve and Neuber curve, hysteresis loops were predicted for same cyclic axial load and torsion load. The hysteresis loops were developed for the material by using the Ramberg - Osgood equations, and developed the other curves by using Neuber equation (K_t^2 Se = σε).

$$\varepsilon = \frac{\sigma}{E} + \left(\frac{\sigma}{K}\right)^{1/n} \quad \text{for first loading}$$

$$\Delta\varepsilon = \frac{\Delta\sigma}{E} + \left(\frac{\Delta\sigma}{2K}\right)^{1/n} \quad \text{for hysteresis loop}$$

$$\gamma = \frac{\tau}{G} + \left(\frac{\tau}{K}\right)^{1/n} \quad \text{for first loading}$$

$$\Delta\gamma = \frac{\Delta\tau}{G} + \left(\frac{\Delta\tau}{2K}\right)^{1/n} \quad \text{for hysteresis loop}$$

For stress concentration factor K_t, 1.6 value was used and developed several curves by changing nominal stress value (S). Then found the common values from the both graphs to predict the Neuber hysteresis loop shown in Figure 5.13. The strain predicted from Neuber was over estimated 36% as FEA.

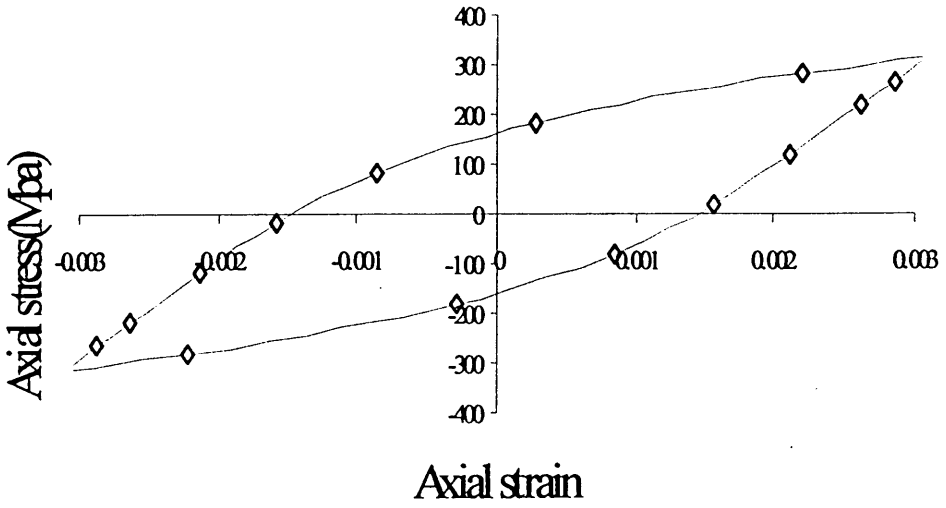

Figure 5.13: Predicted hysteresis loop from Neuber curve for FEA Ref No. 450 in Table 5.1

5.4.2 Cyclic torsion loading

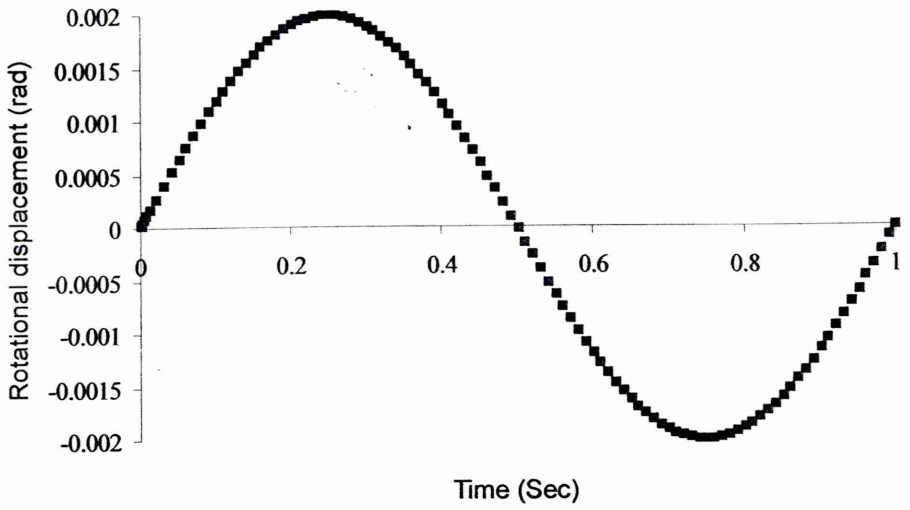

Figure 5.14: FEA results -The amplitude of applied rotational displacement versus time for FEA Ref No. 460 in Table 5.1

For elastic plastic condition cyclic torsional load was applied to the specimen model with the load (rotational displacement) as shown in Figure 5.14. FEA analyses confirm that torsion load range of 70Nm was required to create ±0.002 rad rotational displacement range. Figure 5.15 shows the results for torsional cyclic loading. And the results shown are purely elastic and the maximum shear strain is 0.0012.

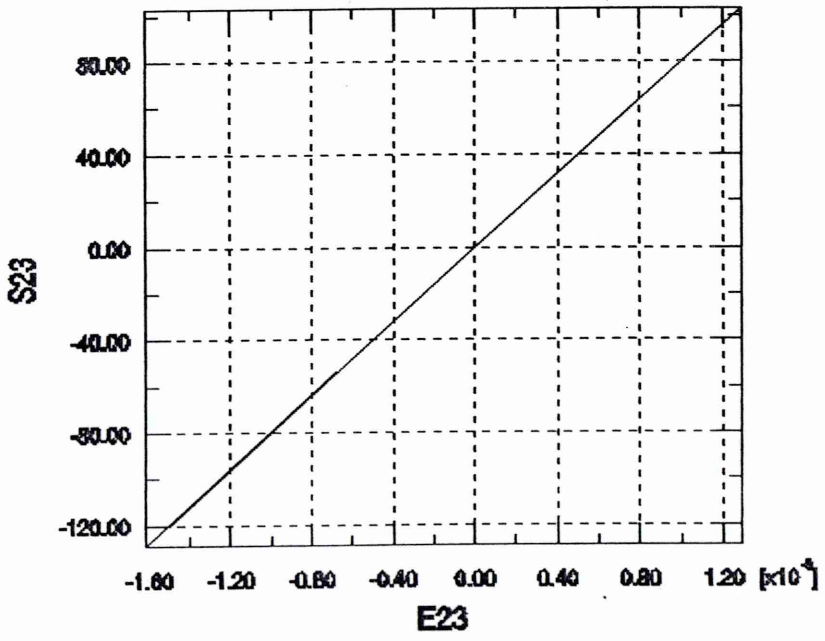

Figure 5.15: FEA results - The stress-strain variation at the notch root for FEA Ref No.460 in Table 5.1

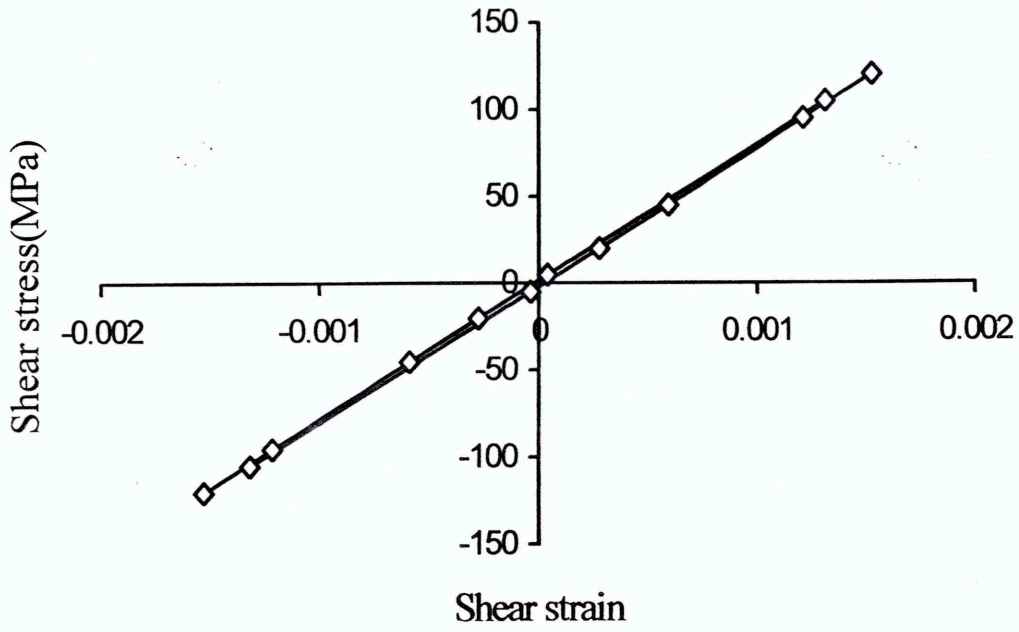

Figure 5.16: Predicted hysteresis curve using Neuber's equation for cyclic torsion load for FEA Ref No.260 in Table 5.1

As the Figure 5.16, using material cyclic shear stress-shear strain curve and Neuber's equation, hysteresis loop was predicted for same cyclic torsion load. The strain predicted from Neuber was over estimated 25% comparing with FEA.

5.5 Axial-Torsion proportional loading

When the two cyclic stress components are in phase and proportional to each other, the loading is called proportional loading. By using ABAQUS Code the specimen was subjected to a 0.06 mm axial displacement and 0.004 rad rotational displacement, which result in 53 kN load amplitude and 70 Nm torque amplitude for in-phase loading, as shown in Figure 5.17.

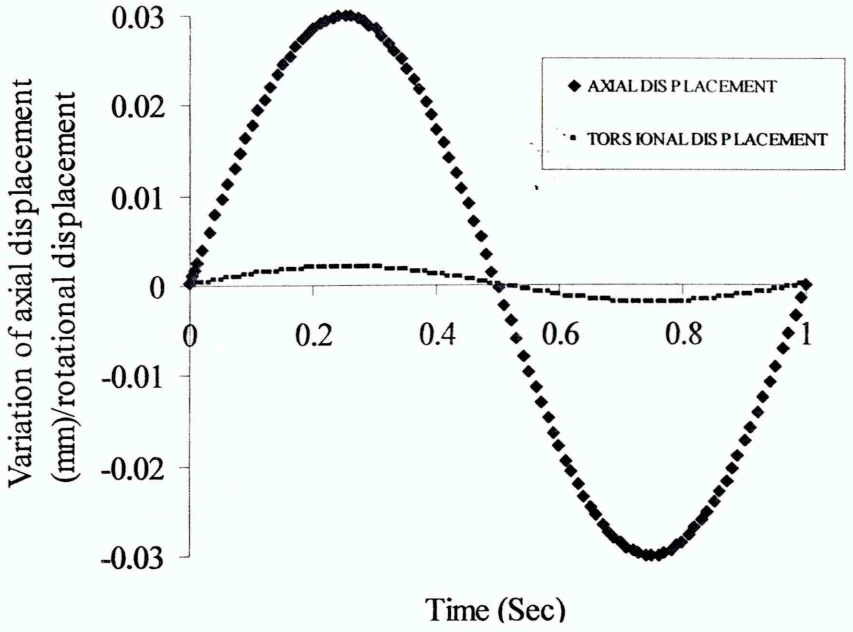

Figure 5.17: FEA results - The variation of the tension and torsion displacements for FEA Ref No.440 in Table 5.1

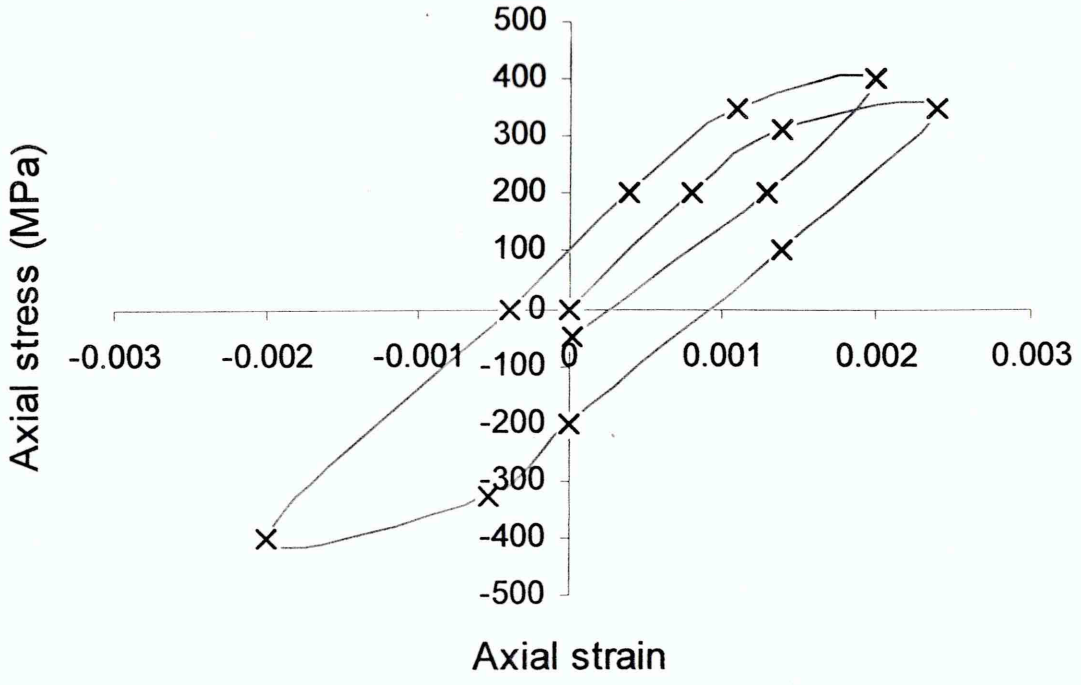

Figure 5.18: FEA results - The graph of axial stress versus axial strain (S22-E22) for FEA Ref No.440 in table 5.1

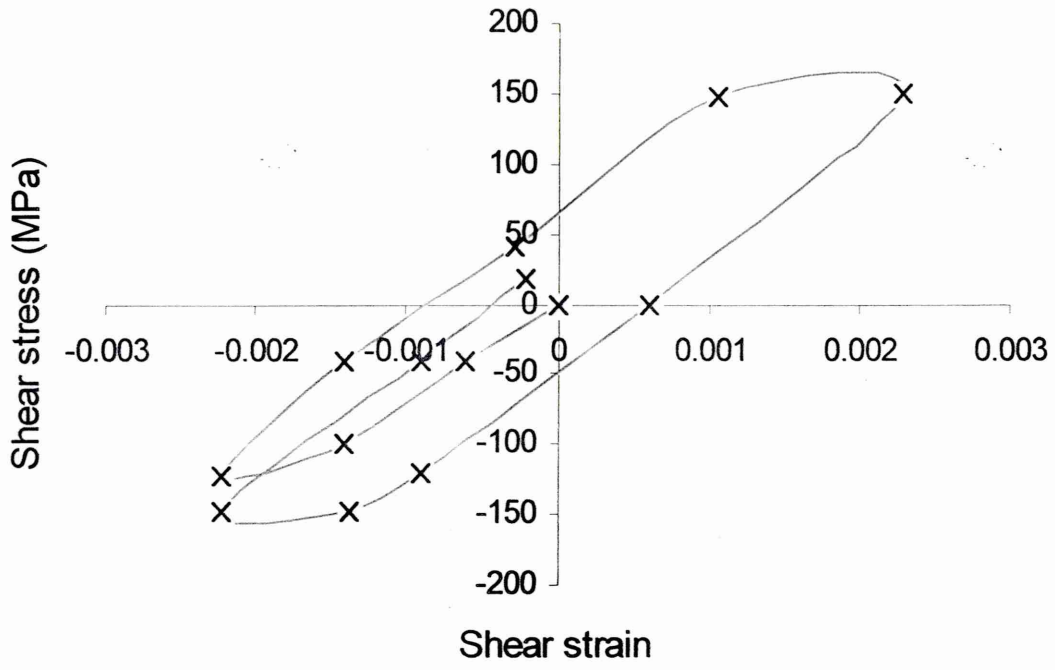

Figure 5.19: FEA results - The graph of shear stress versus shear strain for FEA Ref No.440 in table 5.1

Figure 5.18 and Figure 5.19 show the FEA results for proportional loading FEA Ref No.440, shown in Figure 5.17. Comparing with the loops in the Figures 5.15 and 5.19, shear stress versus shear strain loops shows a little plasticity when applying proportional load. But for the same torsion amplitude, cyclic curve (Figure 5.15) behaves predominately elastic. This means when applying both axial load and torsion, axial load tend to increase the hysteresis energy of the stress-strain curve (S23-E23) in the shear direction.

5.5.1 Axial – Torsion non-proportional loading

When the applied loads cause the directions of the principal stresses and the ratio of the principal stress magnitudes are to change, the loading is termed non-proportional. For the FEA analysis several non-proportional Paths were considered and the results are presented in the following sections.

5.5.1.1 Non-proportional sinusoidal wave Path-A

As shown in the Figure 5.20, the specimen was subjected to a ± 0.025 mm axial displacement (50kN axial load) and or ± 0.0025 rotational displacements, (100Nm torque) with 90^0 phase difference.

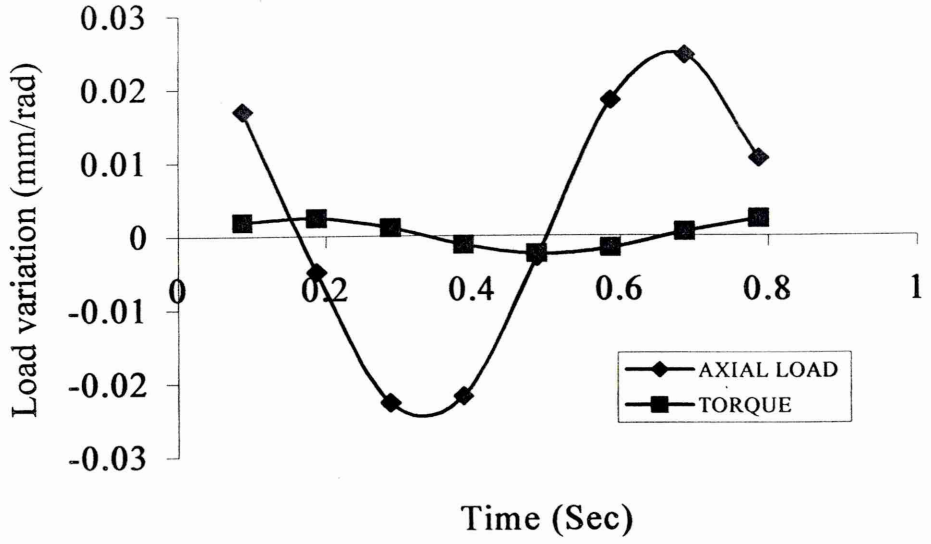

Figure 5.20:FEA results - The axial /torque load variation for out of phase loading Path -A for FEA Ref No.400 in Table 5.1

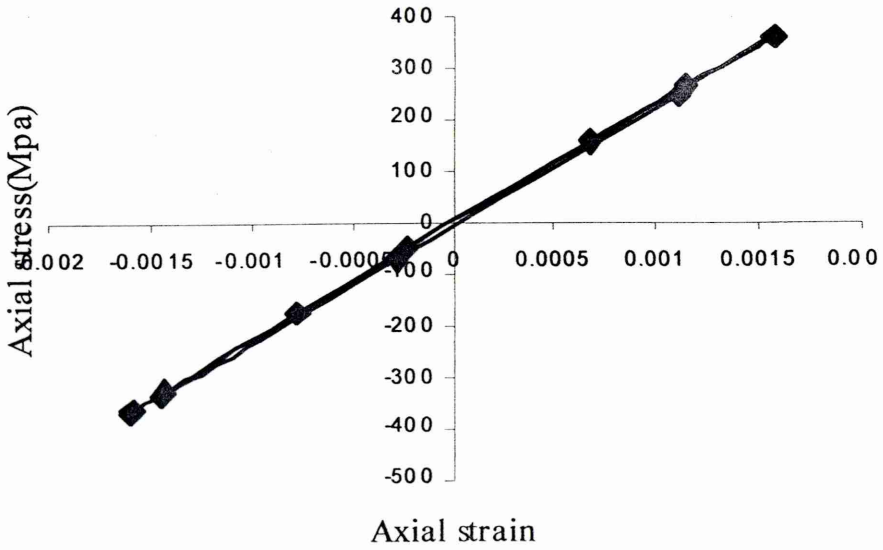

Figure 5.21: FEA results- The axial stress versus axial strain at the notch for FEA Ref No.400 in Table 5.1

As shown in the Figure 5.21, the hysteresis loop shows very little plasticity and the loop is very narrow and long, similar to elastic curve. The gradient of the graph was calculated to be 208000 MPa (Elastic Modulus of the material. $E = \sigma / \epsilon$)

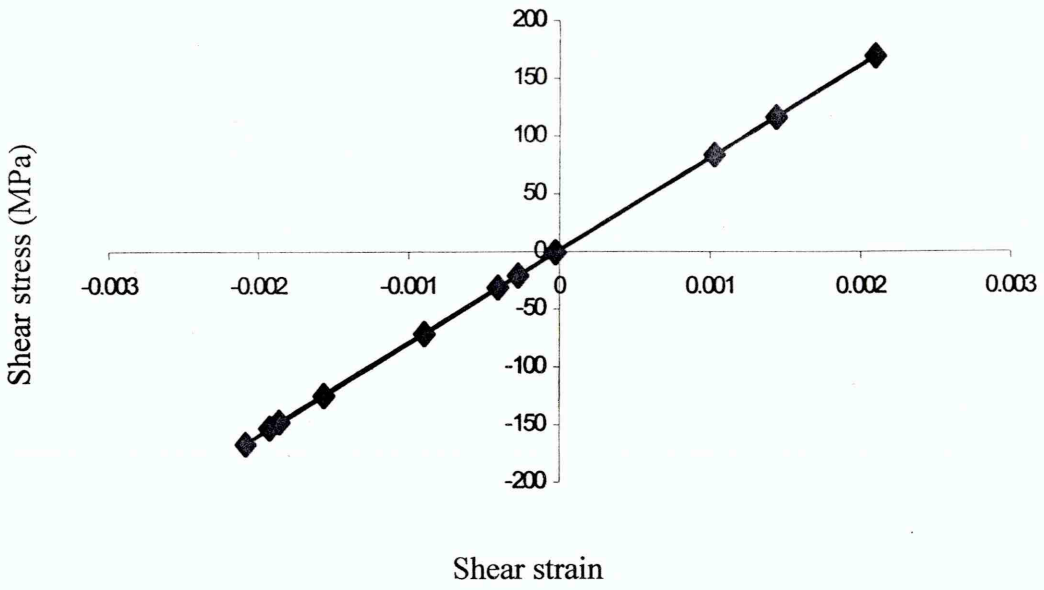

Figure 5.22: FEA results - The shear stress versus shear strain (S23-E23) at notch tip for FEA Ref No.400 in Table 5.1

The Figure 5.22 shows the elastic behavior and the gradient of the graph was calculated to be 80000 MPa. The value is same as the modulus of rigidity of the material.

5.5.1.2 Non-proportional wave Path-B

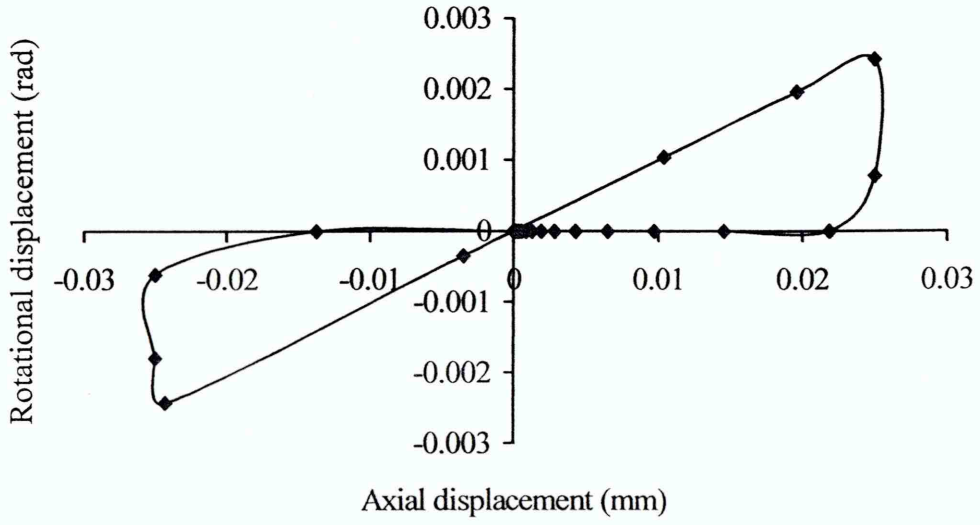

Figure 5.23: FEA results - The rotational displacement versus axial displacement at the notch root for FEA Ref No.410 in Table 5.1

Figure 5.23 shows the applied displacement variations at the notch root for FEA Ref No.410. From the ABAQUS code it was very difficult to take more convergent values for the non-linear analysis. Therefore the shapes of the loops were little different with expected loops as shown in Figure 5.23. Same behaviour will show for the shear strain versus axial strain at the notch root for the non-proportional load Path-B

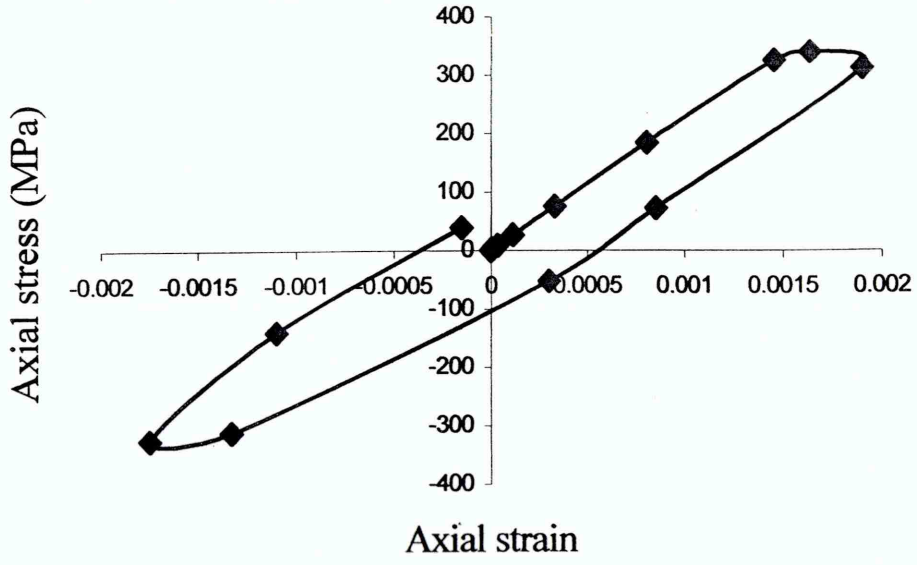

Figure 5.24: FEA results -The axial stress versus strain (S22-E22) at the notch tip for loading Path–B for FEA Ref No.410 in Table 5.1

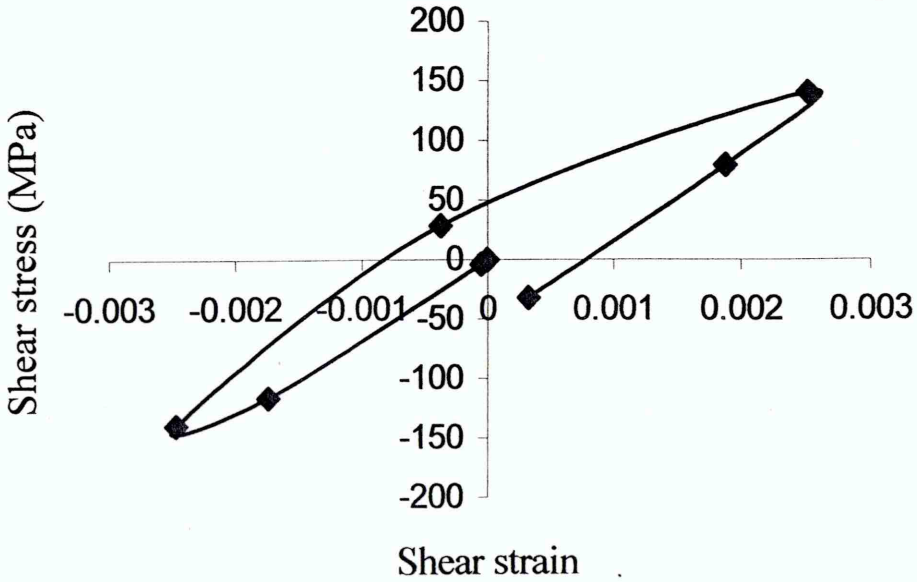

Figure 5.25: FEA results - The shear stress versus shear strain (S23-E23) at the notch tip for loading Path-B for FEA Ref No.410 in Table 5.1

As shown in the Figures 5.24 and 5.25, the both hysteresis loops in Path-B, have more energy than the hysteresis loops in Path-A. But there are no noticable differences between maximum strain values of the Paths-A and B.

5.5.1.3 Non-proportional wave Path-C

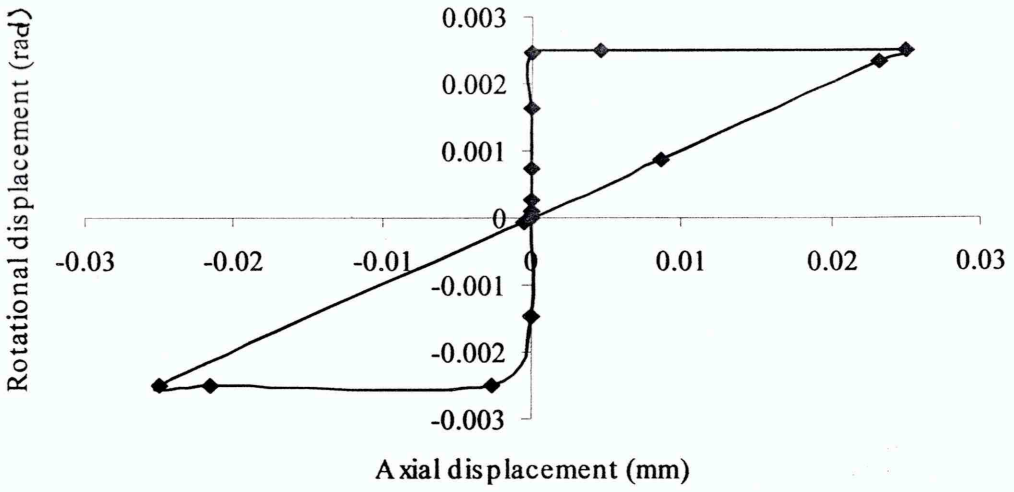

Figure 5.26: FEA inputs for non-proportional loading Path-C

Table 5.1 shows the load set used for non-proportional loading Path-C for FEA Ref No. 420. Figure 5.26 shows the variation of torque versus axial load throughout the wave applied for FEA. The variation expected to be same for shear strain γ versus axial strain ε for the Path-C loading.

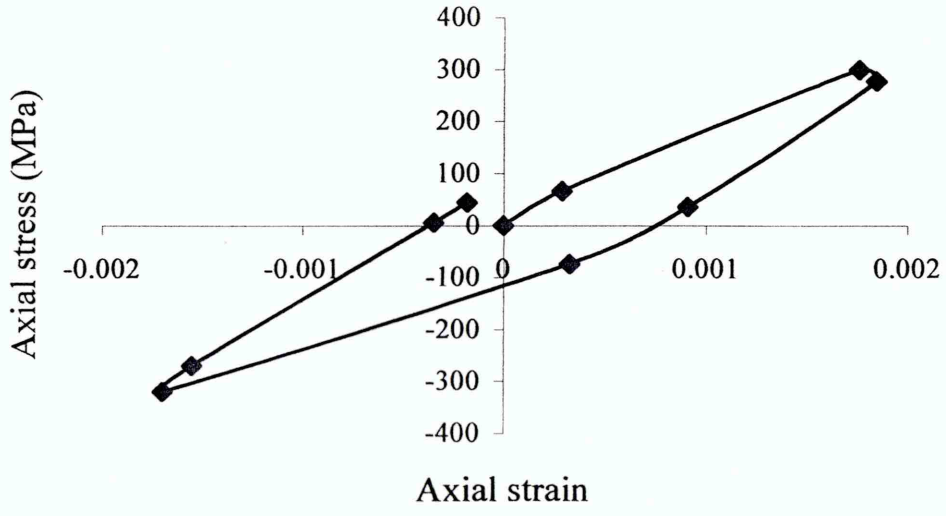

Figure 5.27: FEA results – The axial stress versus axial strain at notch tip for the loading Path-C for FEA Ref No.420 in Table 5.1

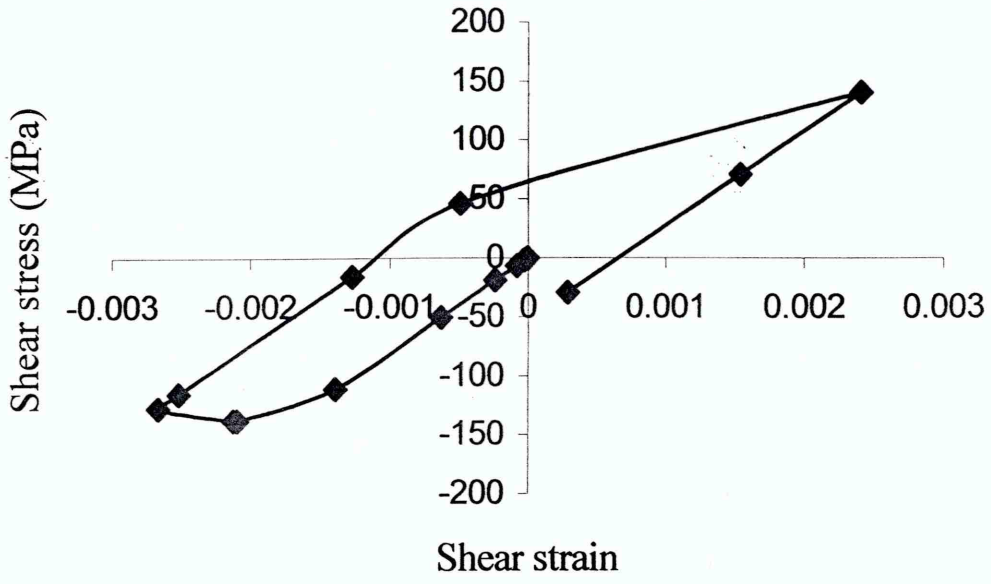

Figure 5.28: FEA results - The shear stress versus Shear strain (S23-E23) at the notch tip for loading Path-C for FEA Ref No.420 in Table 5.1

The Figures 5.27 and 5.28 show the axial stress/strain and shear stress/strain loops for Path-C loading, FEA Ref No. 420. Both loops show plastic energy and comparing the results of Path–B, maximum strain ranges are same for both loops. But the shapes of the hysteresis loops were different.

5.5.1.4 Non-proportional wave Path-D

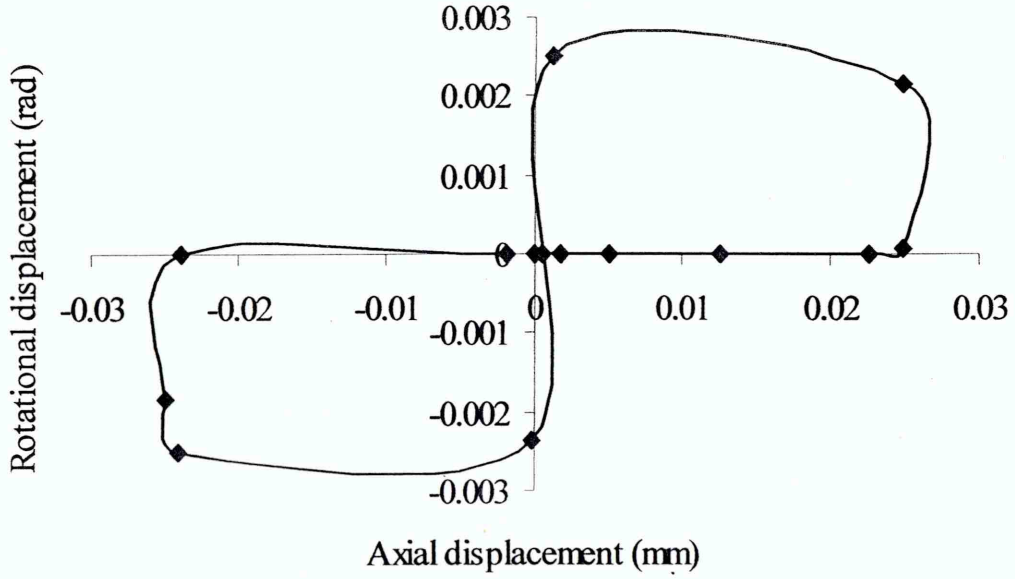

Figure 5.29: FEA inputs for non-proportional loading Path-D for FEA Ref No. 430 in Table 5.1

Table 5.1 shows the load set used for non-proportional load Path-D Test No. 430 and Figure 5.29 shows the variation of rotational displacement versus axial displacement throughout the wave applied for FEA. As the ABAQUS always does not give many convergent values, the shape of the variation was different as Figure 5.29. The variation is expected to be same for shear strain γ versus axial strain ε for Path-D loading.

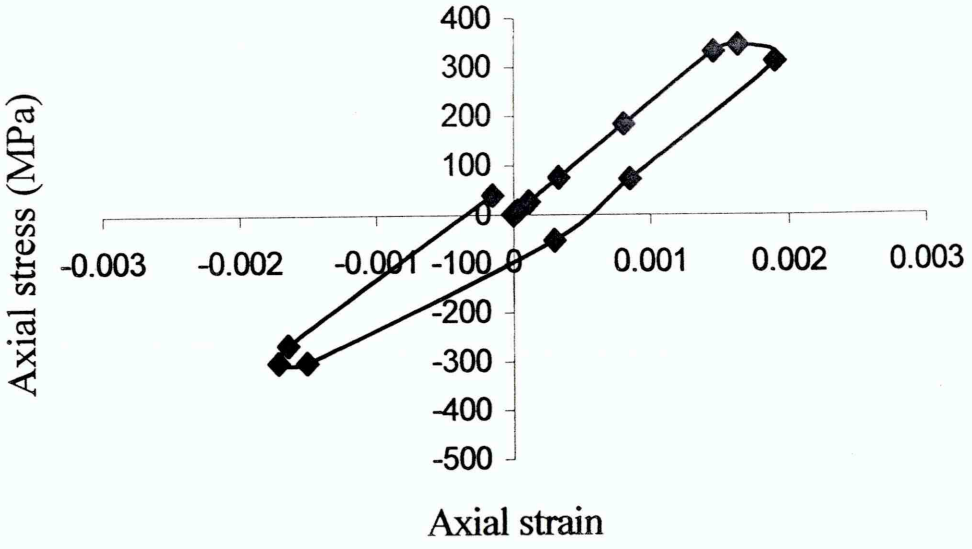

Figure 5.30: FEA results-The axial stress versus axial strain at notch tip for the loading Path – D for FEA Ref No.430 in Table 5.1

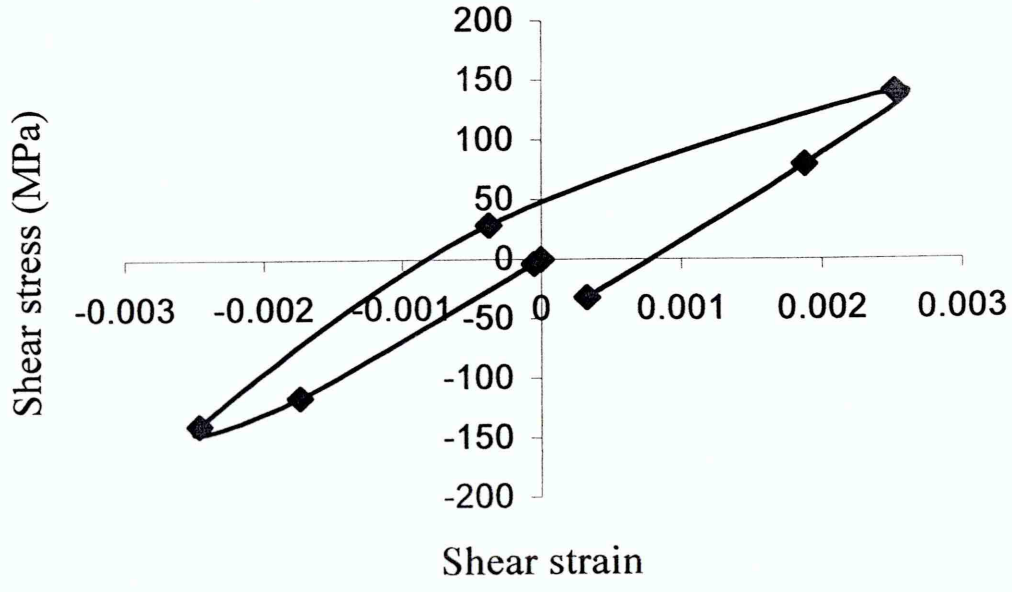

Figure 5.31: FEA results - The shear stress versus shear strain graph for Path-D for FEA Ref No.430 in Table 5.1

Figure 5.30 and Figure 5.31 shows the hysteresis loops were obtained for Path-D non-proportional loading, FEA Ref No.430 in Table 5.1. The both loops show plastic deformation and the shapes of the loops are completely different.

The size of the elements and the type of elastic-plastic theory used can influence the results yielded by the finite element analysis. Another factor that can influence finite element results is the assumptions made in the numerical solution. However the finite element analyses did show that the stresses and strains are higher at the notch root. However, appropriate experiments are essential to check the accuracy of the finite element. The comparison of the experimental results and the finite element results are discussed in Chapter 7.

Chapter 6

Experimental Programme and Results

6.1 Introduction

In order to understand the cyclic deformation of the carbon steel, fatigue test had been carried out under tension and torsion combined loading. The material used was conventional industrial medium carbon steel, EN 8 (SAE Grade 1035) whose yield stress is 320 MPa and ultimate strength is 730 MPa. Tests were carried out using solid notched specimens. The experimental programme involved uniaxial, torsion, proportional loading and various combinations of non-proportional loadings. Experiments were performed at room temperature under displacement control for both torsion and tension loadings.

The tests were carried out using a biaxial servo-hydraulic machine ESH, with an electronic control system. A special mechanical system adapted to the machine in order to accomplish easier mounting of the test specimen and also to apply the required torsion and push pull loading. The test were carried out on solid specimens and were mechanically polished to obtain a smooth surface without defects and especially notch area was finished with emery paper through grade No. 1200.

The required strains amplitudes were measured by using strain gauges attached to the specimen. The specimen was fitted with a three-gauge strain gauge rosette, at the notch root. They were connected to the amplifiers to read the strains in three directions. The signals were recorded, by digitising and storing on to a computer data file as voltage. Recordings were obtained for uniaxial, torsion, proportional and non-proportional loadings.

6.2 Material

The material used in this research work was medium carbon steel with equivalent BS specification is BS 970 080A42. Material received in cold finish bright bar manufactured to BS EN ISO 9002:1994. This is general-purpose steel, which when heat-treated demonstrates good ductility and resistance to fatigue. The material is widely used in the automotive industry for gears, connecting rods, axles and crankshafts. The mechanical properties and the chemical composition of the material is given in, Tables 6.1 and 6.2. The monotonic and cyclic stress strain curves of the material are given in Figure 6.1. The S-N curve for the material is given in Figures 6.2

and 6.3. The stress amplitudes of the fatigue tests were so chosen that the fatigue life is within 10^4 and 10^6 cycles.

Table 6.1: Mechanical Properties of the medium carbon steel

E –Yong's Modulus	2.08E5 MPa
G-Modulus of Rigidity	80000 MPa
υ - Poisson's Ratio	0.3
σ_y _ Yield or 0.2% Proof strength	320 MPa
σ_u – Ultimate tensile strength	730 MPa

Table 6.2: Nominal chemical composition (%) of the medium carbon steel

Mn	C	Si	S	P
0.780	0.421	0.219	0.008	0.011

It is customary to use monotonic stress-strain curves to obtain design parameters and limiting stresses on engineering structures and components subjected to static loading. Similarly, cyclic stress-strain curve is useful for assessing the durability of structures and components subjected to repeat loading [5].

The equation for hysteresis loop is,

$$\Delta\varepsilon = \frac{\Delta\sigma}{E} + 2\left[\frac{\Delta\sigma}{2K}\right]^{1/n}$$

For the material, n = 0.19 and K for uniaxial and torsion loadings are 1148 MPa and 529 MPa, respectively. The hysteresis curve for the carbon steel used is

For uniaxial $\Delta\varepsilon = \frac{\Delta\sigma}{E} + \left[\frac{\Delta\sigma}{2013}\right]^{1/0.19}$, and torsion $\Delta\gamma = \frac{\Delta\tau}{G} + \left[\frac{\Delta\tau}{1185}\right]^{1/0.19}$

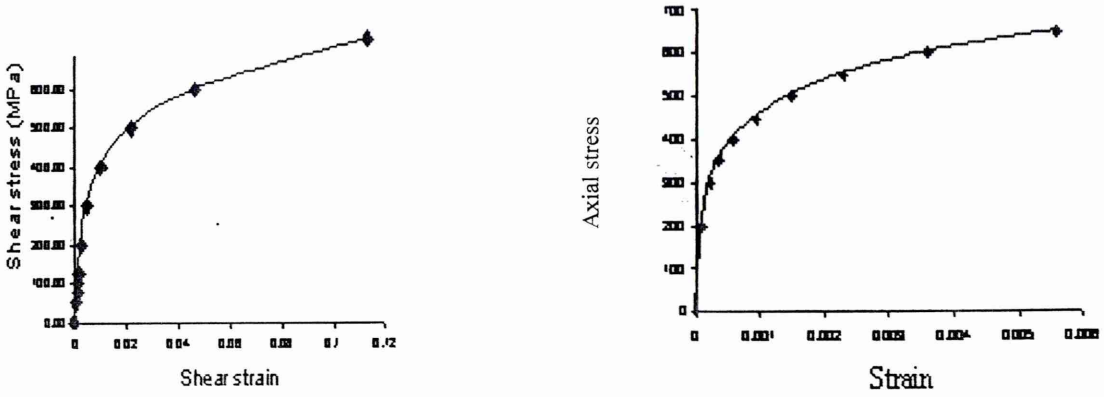

Figure 6.1: Cyclic stress- strain curves for the material EN-8

For the material, the uniaxial fatigue properties are

Fatigue strength coefficient = 453 MPa

Fatigue strength exponent (b) = -0.11

Fatigue ductility exponent (c) = -0.47

Fatigue ductility coefficient = 0.33

For the material torsion fatigue properties are

Fatigue strength coefficient = 906 MPa

Fatigue strength exponent (b) = -0.11

Fatigue ductility exponent (c) = -0.47

Fatigue ductility coefficient = 0.495

By using these data strain-life curve for axial loading and shear strain life curve for torsion loading were obtained for the material EN 8 as in Figure 6.2 and 6.3

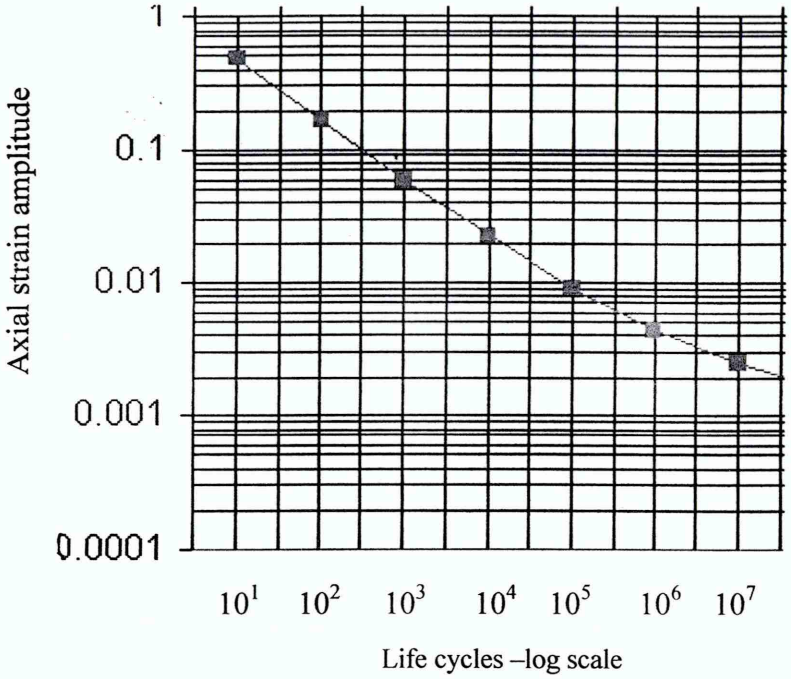

Figure 6.2: The strain life curve for material EN 8

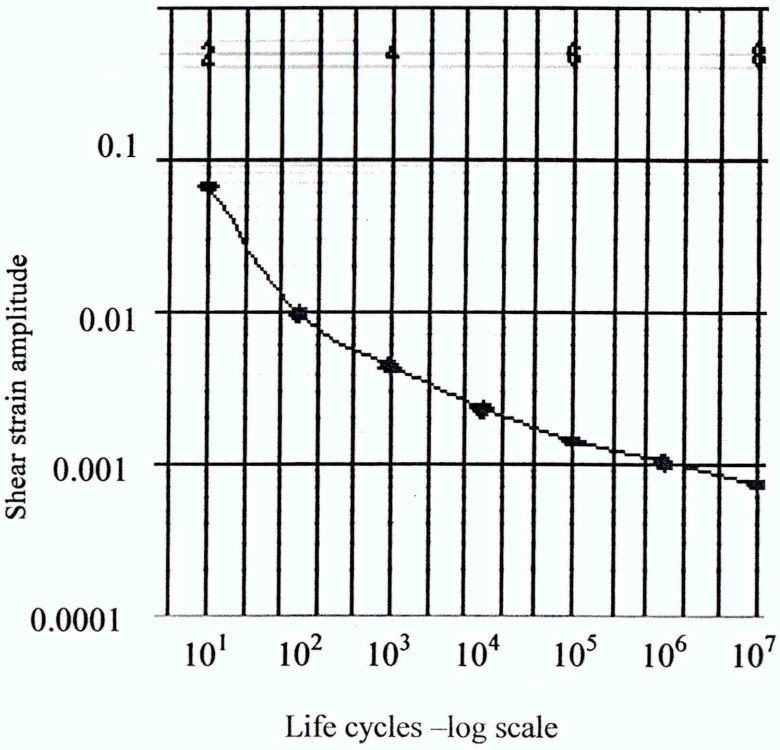

Figure 6.3: The shear strain against life cycle curve for material EN 8

6.3 Specimen configuration

To obtain the maximum area of plasticity at the notch root, the diameter at the notch should be large. According to the machine specification, maximum allowable notch diameter, length of the specimen and the other dimensions were calculated for the specimen.

The tests were carried out on solid specimens, which have an outer diameter of 35mm, notch diameter of 15mm and notch root diameter of 10mm. Surfaces were mechanically polished to obtain a smooth surface without defects and especially notch area was finished with emery paper through grades of 320, 400, 600, 800 and 1200.

The geometry of test specimen is presented in Figure 6.4 (a).

(a)

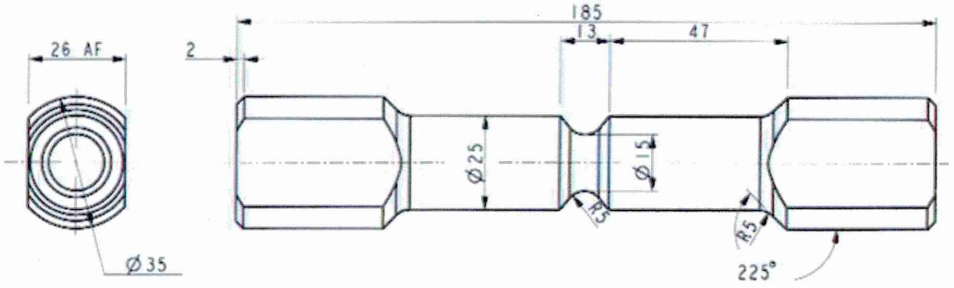

Figure 6.4:(a) Model of the specimen and (b) The dimensions of the specimen (mm)

6.4 Strain measurements

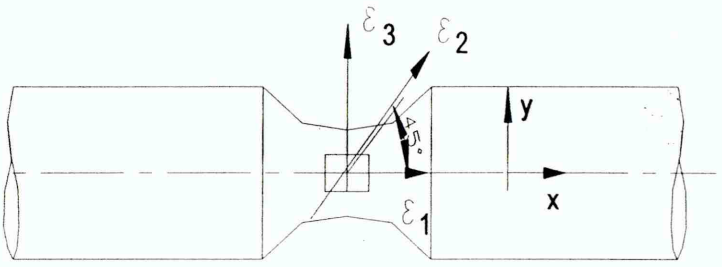

Figure 6.5: The strain gauge position and direction

Considering the Figure 6.5, for axial loading (only), $\varepsilon_1 = \varepsilon_x$, $\varepsilon_3 = -\nu\varepsilon_x$ and

$\varepsilon_2 = \varepsilon_x (1-\nu)/2$

For torsion loading (only), $\varepsilon_1 = \varepsilon_3 = 0$ and $\varepsilon_2 = \gamma_{xy}/2$

For combined tension and torsion loading, $\varepsilon_1 = \varepsilon_x$, $\varepsilon_3 = \varepsilon_y$ and

$\gamma_{xy} = 2\varepsilon_2 - \varepsilon_1 - \varepsilon_3$

For the current research, rosette strain gauges were used to measure strain at the notch root. Gauges were arranged as in Figure 6.5. The strain was determined in three different directions for tension and torsion combine loading. Zero (0^o) angle was used to measure strain in ε_1 direction, 90^o angle was used to measure strain in ε_3 direction and 45^o angle was used to measure strain in ε_2 direction as indicated in Figure 6.5. The details of the strain gauge used are;

Strain Gauge Type: Rectangular rosette Size: 1mm, Gauge Factor: 2.071

The tension and torsion-combined loads were applied to the specimen and strain histories were recorded by a special computer connecting to the machine. Three amplifiers were used as shown in Figure 6.6. These amplifiers were used to condition the strains in three different directions. These readings were recorded by voltage. To convert the voltage reading to strain reading, strain calibrations were conducted using the same amplifiers.

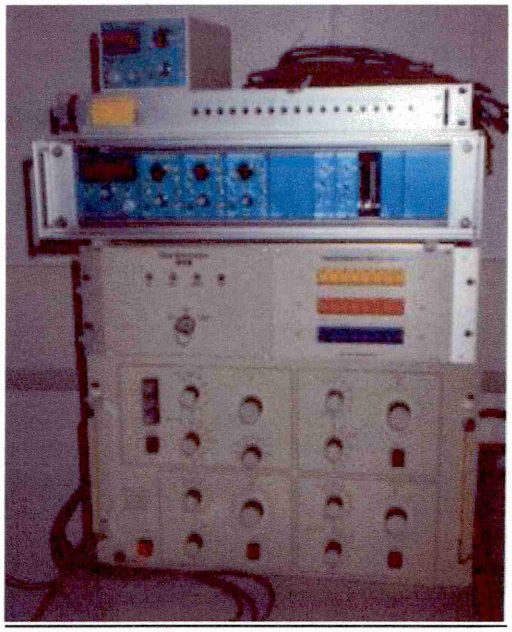

Figure 6.6: Amplifiers for 3 strain readings and torque

6.5 Multiaxial loading machine

The test had been carried out using a biaxial closed-loop ESH servo-hydraulic test machine that comprises of four actuators, two positioned in the vertical axis and two in the horizontal axis with an electronic control system. The movement of all the actuators are purely axial centred on the x and y planes. Pictorial views of the machine are shown in Figure 6.7 and 6.8.

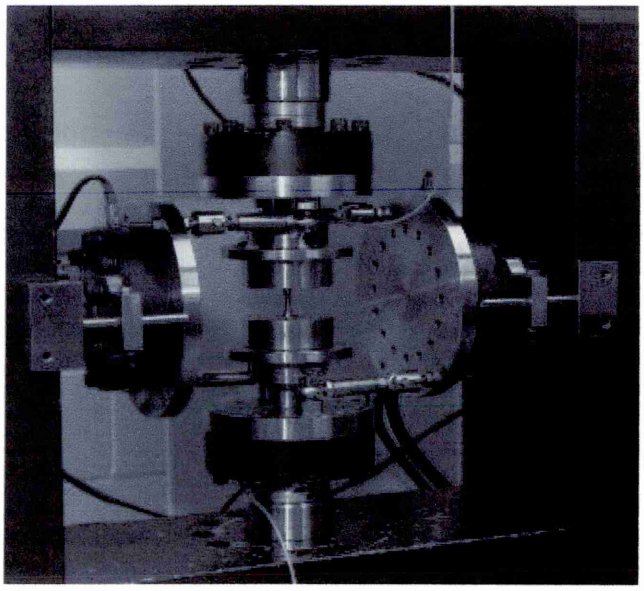

Figure 6.7: Specimen housing for torsion and axial cyclic loading

This specimen housing consisted of four plates. Two of them were connected to the upper and lower load cells to apply push-pull loads; and other two worked as torque

plates in right and left hands of the specimen. Torque for the specimen was given by the torque pins connected to the torque plates.

The specimen was connected to the loading rings by using clutches, and load rings were connected to the upper and lower plates. The actuators are controlled by the electronic control panel. The complete test procedure can be divided into 4 main parts which are loading system, control system, torque and strain measuring system and wave generating system.

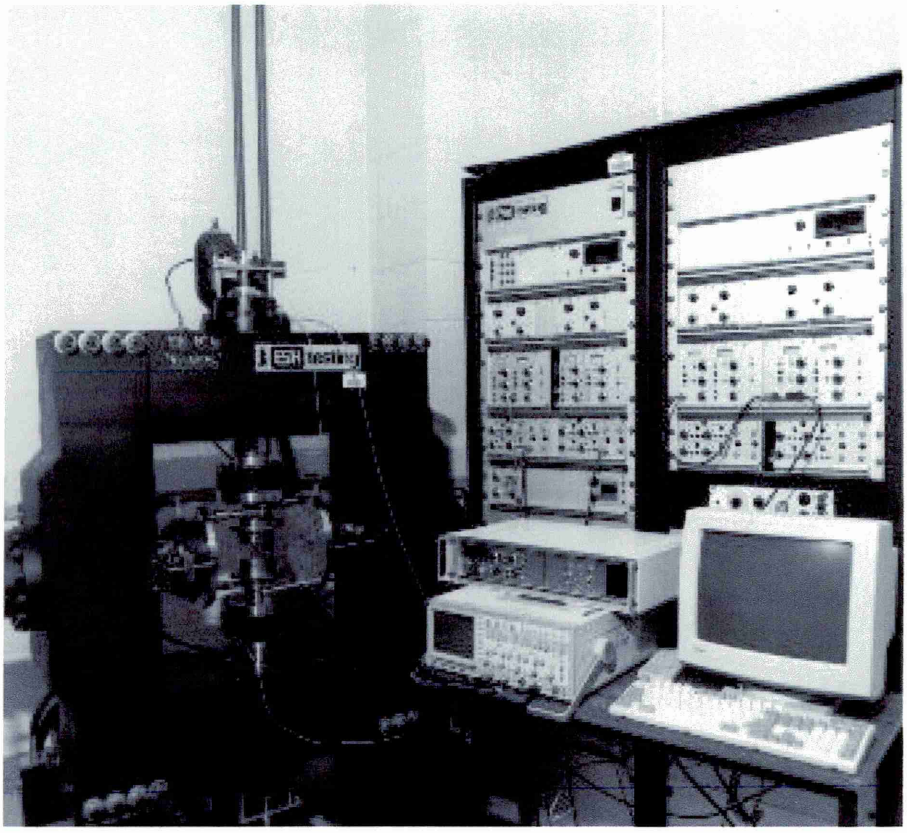

Figure 6.8: The pictorial view of the fatigue equipment

6.6 Calibration of the Strain Results

6.6.1 Calibration of strain gauge at the notch root

A computer connected to the machine was used to generate the waveforms and record the strain readings. All the strain readings were recorded in voltage. Therefore to convert these voltages to strain values calibration was done to the amplifiers. Initially the strain gauge was fixed to the notch root and initial strain reading was taken by using a strain meter box. Then the three gauges were attached to the three amplifiers and the

readings were taken for corresponding strains. Typical results for the specimen no.01 are given in Table 6.3, and the relevant graph is shown in Figure 6.9.

Amplifier settings: 10mV input range, Gain: 840, Supply voltage: 6V

Table 6.3: The strain calibration results

Gauge angles	0°	45°	90°
Strain meter reading (μE)	+1081	-1644	+259
Amplifier reading (V)	1.05	-9.03	-1.73

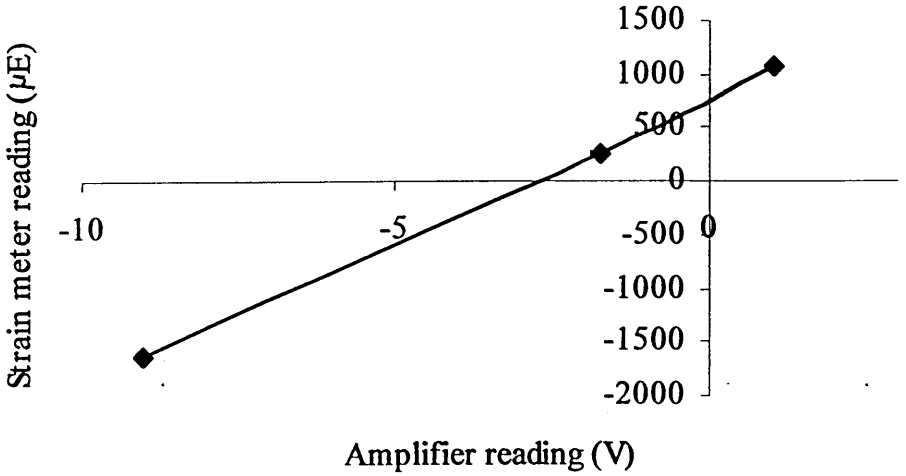

Figure 6.9: The graph for calibration readings

Considering the gradient of the graph, 1V = 272.5 μE

6.6.2 Calibration of torque load cell

For the specimen, torque was applied by using a displacement control mode and it was appeared as a voltage through a fourth strain amplifier. Therefore to convert the voltage reading to torque; Nm, calibration was performed and the results are shown in Table 6.4 and the Figure 6.10.

Amplifier settings: 10mV input range, Gain 2.00

Table 6.4: The results for calibrating applied torque

Torque (Nm)	Strain Meter Readings (μE)	Amplifier Readings (V)
5	0052	0.58
6	0062	0.70
7	0072	0.80
8	0083	0.89
9	0093	1.01
10	0103	1.10
11	0113	1.24
12	0123	1.40
13	0133	1.48
14	0143	1.59
15	0154	1.74
16	0168	1.86
17	0175	1.98
18	0184	2.04

Torque (Nm)	Strain Meter Readings (μE)	Amplifier Readings (V)
19	0194	2.20
20	0205	2.29
21	0215	2.43
22	0226	2.51
23	0236	2.63
24	0248	2.81
25	0256	2.90
26	0266	3.00
27	0277	3.10
28	0287	3.20
29	0298	3.36
30	0309	3.47
31	0320	3.55
32	0330	3.69

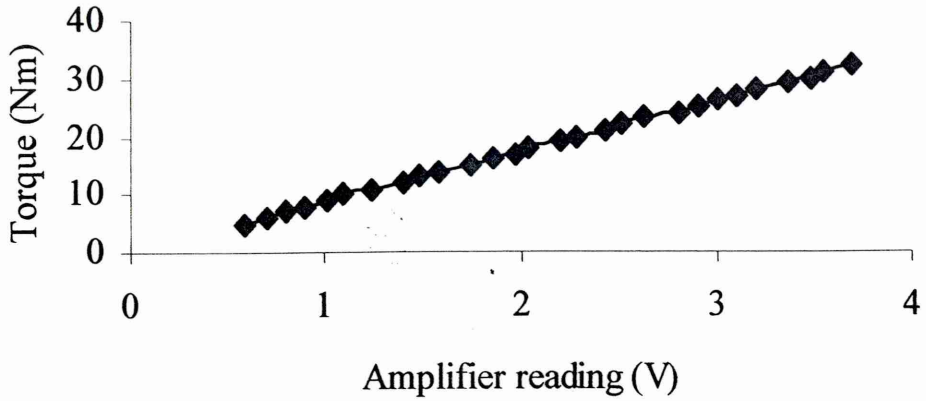

Figure 6.10: The graph of torque (Nm) verses amplifier reading (V)

Using Figure 6.10, the following torque calibration was obtained.

1V Amplifier reading = 9 Nm

6.7 Experimental procedure

Generally the specimen was fixed to the ESH machine and it was subjected to a tension-torsion load under different loading Paths. Three strains were measured by using three amplifiers. The attached computer was set-up to obtain the required load waves and torque waves for the machine. And the machine was under load control mode and load range was fixed to 100 kN. The results of the tests are discussed in chapter 7.

Chapter 7

Results and Discussion

7.1Comparison of the results of FEA and experiments

7.1.1 Introduction

The results predicted by Finite Element Analyses were compared with experimental results. As previously described, the cyclic deformation behaviour (hysteresis loops) of EN 8 steel was recorded from experiments, for axial load, torsion and combined loading cases. During tests, the amplitudes of axial load and torsion were increased gradually in steps and for each combination of axial load amplitude and torsion load amplitude hysteresis loops were recorded. Similar tests were performed for uniaxial and pure torsion, combined in-phase load, 90° out of phase load and three different multiaxial loading paths. For each loading case, the hysteresis loops predicted by FEA are compared with the experimental results for two different amplitudes of loading.

7.2 Axial load (within elastic range)

Initially, the experimental results for uniaxial loading were compared with the FEA results. For the experiment, the specimen was fixed to the ESH machine and subjected to tension and compression loads. The load range was selected to be within elastic region. Three strain readings were measured by using amplifiers. Channel 1 was used to measure strains in 0^0 direction and Channel 2 and 3 were used to measure strains in 45^0 and 90^0 directions respectively. The results are given in Table 7.1.

Table 7.1: Strain values for different loads

Load (kN)	Channel 1 Strain 0° (V)	Channel 2 Strain 45° (V)	Channel 3 Strain 90° (V)
0	0	0	0
5	0.75	0.24	-0.05
10	1.46	0.46	-0.10
15	2.19	0.70	-0.15
20	2.93	0.92	-0.20
25	3.67	1.15	-0.25
0	0	0	0
-5	-0.76	-0.21	0.05
-10	-1.47	-0.44	0.09
-15	-2.21	-0.68	0.14
-20	-2.95	-0.91	0.20
-25	-3.69	-1.14	0.25

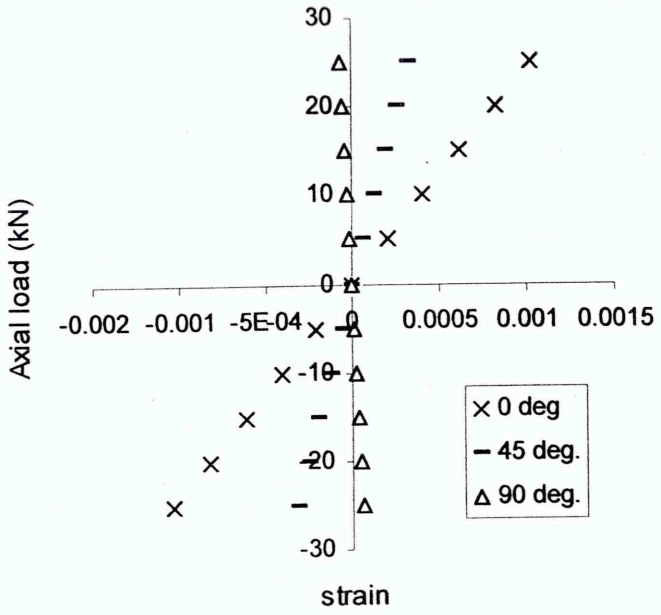

Figure 7.1: Strain values in each direction for different loads

Figure 7.1 shows the variation of strain for each direction for different axial loads given in the Table 7.1. The strain in 45^0 direction was less than that of strain in 90^0 but it increased with the increasing axial load. The strain value in 90^0 direction (E33) was nearly zero as there was no strain while applying axial load.

Considering Finite Element results (Figure 5.1 and Figure 5.2) from ABAQUS, when a 0.1mm displacement is applied to the specimen,

Load range $= 88.0$ kN

Strain in axial direction (E22) $= 4.08 \times 10^{-03}$

Therefore axial displacement for 5kN load $= \frac{0.1 \times 5}{88} = 5.68 \times 10^{-03}$ mm

The strain for 5.68×10^{-03} mm displacement $= \frac{4.08 \times 10^{-3} \times 5.68 \times 10^{-3}}{0.1} = 2.2 \times 10^{-04}$

Experimental, value as given in Table 7.1, for 5 kN load, strain in 0° direction is 0.75V. Since 1V=272.5 μE (calibration) strain in 0^0 direction is 2.1×10^{-04}. This shows that the experimental result compatible with FEA results. For the same load, strain measured in E33 direction is 3.23×10^{-04} and the FEA predicted strain is 0.14×10^{-04}. The results suggest that FEA predictions are comparable to experimental results.

Table 7.2: The results of FEA and Experiment within elastic region

Types of analysis	Strain - 0° direction	Difference % with experiment value	Strain - 90° direction	Difference % with experiment value
FEA	2.2×10^{-03}	4.7	0.18×10^{-04}	28
Experimental	2.1×10^{-03}	-	0.14×10^{-04}	-

7.3 Torsion (within elastic range)

During these experiments, the specimen was fixed to the ESH machine and subjected to a torsion load within elastic condition. The machine was given an input voltage from an external supply to produce the torque required. The torsion load was calculated from the calibrated amplifier. The results are shown in Table 7.3 and relevant graph is shown in Figure 7.2.

Table 7.3: Strain values for cyclic torque

Torque (Nm)	Channel 1 Angle 0° (V)	Channel 2 Angle 45° (V)	Channel 3 Angle 90° (V)
0	0	0	0
4.5	-0.05	-0.18	0.01
9.09	-0.08	-0.37	0.03
13.5	-0.12	-0.55	0.05
0	0	0	0
-4.5	0.04	0.18	-0.01
-9.09	0.07	0.36	-0.04
-13.5	0.11	0.55	-0.07

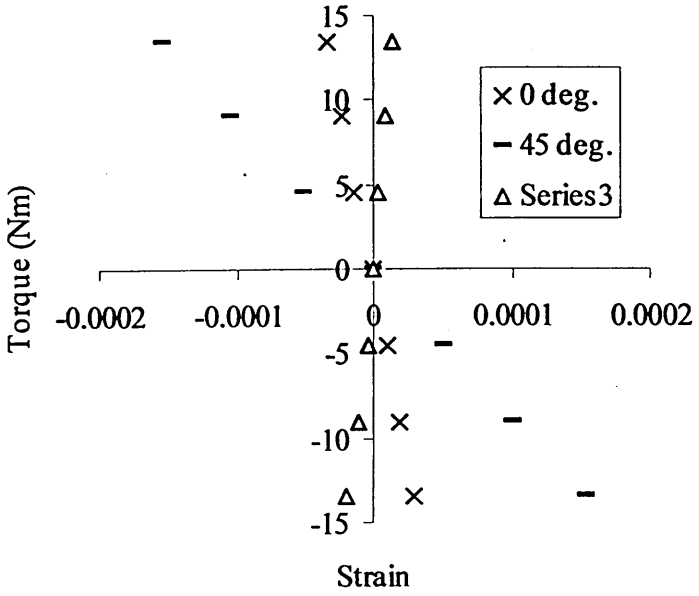

Figure 7.2: Strain values for each direction for torque

Figure 7.2 shows that while increasing the torsion load, the shear strain (E23) also increased. The strain value of E22 was less than E23. The strain value in 90^0 direction (E33) was nearly zero as there was no strain for that direction while applying a torque.

Considering FEA results from ABAQUS (Figure 5.5 and Figure 5.7), when a 0.01rad displacement is applied to the specimen, the relevant torque is 0.20914 kNm

The corresponding strain in γ_{23} direction $= 5.14 \times 10^{-03}$

Therefore displacement relevant to 13.5Nm torque $= \frac{0.01 \times 13.5}{0.20914}$ rad

The strain for 0.645×10^{-03} rad displacement $= \frac{5.14 \times 10^{-3} \times 0.645 \times 10^{-3}}{0.01} = 3.31 \times 10^{-04}$

But when applying torsion, $\gamma_{23} / 2 = \gamma_{45}$, where γ_{45} is strain in 45° direction. Experimental, value as given in Table 7.3, for 13.5 kNm torque, strain in 45° direction is -0.55V. Since 1V=272.5 μE (calibration) strain in 45^0 direction is 1.55×10^{-04}.

Table 7.4: The results of FEA and Experiment with elastic region

Types of analysis	Strain - 45° direction	Difference % with experiment value
FEA	1.65×10^{-04}	6
Experimental	1.55×10^{-04}	-

Tables 7.2 and 7.4 show the error percentages in FEA respect to the experimental results, for axial and torsion loadings. The differences are small and the FEA results are compatible with the experimental results.

7.4 Cyclic axial loading tests

Cyclic loads are more harmful than the static loads and they affect the fatigue life of the material. So the cyclic axial load and the cyclic torsion were applied to the notched specimen to study the behaviour on the hysteresis loops. Previously explained experimental procedure was carried out for the test and from the computer, connected to the ESH machine, the required sinusoidal waves were produced and the results are shown in Figure 7.3 and Figure 7.4.

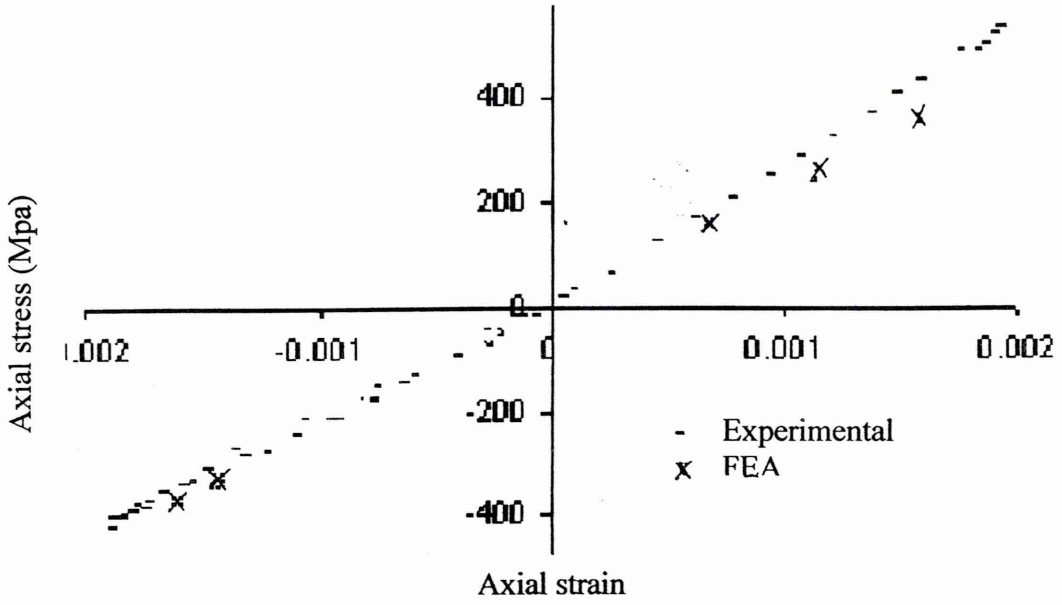

Figure 7.3: The comparison of experimental and FEA results for Test No. 250 and FEA Ref No. 450 in Table 5.1

Figure 7.3 shows the comparison of experimental and FEA results for Test No. 250 and FEA Ref No. 450 in Table 5.1. Both experimental and finite element results are shown a slight plasticity.

7.5 Cyclic torsion loading tests

The results for cyclic torsion (Test No. 260 and FEA Ref No. 460) are shown in Figure 7.4

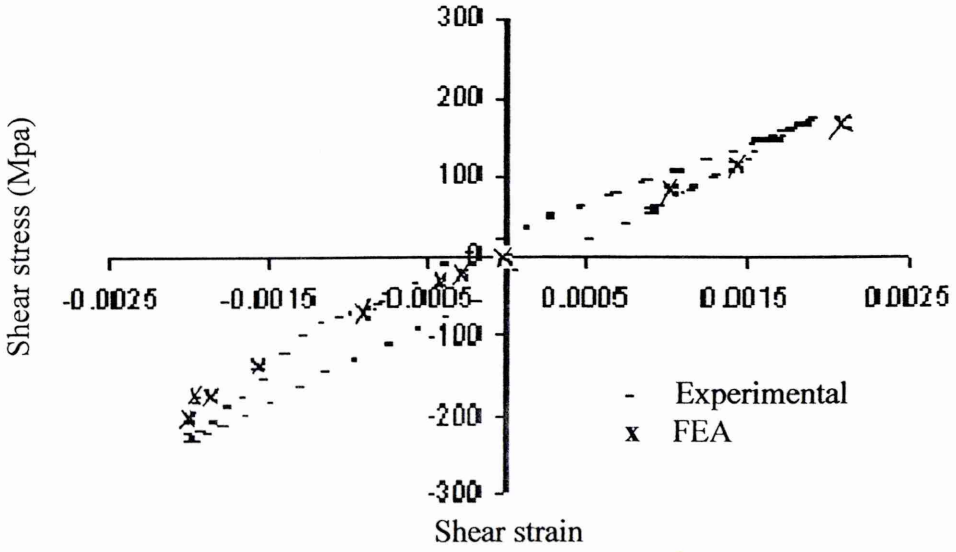

Figure 7.4: Comparison of shear stress versus shear strain for the cyclic torsion loading for Test No.260 and FEA Ref No.460

Considering the experimental and FEA results for torsion loading, hysteresis loop for experiments shows slight plasticity than that for FEA. But the FEA predicted elastic region was similar to the experimental results. The increase in strain amplitudes results in larger and longer hysteresis loops. This means that the plastic strain amplitude has increased. Therefore the estimated fatigue lifetime is expected to decrease as the applied strain amplitudes increase since the plastic strain energy developed in the material affects the fatigue behaviour.

7.6 Selected multiaxial paths

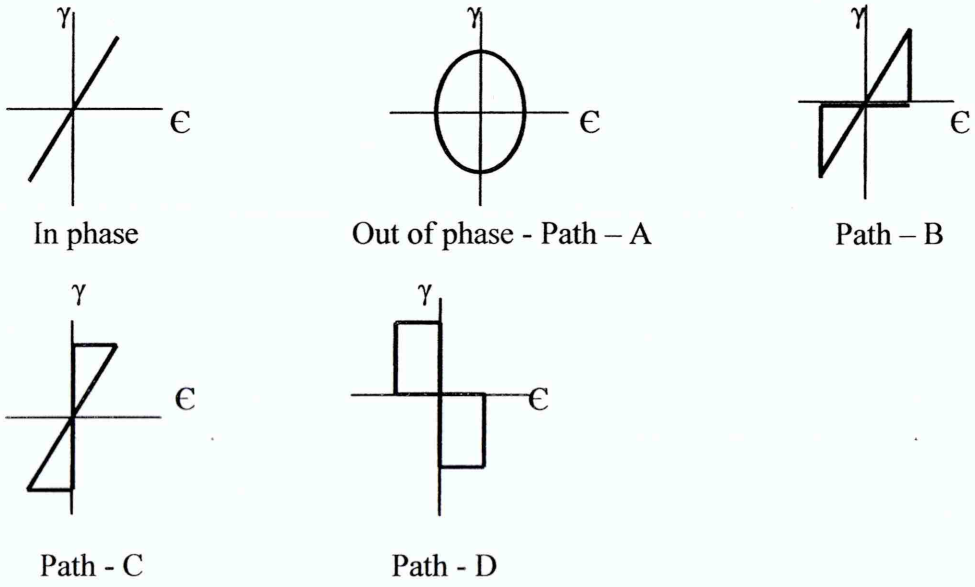

Figure 7.5: Experimental strain paths

Figure 7.5 shows the strain paths selected in the experiments. The axial load and torque wave paths for the ESH machine were created according to these paths.

7.6.1 Combined axial – torsion in phase loading

For the experiment, different proportional (axial-torsion) load sets were used as in Table 5.1. Figure 7.6 shows the torque versus axial load variation at the notch root for three proportional loading tests.

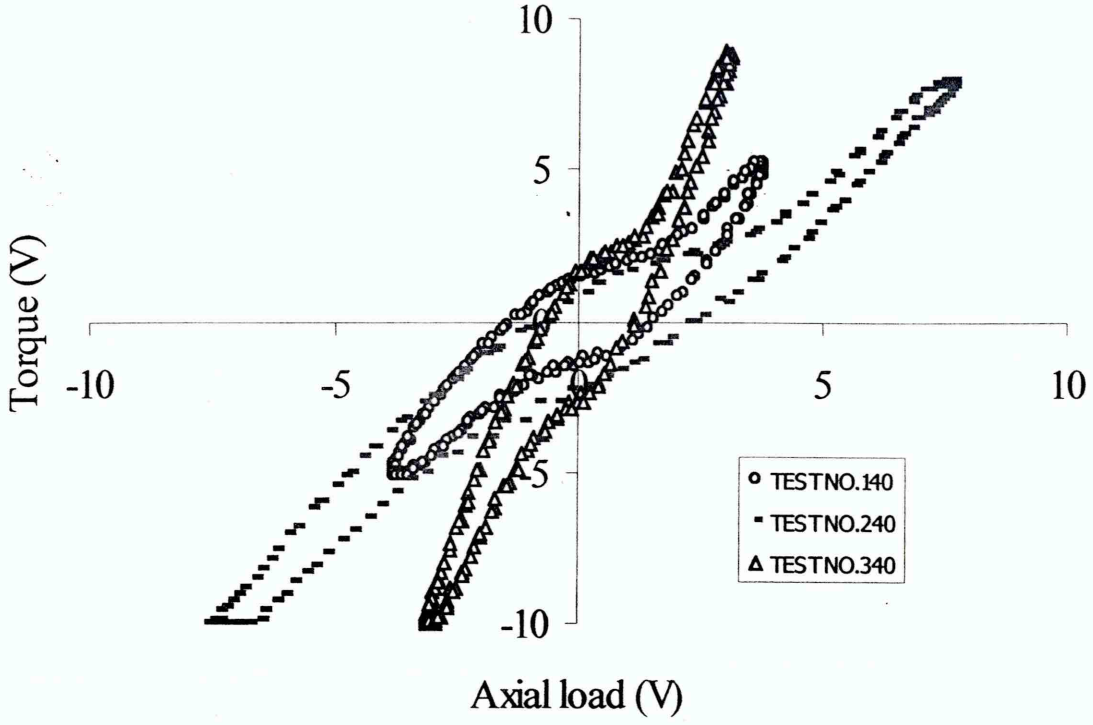

Figure 7.6: Torque versus axial load for different proportional loading test

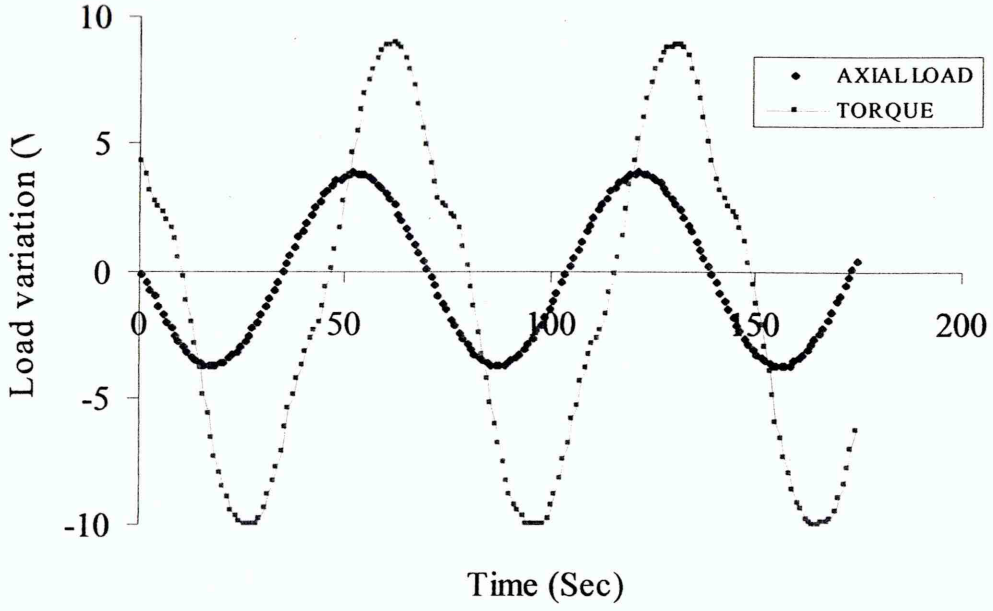

Figure 7.7: The recorded axial load and torque amplitudes with time for Test No.340 in Table 5.1

As shown in the Figure 7.7, the path followed by the material in the experiment is slightly different from that imposed to it. The torque wave pattern was slightly different from the sinusoidal wave. However the shape considered is acceptable. This means that the material does not necessarily follow the strain path. This is due to inaccuracies of

load control. Considering the Figure 7.5, torque versus axial load should have been a straight line for the proportional loading but the machine had not taken the actual proportional wave pattern given. Hence some non-proportionality was indicated.

Figure 7.7 shows the applied axial load wave pattern, followed by the material, was same as the input wave pattern. Therefore the hysteresis loop, plotted for axial stress versus axial strain for in-phase loading (Figure 7.8) shows the expected shape. The applied torsion wave pattern was slightly different from the input pattern as per Figure 7.7. Therefore the shape of the hysteresis loop (Figure 7.9) between shear stress versus shear strain was slightly different.

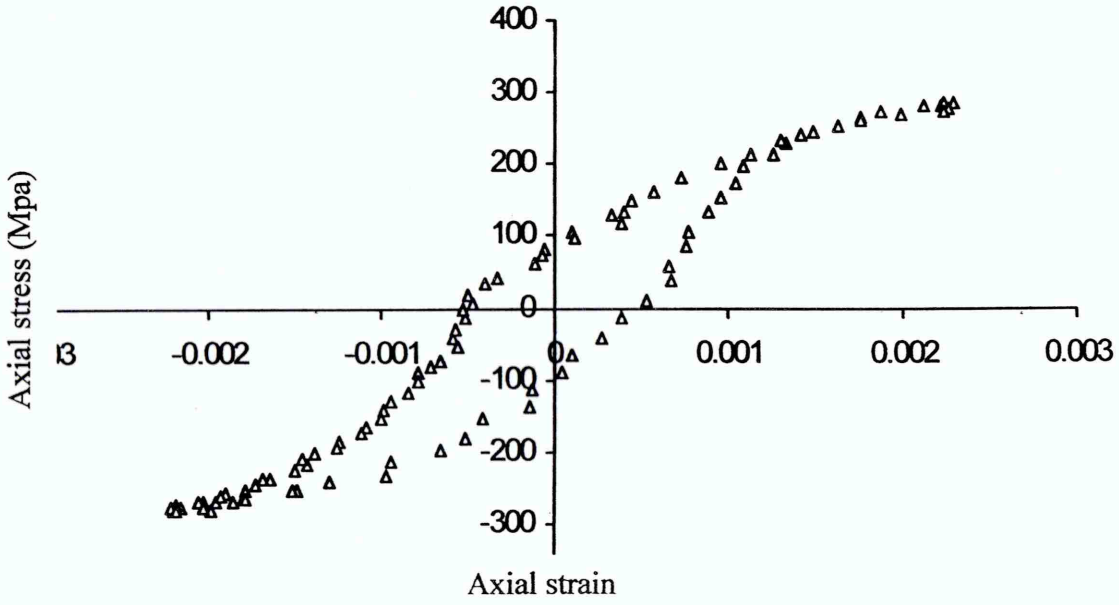

Figure 7.8: The axial stress versus axial strain for Test No. 340 in Table 5.1

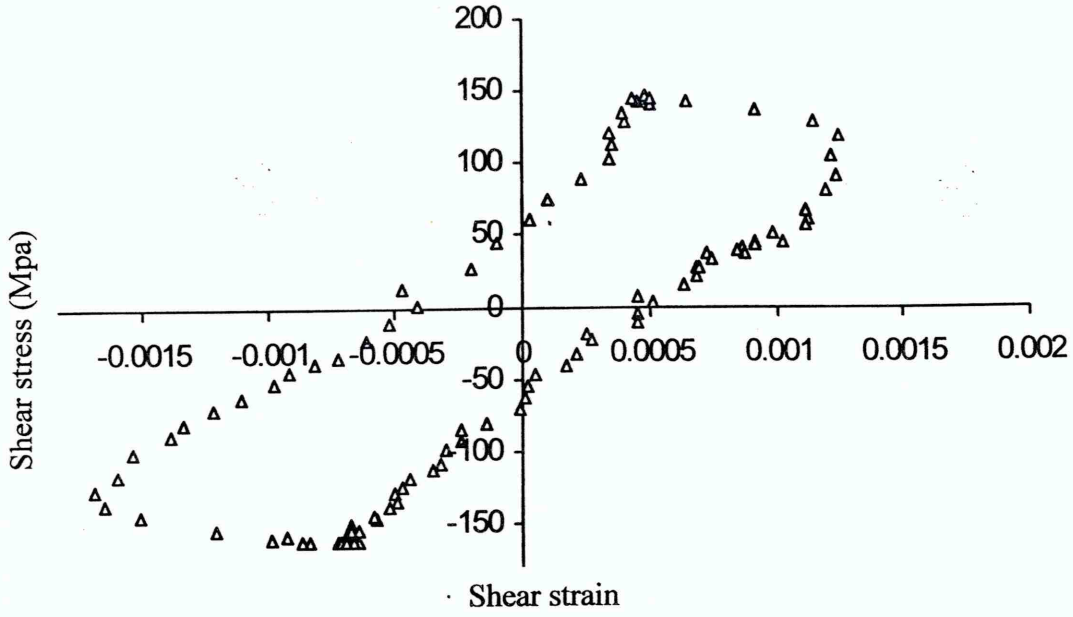

Figure 7.9: The shear stress versus shear strain for Test No.340 in Table 5.1

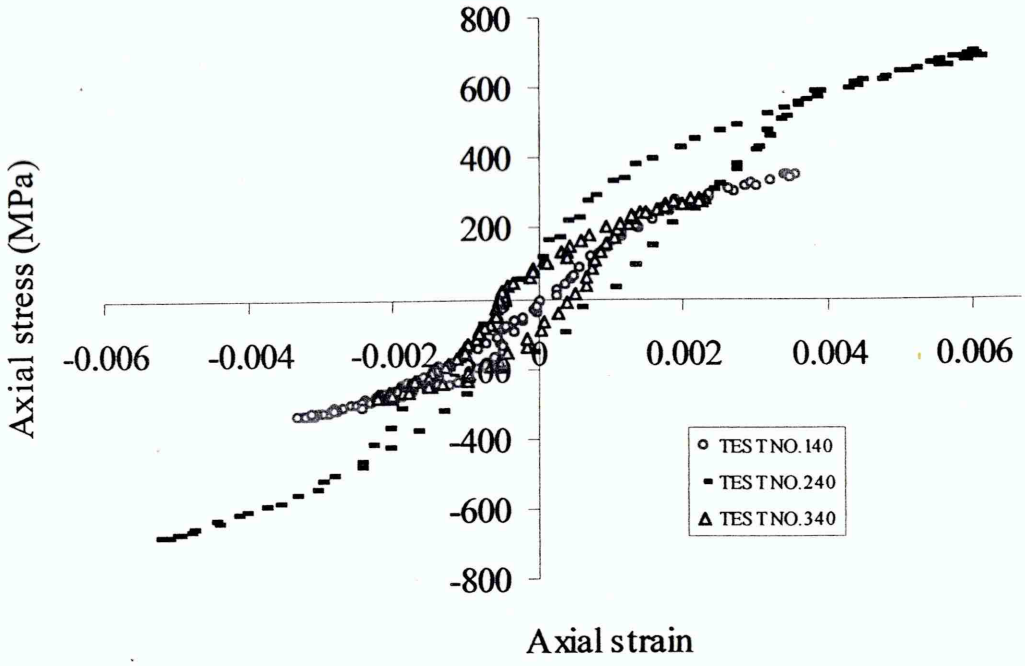

Figure7.10: The axial stress versus axial strain (S22-E22) for different proportional load sets

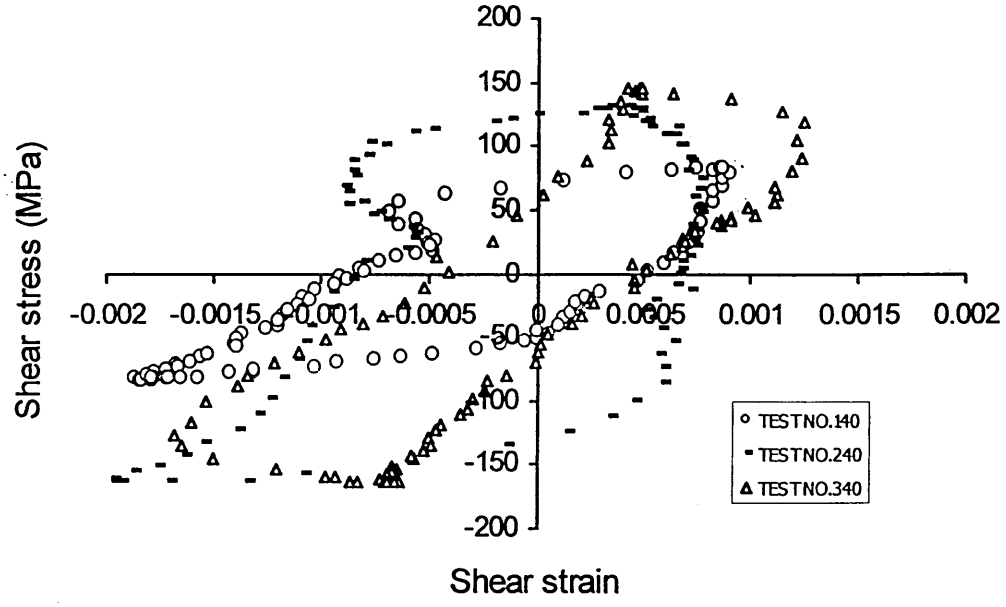

Figure 7.11: The shear stress versus shear strain for different proportional load sets

Figure 7.10 shows the hysteresis loops for different proportional load sets given in Table 5.1. During these types of loadings the size of the hysteresis loops increases as the applied axial load becomes higher. Therefore the axial strain also increases with increasing amplitudes of loads. But the plastic area of the S22-E22 loop is higher in Test No.340 than in Test No.140 as the applied torque of the Test No.340 is higher than that of Test No.140. That means the torque also plays a vital role in increasing the plastic energy of the axial stress-strain loop. It can be expected to have shorter lives for higher applied load.

As shown in the Figure 7.11, the size of the hysteresis loops increased when applied torques were increased. The plastic energy is higher in shear stress versus shear strain loops. Considering the Table 5.1, the Figure 7.10, and the Figure 7.11, when the axial load and torque are low, the areas of the hysteresis loops also are low per Test No.140. When applied axial and torsion loads are higher, the plastic area of the loops also higher as Test No. 240. Considering the Test No.340, the axial load is low, but torsion load is very high and therefore the area of the shear stress versus shear strain hysteresis loop is larger than that of the loop obtained in Test No.140. Therefore the material lifetime expected to be shorter for a hysteresis with large plastic strain since the plastic work done on the material is believed to determine the cyclic fatigue behaviour of the material.

Comparing the results for in-phase loading hysteresis loops (Figure 7.8 and Figure 5.18, Figure 7.9 and Figure 5.19), peak values of the strains are compatible for both FEA and experiment results. Considering the FEA analysis, the plastic strain is much higher than the experimental results. But considering the elastic part, the gradient was calculated to be 80000 MPa for both FEA and experimental cases. However the shapes of the hysteresis loops were different. For the analysis ABAQUS does not always give convergent results. Therefore it is difficult to obtain the exact shape of the hysteresis loop from FEA.

7.6.2 Combined axial-torsion non-proportional loading

7.6.2.1 Path-A -90^0 out-of phase loads

Table 5.1 shows the different load sets used for 90^0 out-of phase tests. Figure 7.12 shows the variation of torque amplitudes versus the axial load amplitudes throughout the sinusoidal wave applied.

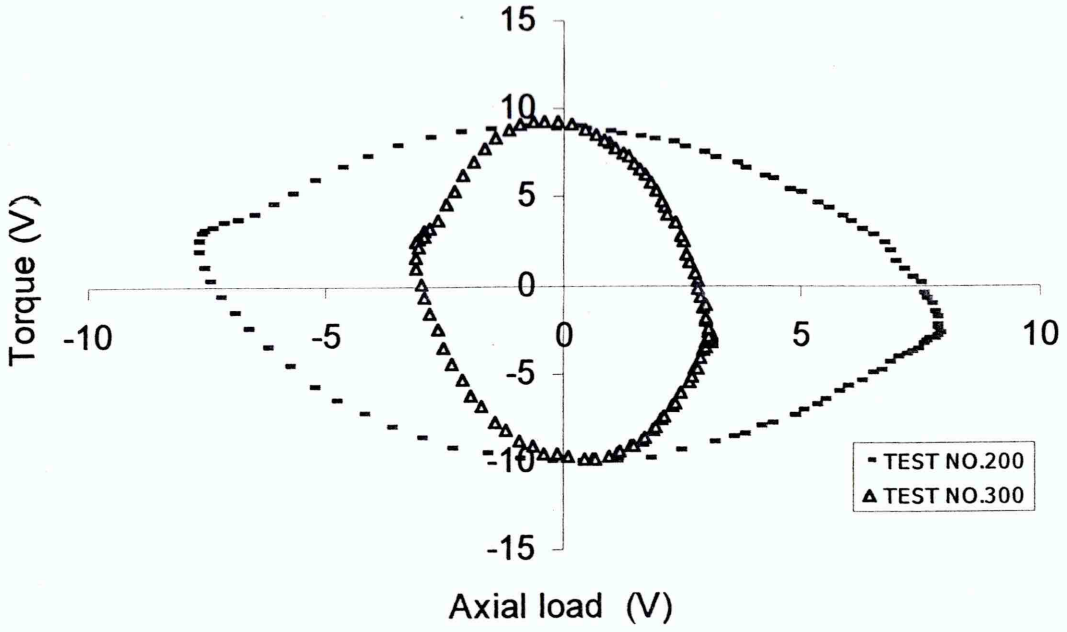

Figure 7.12: The variation of torque versus axial load for non-proportional loading Path-A

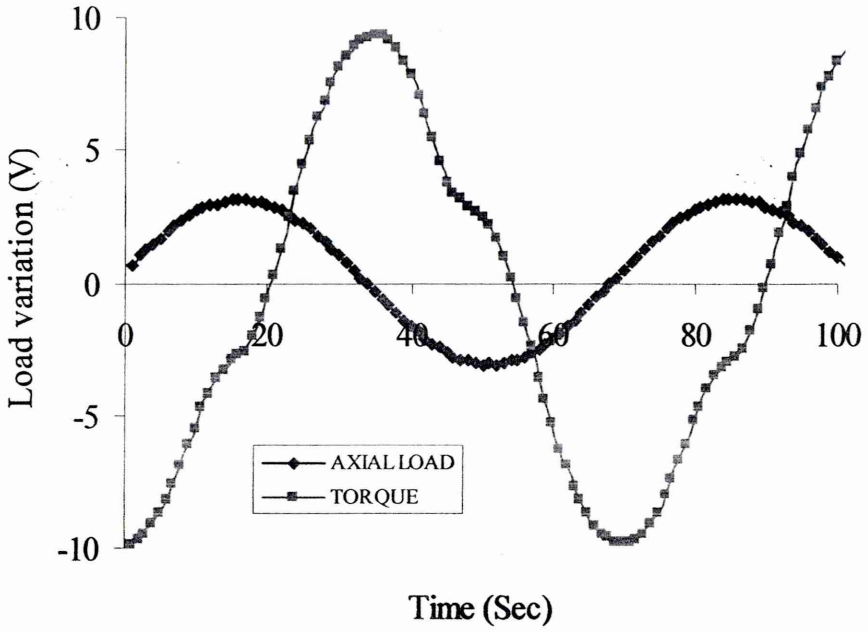

Figure 7.13: The recorded axial load and torque variations with time for Test No. 300 in Table 5.1

The variations of applied torque versus axial load for both cases are shown in Figure 7.12. The shape of the variation shown in Figure 7.12 is expected to be same for shear strain γ versus axial strain ε for the out of phase loading. Figure 7.5 indicates that the imposed loading path was circular and that the path followed by the material during cyclic loading was of circular form even though a slight difference could be noticed as in Figure 7.12. But considering the Figure 7.13, axial load wave pattern was similar to the imposed one but torsion wave pattern was little different due to inaccuracies of load control.

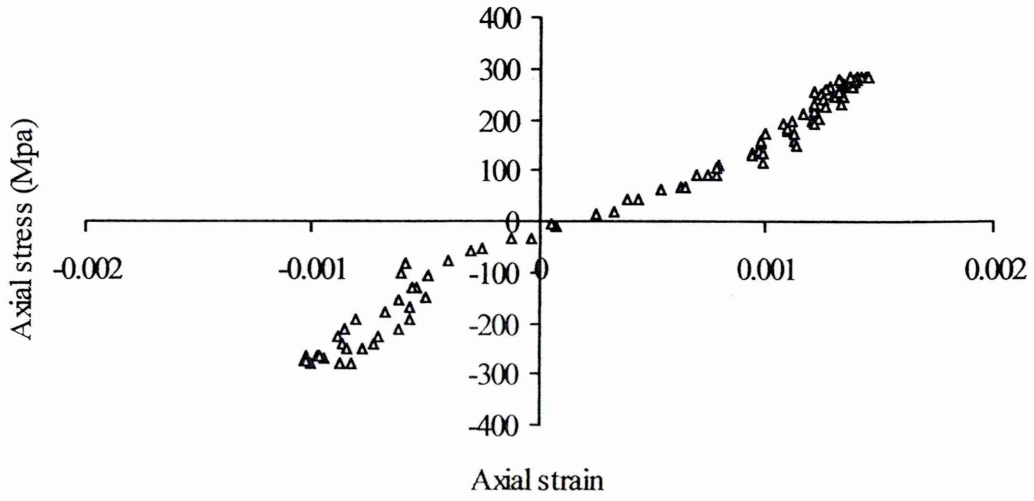

Figure 7.14: The axial stress versus axial strain for Test No.300 in Table 5.1

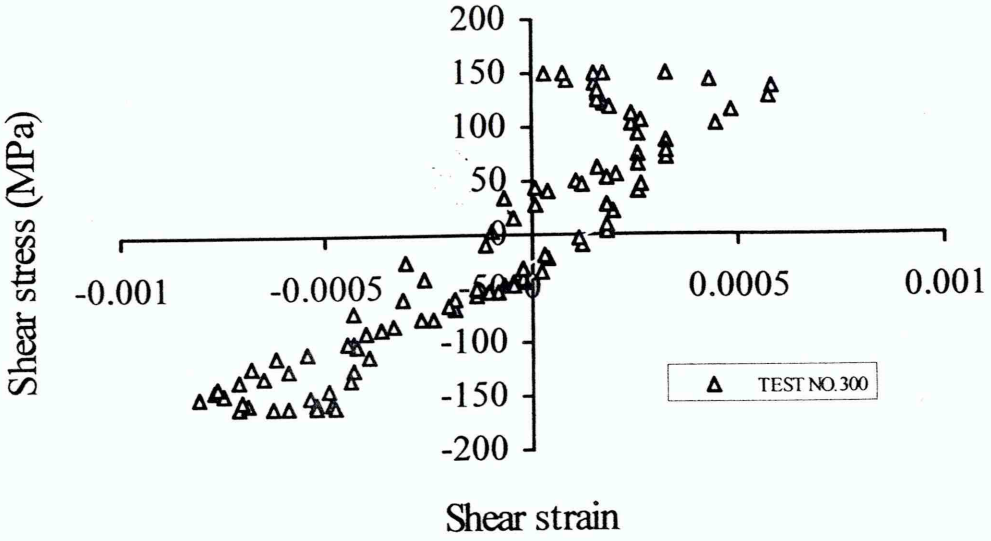

Figure 7.15: The shear stress versus shear strain for Test No. 300 in Table 5.1

Figures 7.14 and 7.15 show that the respective strains follow the applied axial and torsion load wave patterns for Test No.300 in Table 5.1. The out-of phase hysteresis loops obtained from experiments were totally different from those of the in-phase loading.

Comparison of hysteresis loops obtained from experiments for non-proportional loading Path-A

For the non-proportional Path-A, two tests were performed and the hysteresis loops for axial stress/strain and shear stress/strain were compared. As in the Table 5.1, the applied torque was same for the both tests (Test No.200 and Test No.300) and for Test No.200 the applied axial load was doubled as that applied in Test No. 300.

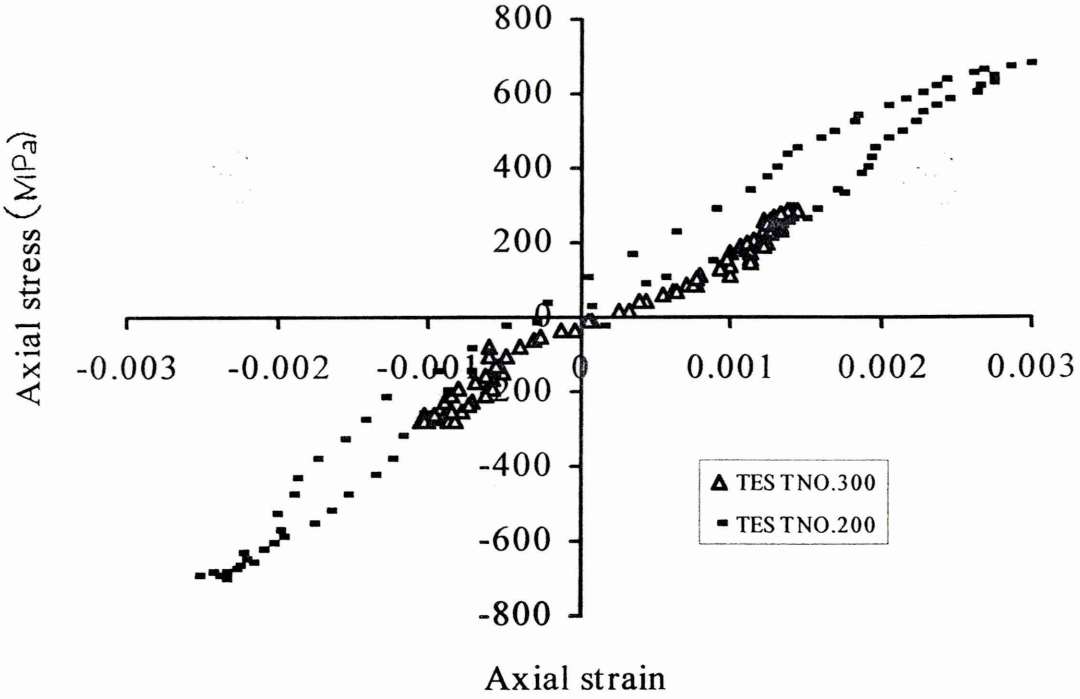

(a)

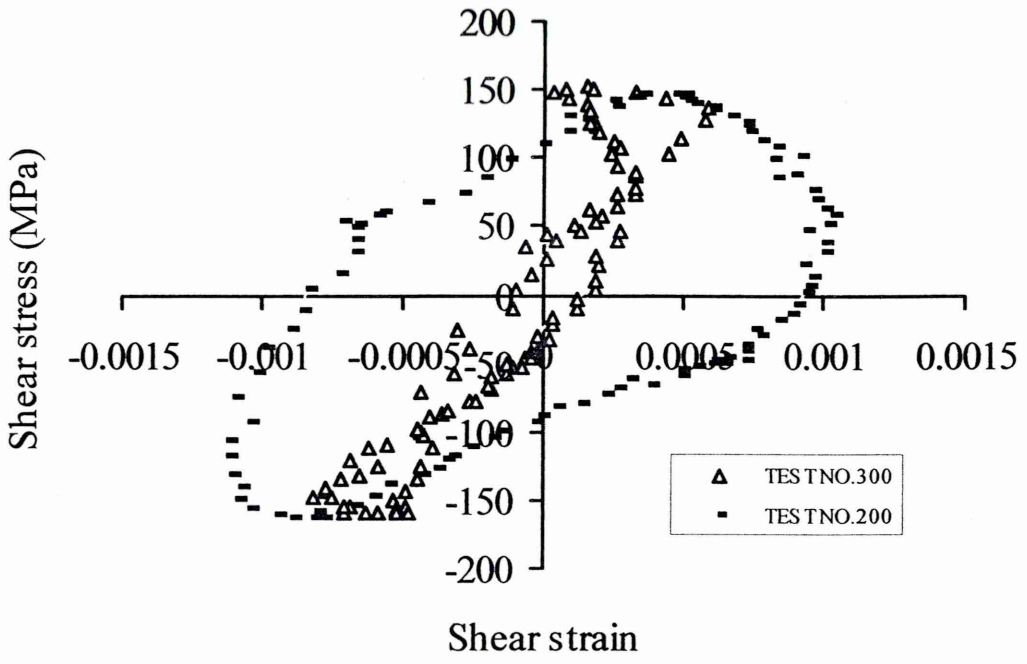

(b)

Figure 7.16: (a) The combined hysteresis loops for axial stress versus axial strain and (b) the combined hysteresis loop for shear stress versus shear strain for out of phase loading Path-A

As indicated in the Figure 7.16 (a) when the amplitude of the applied load increases strain amplitude also increases. The increase in strain amplitude results in a larger and longer hysteresis loops. Test No.200 has bigger plastic area than Test No.300, as the applied axial load was higher than that for Test No. 300.

As can be seen from the Figure 7.16 (b), Test No. 200 has bigger plastic area than Test No. 300; while same torque was applied. That means the axial load helps to increase the shear strain amplitude. Therefore Test No. 200 has more plastic energy than Test No.300. Also the shapes of the out-of-phase hysteresis loops were different when compared with the in-phase hysteresis loops obtained from the experiments.

FEA results for non-proportional loading Path-A

Table 5.1 shows the load set used for 90^0 out-of phase FEA Ref No. 400 and Figure 7.17 shows the variation of torque versus the axial load throughout the sinusoidal wave applied for FEA. The variation is same for shear strain γ versus axial strain ε for the out of phase loading.

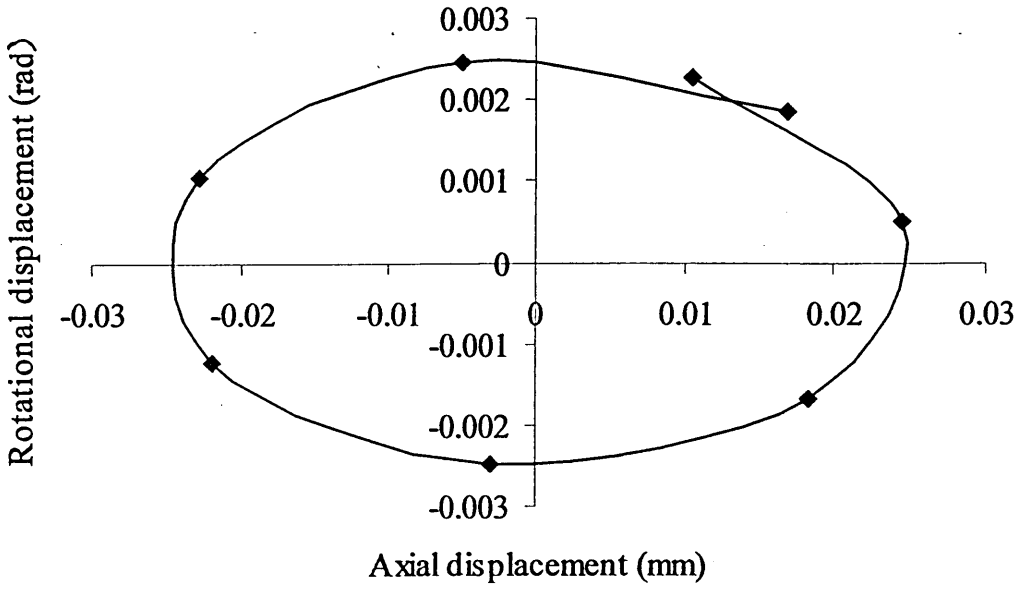

Figure 7.17: FEA inputs for 90^0 out of phase load (Path-A)

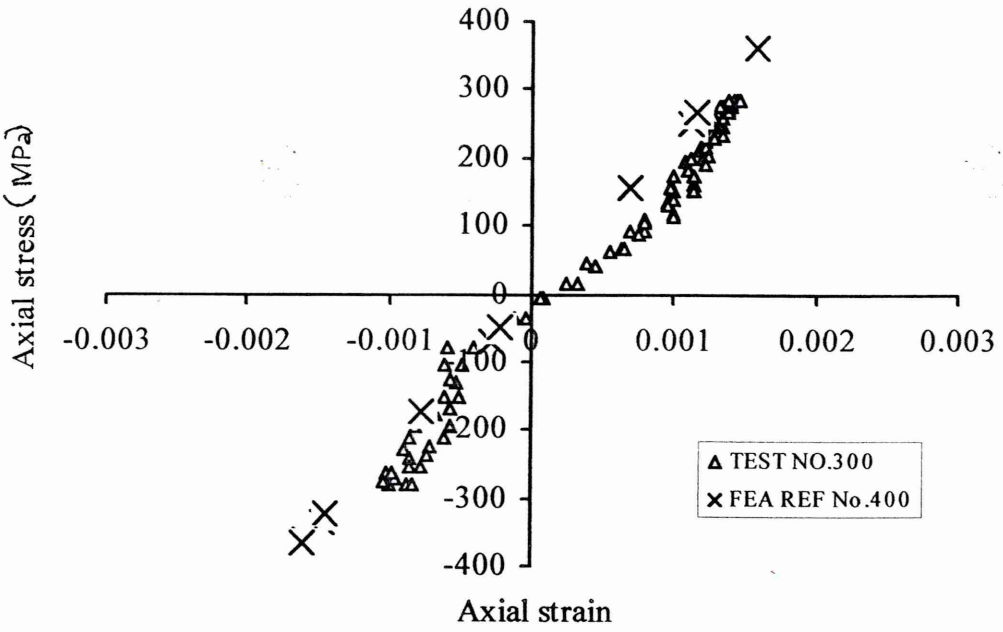

Figure 7.18: The axial stress versus axial strain for Test No. 300 and FEA Ref No. 400 in Table 5.1

Figure 7.21 shows the axial stress versus axial strain loops obtained from FEA and experimental results. Both loops show little plasticity and FEA results behave more elastically. The elastic gradient was same for both hysteresis loops.

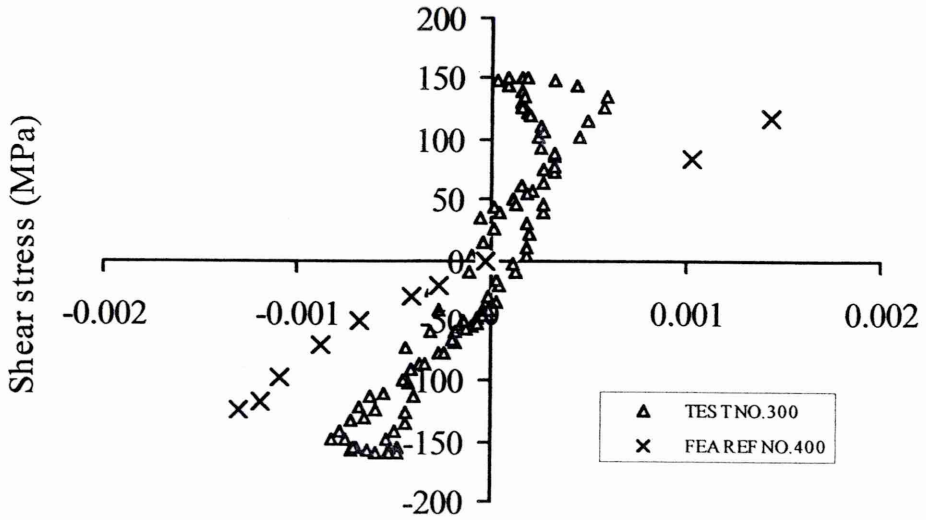

Figure 7.19: The shear stress versus shear strain for Test No. 300 and FEA Ref No. 400 in Table 5.1

Figure 7.19 shows the shear stress versus shear strain for Test No.300 and FEA Ref No. 400. The gradient of the elastic region was same. But the experimental loops have more plasticity as depicted by hysteresis loop.

7.6.2.2 Non-proportional loading Path-B

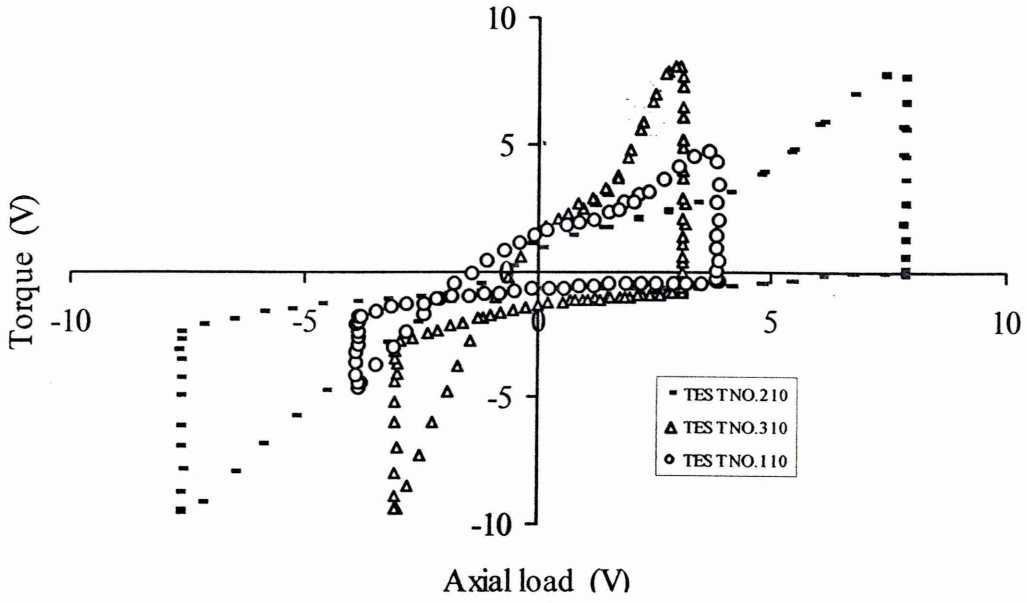

Figure 7.20: The variation of torque versus axial load for Path-B (for load sets shown in Table 5.1)

The variations of applied torque versus axial load for Path-B load cases (Table 5.1) are shown in Figure 7.20. The variation shown in Figure 7.20 is same for shear strain γ versus axial strain ε for the Path-B loading. Figure 7.5 has indicated the desired loading path but the path followed by the material during loading was slightly different as seen from Figure 7.21.

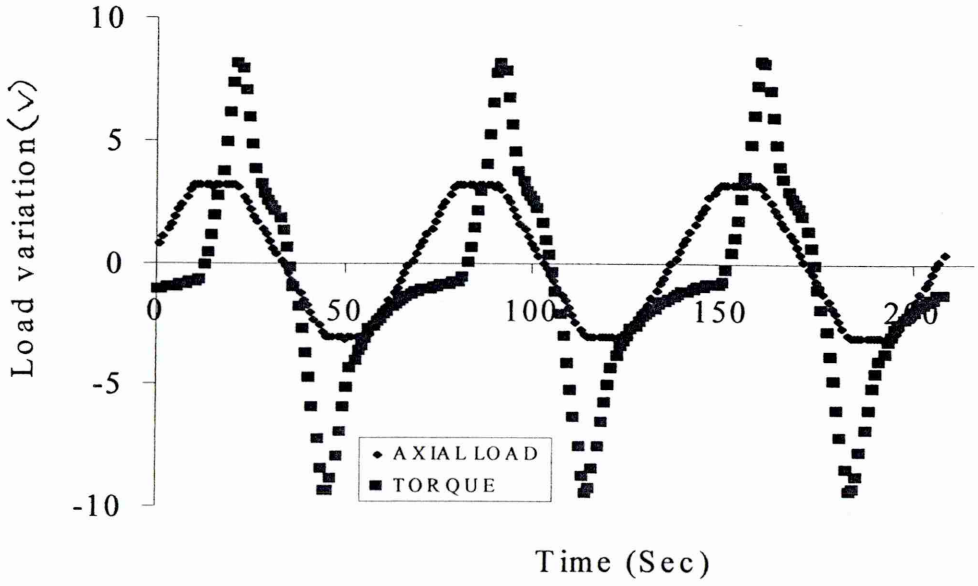

Figure 7.21: The recorded axial load and torque variations with time for Test No. 310 in Table 5.1

Considering the Figure 7.21, axial load wave pattern was similar to the input load pattern to the machine but torsion wave pattern was slight different.

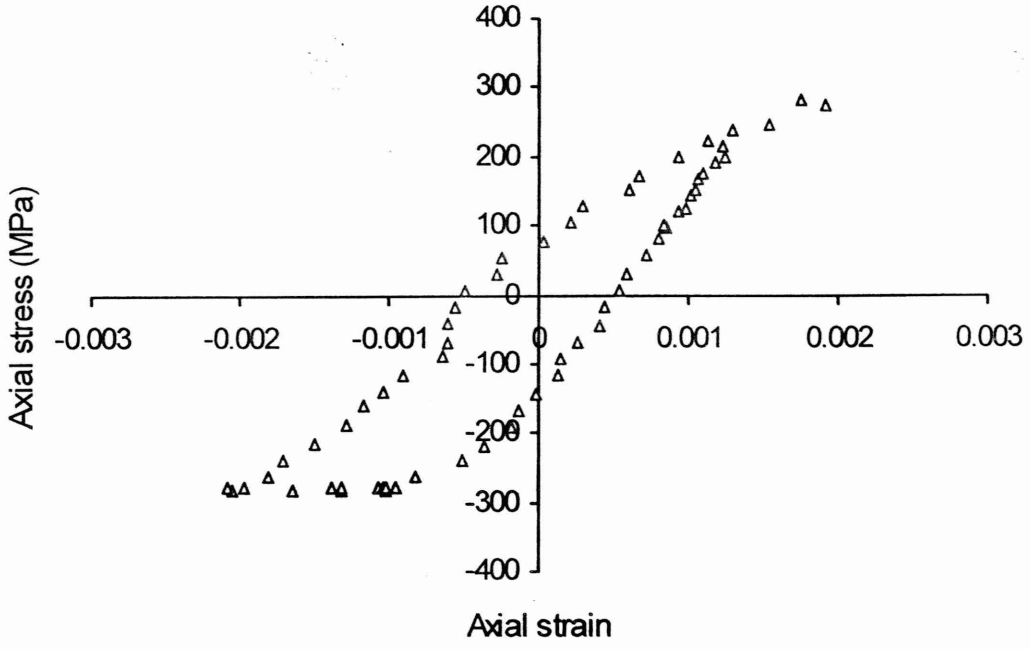

Figure 7.22: The axial stress versus axial strain for Test No. 310 in Table 5.1

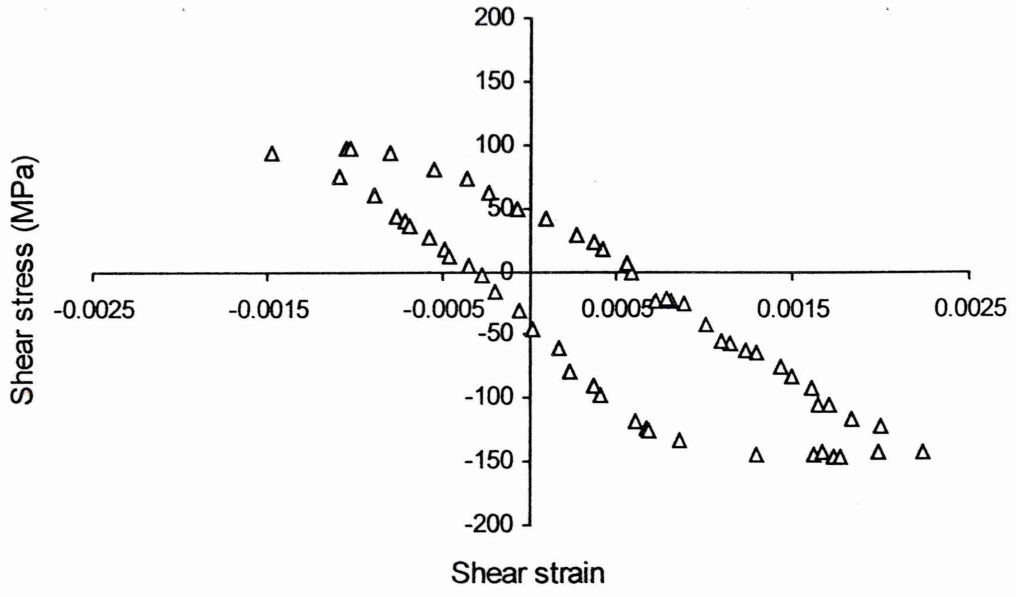

Figure 7.23: The shear stress versus shear strain for Test No. 310 in Table 5.1

Figure 7.22 and Figure 7.23 show that the respective strains follow the applied axial and torsion load wave patterns. The hysteresis loops obtained from experiments for Path-B, were totally different from that of the out-of-phase loading Path-A. As the Figure 7.22 and 7.23, the loops obtained from Path-B, are in general hysteresis loops shape. While

strain amplitudes increase, the size of the hysteresis loops also increase. Therefore the plastic strain energy developed in the material increases.

Comparison of hysteresis loops obtained from experiments for non-proportional loading Path-B

For the non-proportional Path-B, three tests were performed (Table 5.1). The hysteresis loops for axial stress/strain and shear stress/strain were compared. The results for axial stress/strain and shear stress/strain are shown in Figure 7.24(a) and Figure 7.24(b).

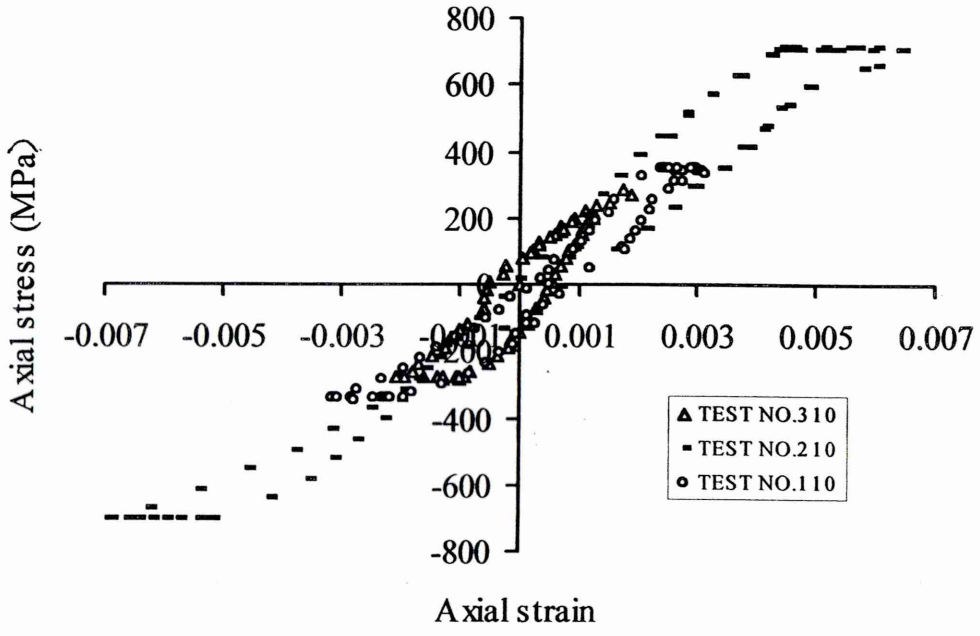

(a)

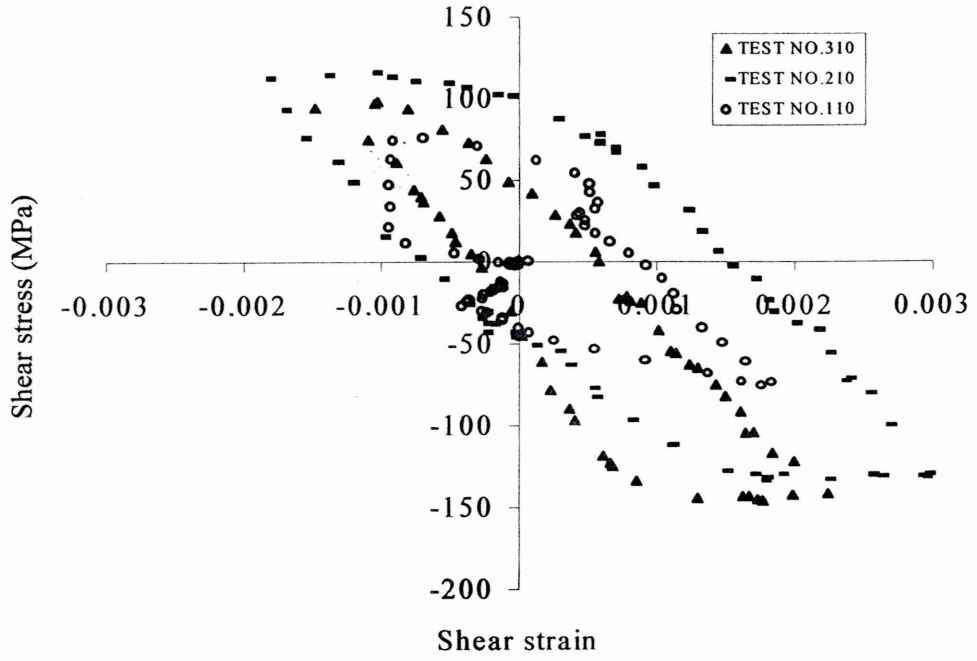

(b)

Figure 7.24: (a) The combined hysteresis loops for axial stress versus axial strain and (b) the combined hysteresis loop for shear stress versus shear strain for non-proportional loading Path-B

As indicated in the Figure 7.24(a), the size of the hysteresis loops increases as the applied axial load becomes higher. Considering the Figure 7.24 (b), Test No. 210 has bigger plastic area than in Test No.310; while they were applying same torque. That means the axial load helps to increase the shear strain amplitude. Therefore Test No. 210 has more plastic energy than Test No.310. Comparing with the out-of-phase hysteresis loops (Path-A), the shapes of the hysteresis loops obtained from Path-B loadings were completely different.

Comparison between FEA and Experimental results: For non-proportional loading Path-B

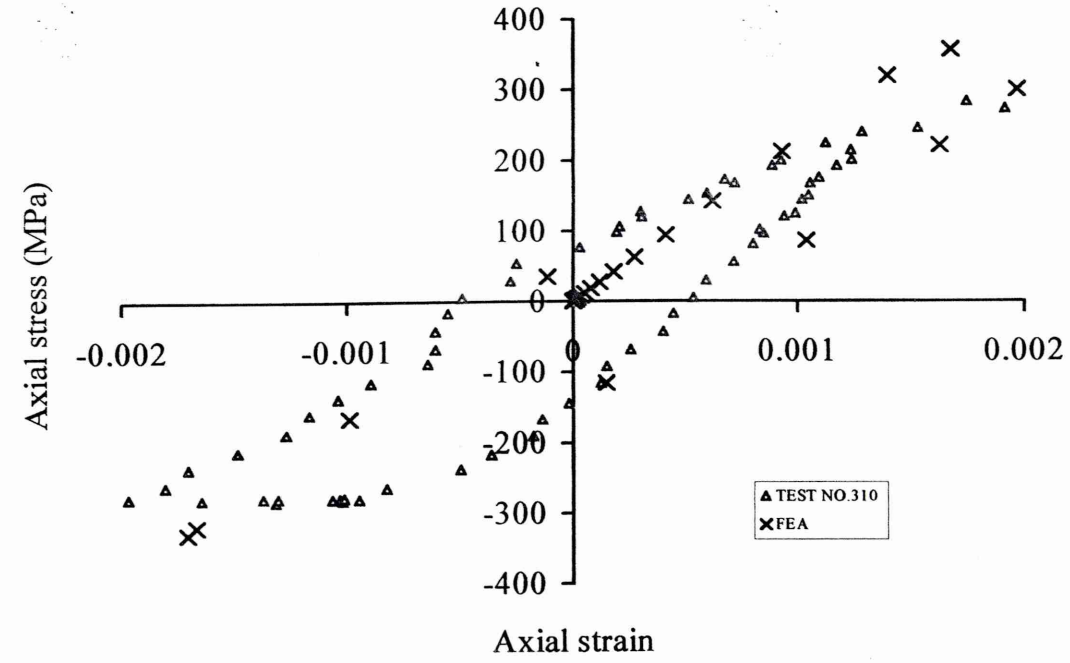

Figure 7.25: Comparison axial stress versus axial strain for Test No. 310 and FEA Ref No. 410 in Table 5.1

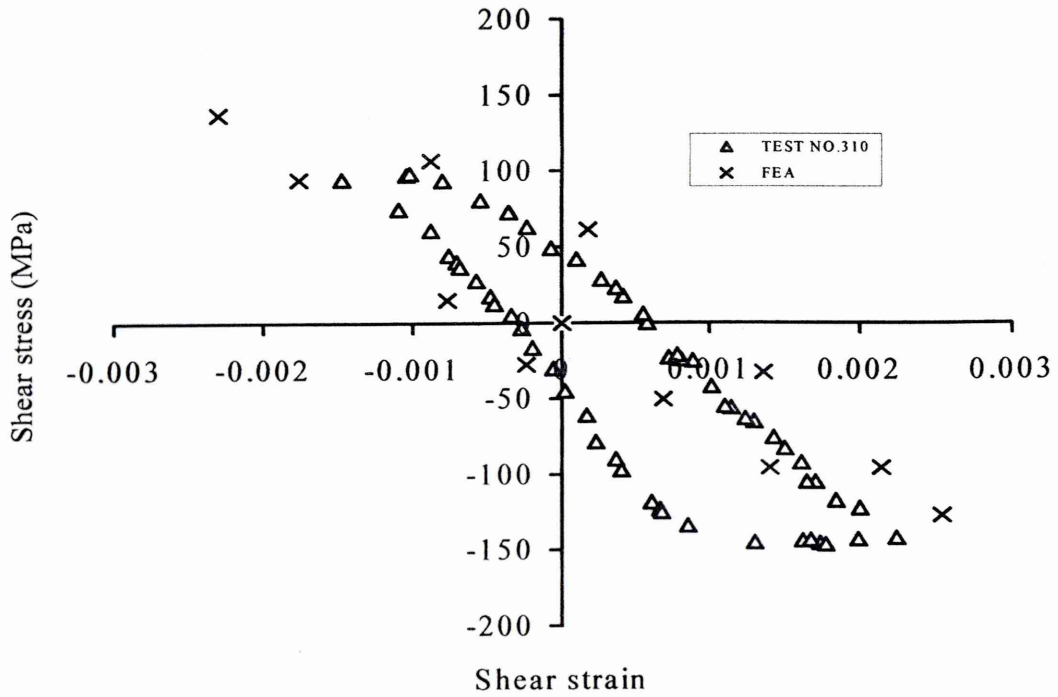

Figure 7.26: Comparison shear stress versus shear strain for Test No. 310 and FEA Ref No.410 in Table 5.1

Figure 7.25 shows the axial stress versus axial strain loops. The shapes of the both loops (FEA and Experiment) were similar. The elastic gradient of the both hysteresis loops were same.

Considering the Figure 7.26, for the shear stress-shear strain loops the elastic gradient was same and both hysteresis loops have more plastic area.

7.6.2.3 Non-proportional loading Path – C

Table 5.1, shows the different load sets used for non-proportional load Path-C and Figure 7.27 shows the variation of torque against the axial load for Path-C load.

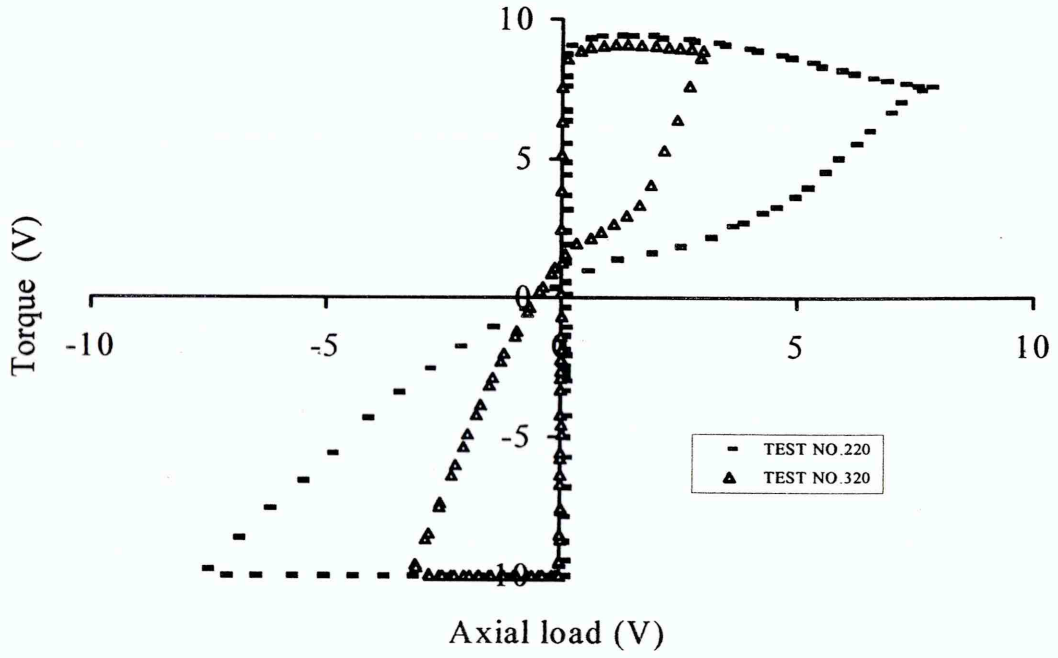

Figure 7.27: The variation of applied torque versus applied axial load for Path-C

The variations of applied torque versus axial load for two non-proportional load Path-C cases are shown in Figure 7.27. The shape of the variation (Figure 7.27) is same for shear strain γ versus axial strain ε for the Path-C loading. Figure 7.5 indicates the imposed loading path but the path followed by the material in the experiment is slightly different from that imposed to it as the Figure 7.27.

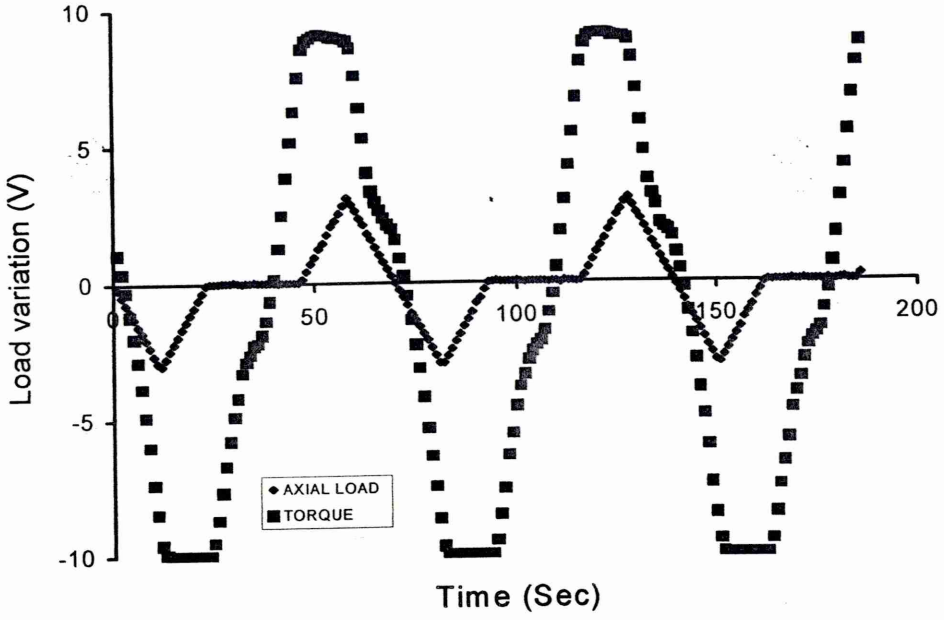

Figure 7.28: The recorded axial load and torque variations with time for Test No. 320 in Table 5.1

Considering the Figure 7.28, axial load wave pattern was similar to the input wave pattern but torsion wave pattern was little different. This is something, which is uncontrollable situation through out the research.

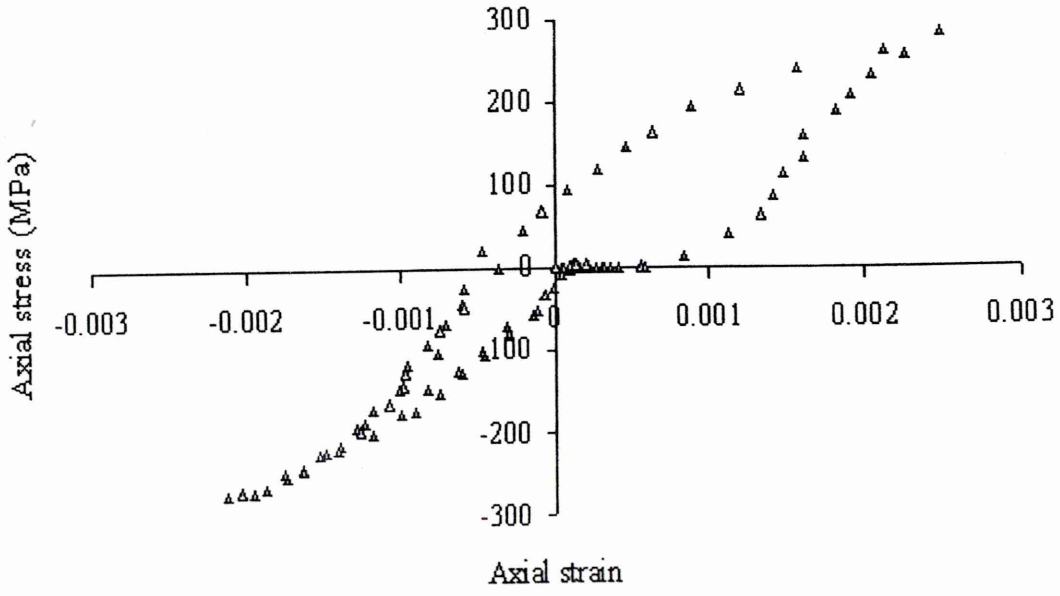

Figure 7.29: The axial stress versus axial strain for Test No.320 in Table 5.1

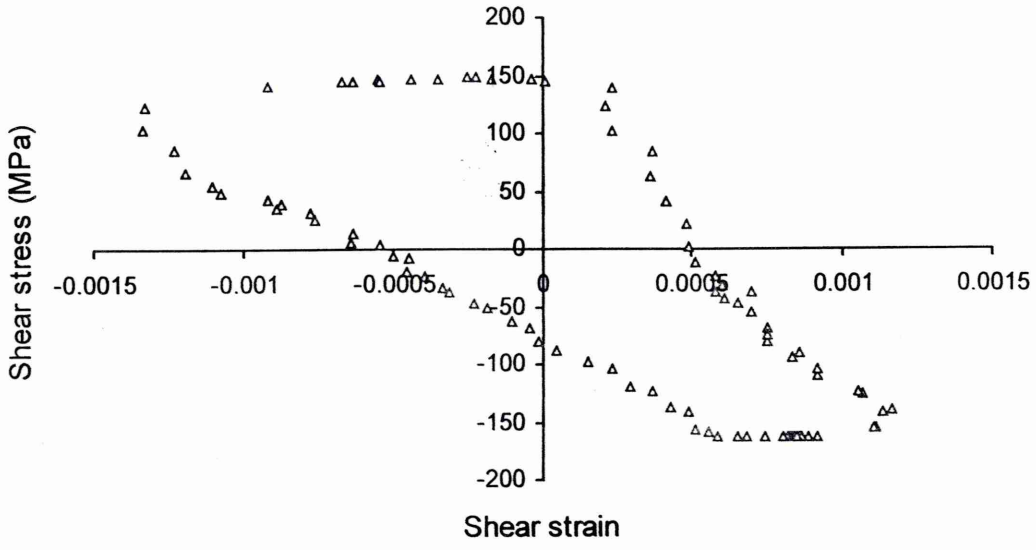

Figure 7.30: The shear stress versus shear strain for Test No.320 in Table 5.1

Figure 7.29 and Figure 7.30 show that the respective strains follow the applied axial and torsion load wave patterns for Test No.320 in Table 5.1.The hysteresis loops obtained for Path-C were totally different from the loops obtained from Path-A and Path-B, non-proportional loadings. As the Figure 7.29 and Figure 7.30 the stress-strain loops obtained from Path-C have slight plasticity. Comparing the Test No.310 and Test No.320, maximum axial strains are same for both tests. But comparing the shear strains, Test No.320 has a lower value than that of Test No.310.

Comparison of hysteresis loops obtained from experiments for non-proportional loading Path-C

For the non-proportional Path-C, two tests were performed and the hysteresis loops for axial stress/strain and shear stress/strain were compared. As in the Table 5.1, the applied torque was same for the both tests (Test No.220 and Test No.320) and for Test No.220 the applied axial load was doubled as that applied in Test No. 320.

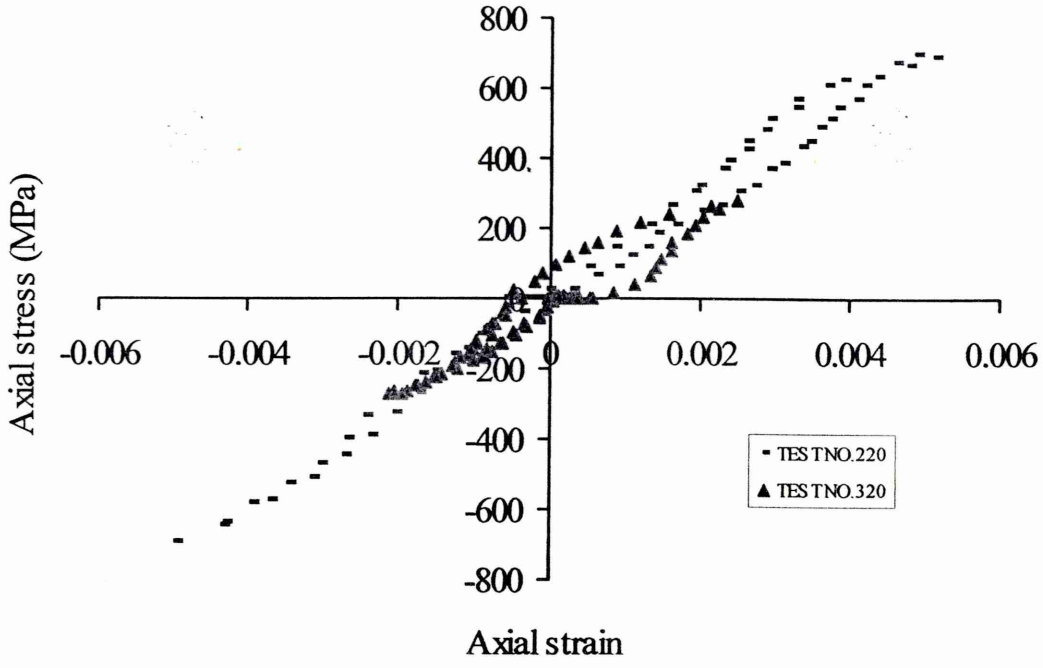

(a)

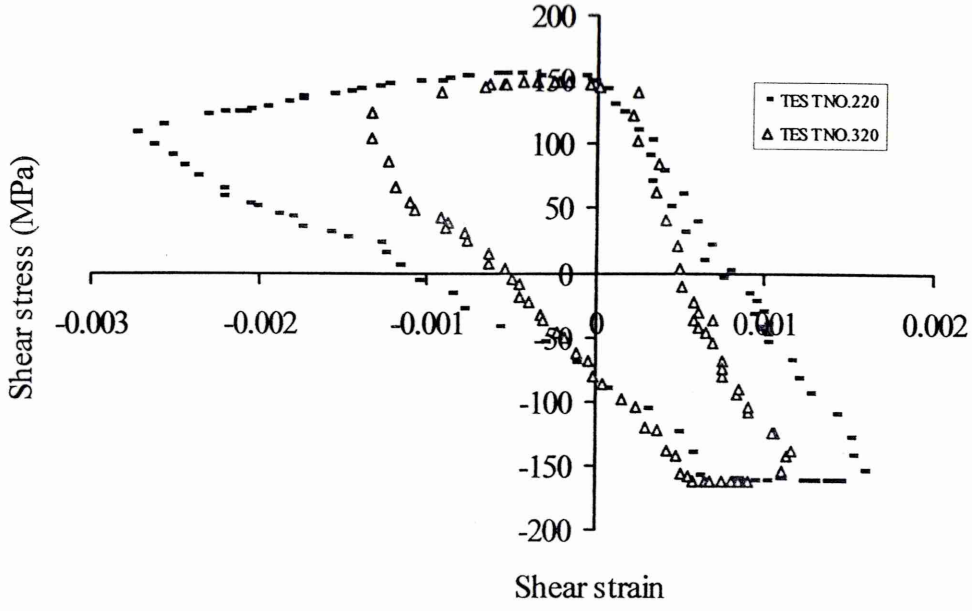

(b)

Figure 7.31: (a) The combined hysteresis loops for axial stress versus axial strain and (b) the combined hysteresis loop for shear stress versus shear strain for out of phase loading Path-C

As the Figure 7.31(a), that the applied load amplitude increases the developed strain amplitude also increases. The increase in strain amplitude results in a larger and longer hysteresis loops

Considering the Figure 7.31 (b), Test No. 220 has bigger plastic area than that of Test No. 320; while they were applying same torque. That means the axial load helps to increase the shear strain amplitude. Therefore Test No. 220 has more plastic energy than Test No.320. Also comparing with the non-proportional loading path-A/Path-B hysteresis loops, the shapes of the hysteresis loops obtained for Path- C were completely different from those of Path A and B.

Comparison between FEA and Experimental results: For non-proportional loading Path-C

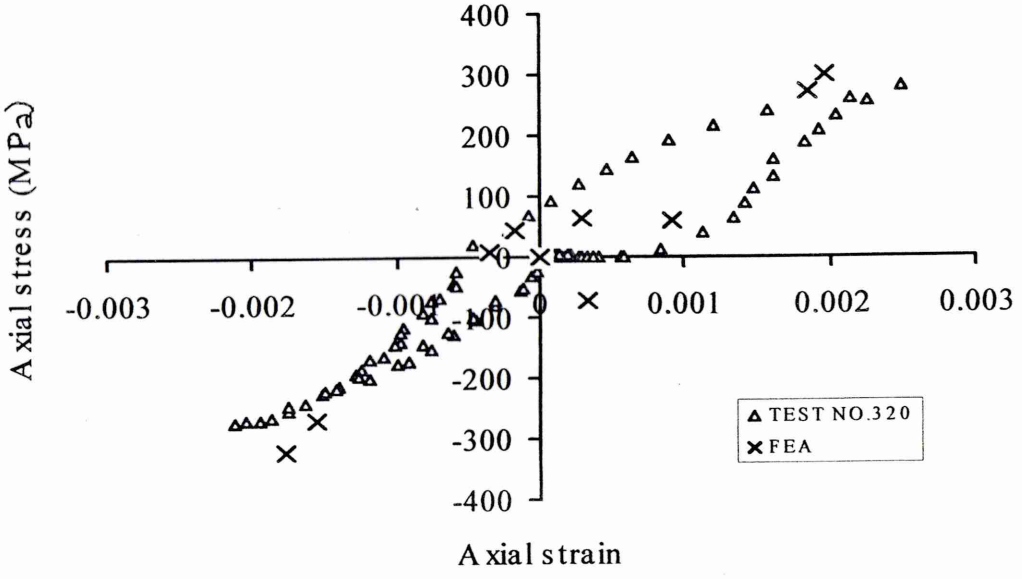

Figure 7.32: Comparison of axial stress versus axial strain for Test No. 320 and FEA Ref No. 420 in Table 5.1

Figure 7.32 shows the axial stress versus axial strain loops and both loops have plasticity. The elastic gradient of both hysteresis loops also were same.

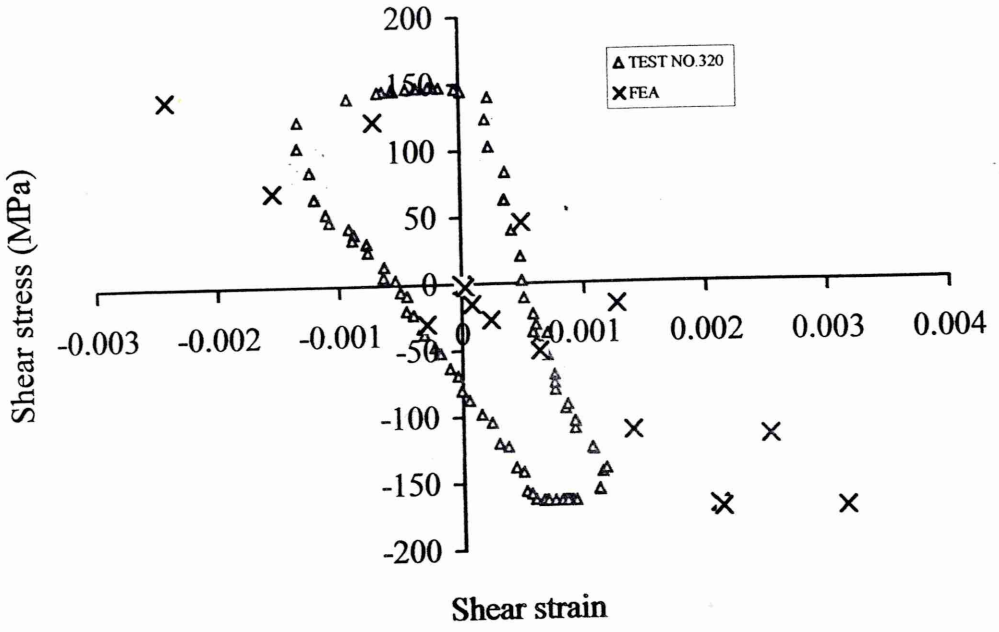

Figure 7.33: Comparison of shear stress versus shear strain for Test No. 320 and FEA Ref No. 420 Table 5.1

Considering the Figure 7.33, for the shear stress-shear strain loop has more plasticity as depicted by hysteresis.

7.6.2.4 Non-proportional load Path-D

Table 5.1 shows the different load sets used for non-proportional load tests for Path-D and Figure 7.34 shows the variation of torque versus the axial load through out the wave applied.

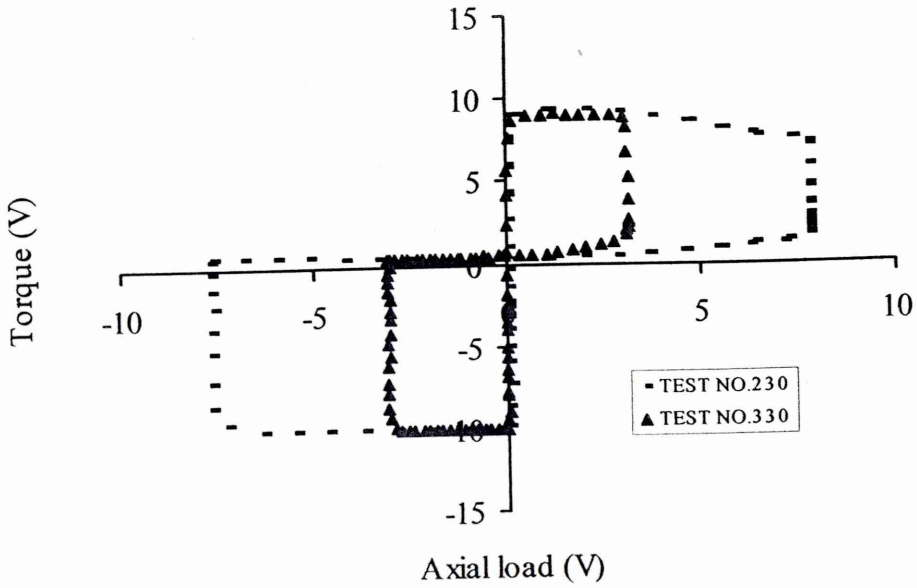

Figure 7.34: The variation of torque versus axial load for Path-D

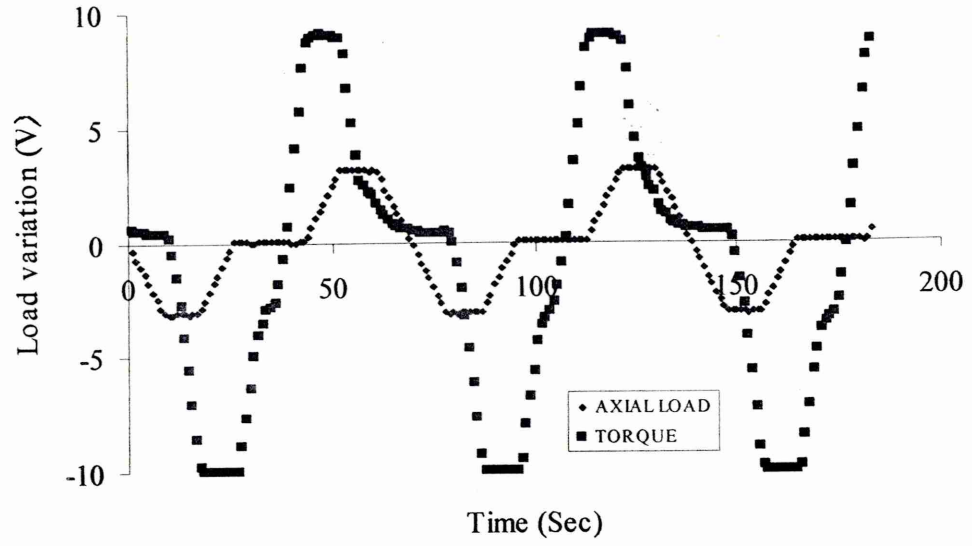

Figure 7.35: The recorded axial load and torque variations with time for Test No. 330 in Table 5.1

The variation of applied torque versus axial load for all Path-D load cases is shown in Figure 7.34. The shape of the variation shown in Figure 7.34 is expected to be same for shear strain γ versus axial strain ε for the Path-D loading. Figure 7.5 indicates the imposed loading path but the path followed by the material during loading was slightly different as shown in Figure 7.34 and 7.35. But considering the Figure 7.35, axial load wave pattern was similar to the imposed one but torsion wave pattern was little different.

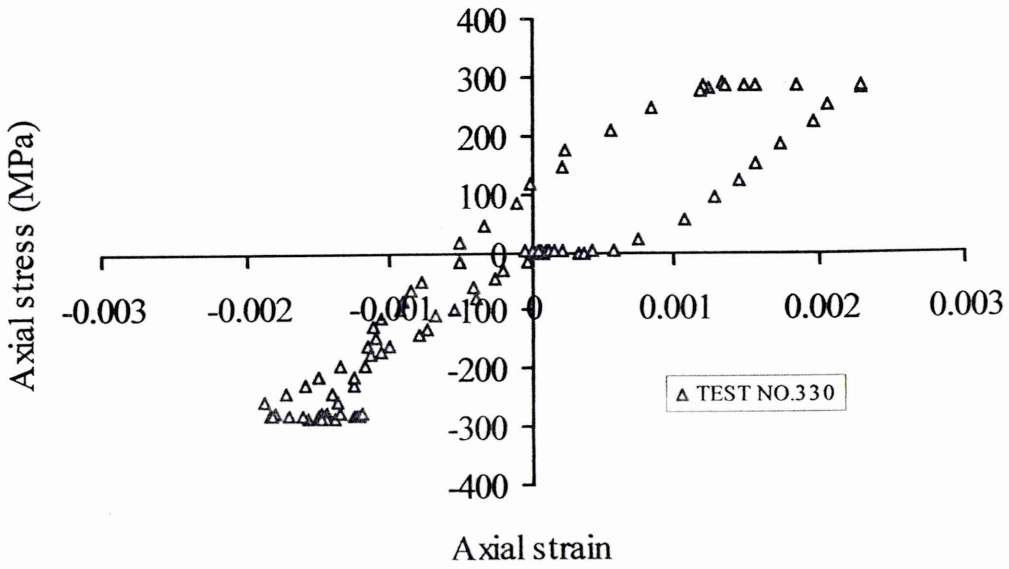

Figure 7.36: The axial stress versus axial strain for Test No. 330 in Table 5.1

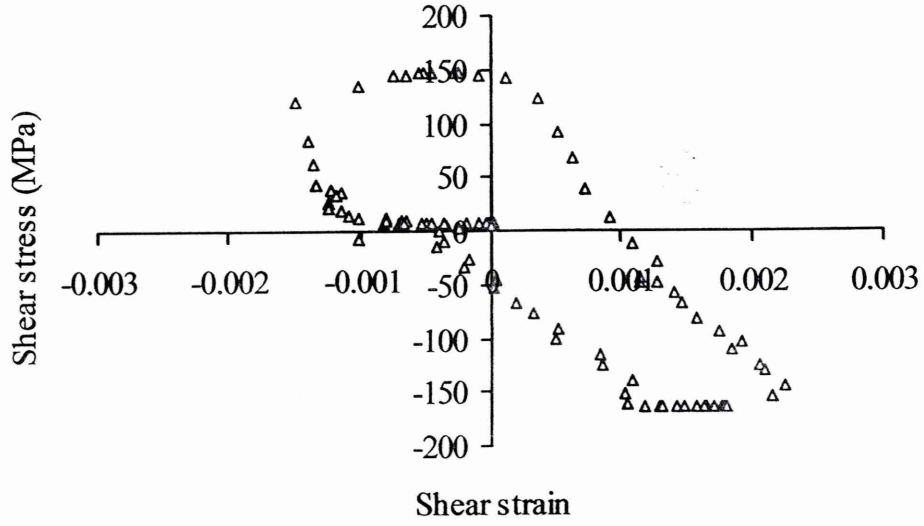

Figure 7.37: The shear stress versus shear strain for Test No. 330 in Table 5.1

Figure 7.36 and Figure 7.37 show that the respective strains follow the applied axial and torsion load wave patterns. The hysteresis loops obtained for Path-D were different from the Path-A, B and C non-proportional loadings. As the Figure 7.36 the axial stress-strain loop obtained from Path-D has more plasticity. But the shear stress/strain loop shown in Figure 7.37, has more plastic energy than axial stress/strain loop as it has a big plastic area. For Test No.330, the applied torque was larger than applied axial load as in Table 5.1. Therefore, while strain amplitudes increase the size of the hysteresis loops also increase as shown in Figure 7.37. Therefore the plastic strain energy developed in the material also increases. Comparing the Test No. 320 and Test No. 330, maximum axial strains are not much different for the both tests. But comparing the shear strains, the Test No. 320 has a lower value than Test No. 330.

Comparison of hysteresis loops obtained from experiments for non-proportional loading Path-D

For the non-proportional Path-D, two tests were performed and the hysteresis loops for axial stress/strain and shear stress/strain were compared. As the Table 5.1, the applied torque were same for the both tests (Test No.230 and Test No.330), but for Test No.230, the applied axial load was doubled as Test No. 330.

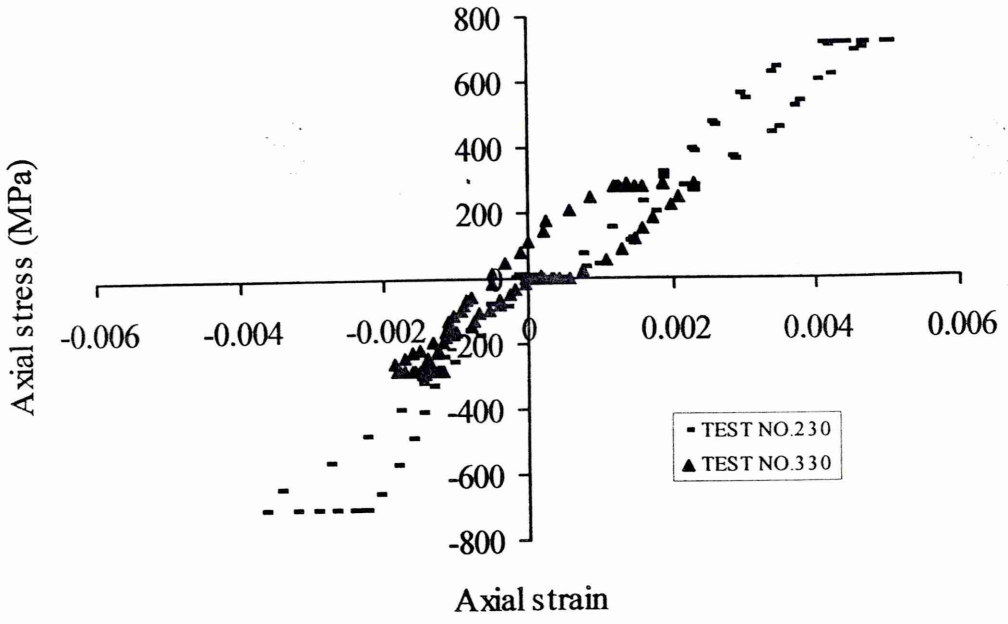

(a)

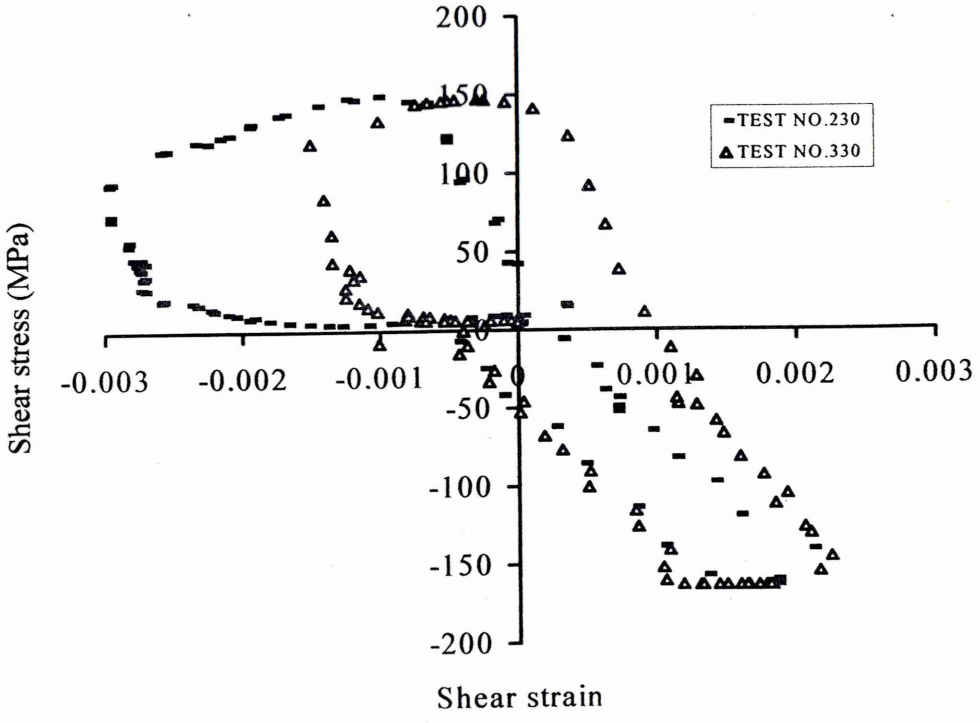

(b)

Figure 7.38: (a) The combined hysteresis loops for axial stress versus axial strain and (b) the combined hysteresis loop for shear stress versus shear strain for non-proportional loading Path-D

As the Figure 7.38(a), while the load amplitude increases the developed strain amplitude also increases. Therefore the increase in strain amplitude results in a larger and longer hysteresis loops as the other non-proportional paths (Path-A, B and C).

Considering the Figure 7.38 (b), Test No. 230 has bigger plastic area than Test No. 330; while they were applying same torque. That means the axial load helps to increase the shear strain amplitude. Therefore Test No. 230 has more plastic energy than Test No.330. Considering the non-proportional loading Path-A, Path-B, Path-C and Path- D, the shapes of the hysteresis loops obtained were completely different.

Comparison between FEA and Experimental results: For non-proportional loading Path-D.

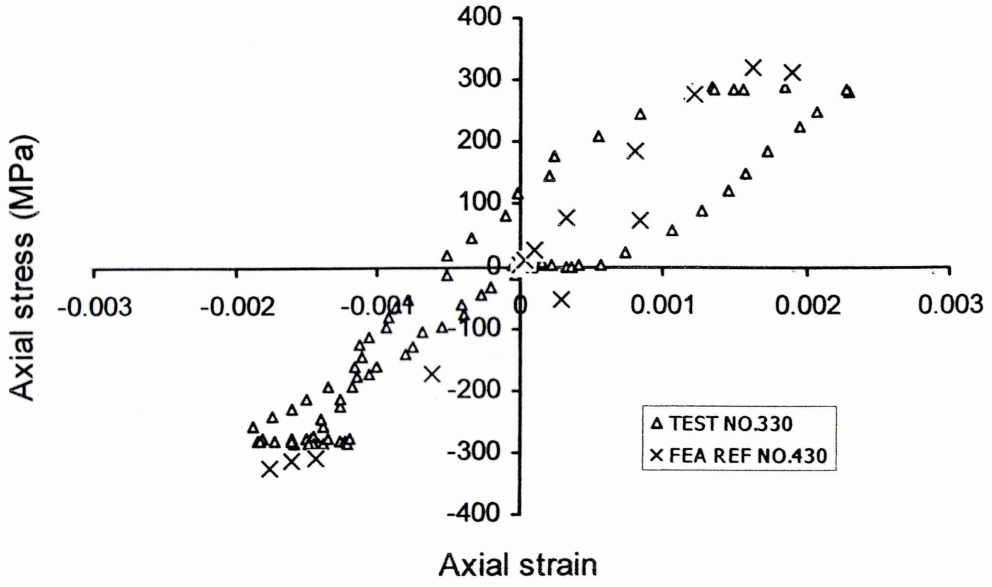

Figure 7.39: Comparison axial stress versus axial strain for Test No. 330 and FEA Ref No. 430 in Table 5.1

Figure 7.39 shows the axial stress versus axial strain loops and both loops have plasticity. The elastic gradient of the both hysteresis loops were same.

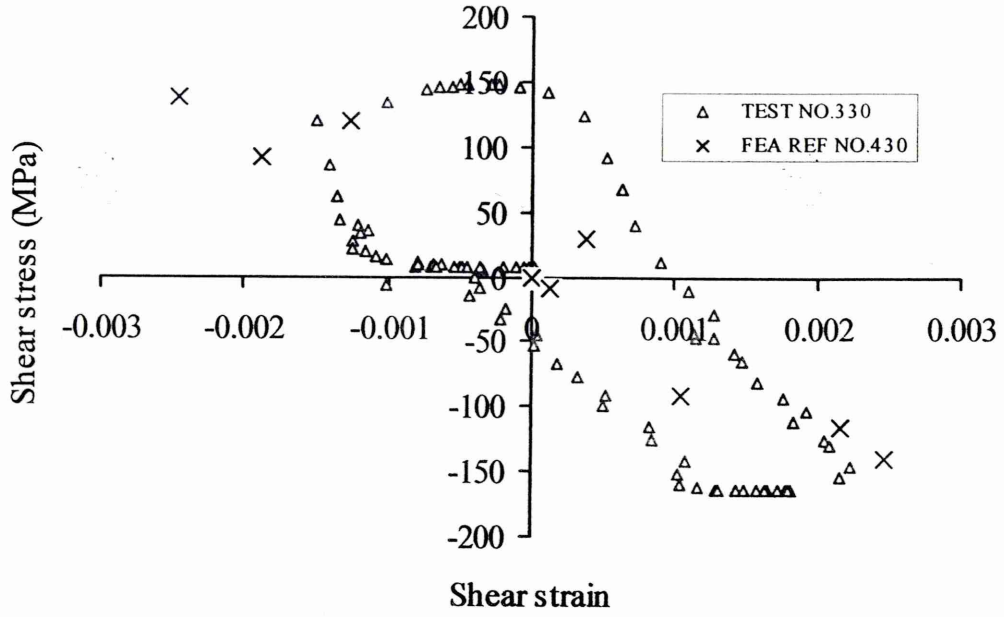

Figure 7.40: Comparison shear stress versus shear strain for Test No. 330 and FEA Ref No. 430 in Table 5.1

Figure 7.40, for the shear stress-shear strain loops have more plasticity as depicted by hysteresis loops. Considering the loads of the Test No.330 and Test No. 430, the obtained hysteresis loops for experiment and FEA were different but the elastic gradient was the same for the both tests.

Table 7.5 shows the axial and shear strain ranges for each experiment and FEA test.

Table 7.5 : The axial and shear strain ranges for each test

Test No./FEA Ref No.	$\Delta\varepsilon$	$\Delta\gamma$
250	0.0039	
450	0.0034	
260		0.0040
460		0.0040
140	0.0076	0.0028
240	0.0055	0.0028
340	0.0061	0.0029
440	0.0045	0.0045
200	0.0028	0.0022
300	0.0026	0.0014
400	0.0030	0.0029
110	0.0062	0.0026
210	0.0140	0.0049
310	0.0042	0.0027
410	0.0038	0.0035
220	0.0104	0.0043
320	0.0049	0.0025
420	0.0040	0.0055
230	0.0090	0.0055
330	0.0045	0.0035
430	0.0040	0.0050

For the Finite Element Analysis, CGAX axisymmetric elements were used and these elements did not behave for load and torque at the same time. For these elements axial and rotational displacements were applied instead of load and torque. When converting to load and torque from displacements there were some errors, which was unavoidable.

Comparing the results of FEA and experimental it can be seen the general shape of the hysteresis loops are similar. However FEA results showed less plastic deformation as apparent from the thinner loop compared to experiments. This may be due to the control errors of the experiments.

Results show significant difference in hysteresis behaviour under non-proportional loading. The loops observed for out-of phase paths, path B, C and D in particular one of complex shape. This suggests that analytical predictions of these loops are extremely difficult. However, since similar loop results observed from FEA, FEA can be used to predict hysteresis loops with confidence.

The present work shows the complex loop patterns for non-proportional paths, which has not been investigated before. Considerable experiment is needed to explain the shapes and they cannot be derived from simple theory like Neuber method.

The results also show that for some amplitudes of axial load/torque, different plastic strain will occur, dependency on the loading path. Therefore fatigue life may be significantly affected by the path of loading. The study of the effect of plastic strain and loop shape on fatigue life was originally intended however; this is not performed due to time limitations of the project.

As the results shown in Table 7.15 Path-C is more damage and Path-A is least damaging in terms of fatigue life.

Conclusion

The behaviour of hysteresis loops (cyclic deformation) for material EN8 carbon steel under uniaxial, torsion proportion and different non-proportional loadings was studied using the Finite Element Analysis (ABAQUS code) and the experimental techniques. The specimens used for the testing programme were solid cylindrical bars with a notch and the cyclic deformation at the notch root for uniaxial and pure torsional loadings responded as expected.

Comparing the results of FEA and experimental, it can be seen that the general shape of the hysteresis loops are similar. However FEA results showed less plastic deformation as apparent from the thinner loop compared to experimental observations. This may be due to the inaccuracies of the control unit. However, the results indicated significant difference in hysteresis behaviour under non-proportional loading. From the observations, non-proportional loading Path-C is more damaging and Path-A is least damaging in terms of fatigue life.

For future work, the software available in the market for fatigue life prediction can be assessed for the same loadings such as uniaxial, torsional, proportional and different non-proportional loadings by using strain histories.

References

[1] Benham P.P., Crowford R.J. and Armstrong C.G., 1996, Mechanics of Engineering Materials, 2nd Edition, Longman Group, pp 463-544

[2] Ekberg A., Rolling contact fatigue of railway wheels-a parametric study, 1997 Int.J Fatigue Vol.20, No 1, pp 9-34, Elsevier Science Ltd.

[3] Suresh S., 1998, Fatigue of Materials, 2nd ed., Cambridge University Press.

[4] Segerlind L.J., 1976, Applied Finite Element Analysis, John Wiley and Sons.

[5] Bannantine J., Comer J. and Handrock, 1990, Fundamentals of Metal Fatigue Analysis, Prentice Hall.

[6] Dover W.D., Glinka G. and Reynolds A.G., 1986, Fatigue and Crack Growth in offshore Structures, ImechE Conference Publications, pp 458-465.

[7] Devlukia J. and Davis J., 1985, Fatigue Analysis of a Vehicle Structural Component Under Biaxial Loading, Advanced Structural Techniques, BL Technology Limited, Gaydon Proving Ground, Lighthorne Heath, Warwickshire, pp 25-31.

[8] Wang Y., and Pan J., 2000, A Plastic Fracture Mechanics Model for Characterization of Multiaxial low-cycle Fatigue, Int. J fatigue Vol. 20, No 3, pp 248-252, Elsevier Science Ltd.

[9] Abelkis P.R. and Hudson C.M., 1982, Design of Fatigue and Fracture Resistant Structures, Race Street, pp21.

[10] Knop M., Jones R., Molent L. and Wang C., 2000, On the Glinka and Neuber Methods for Calculating Notch Tip Strains Under Cyclic Load spectra, Int. J fatigue Vol. 22, pp 743-755 Elsevier Science Ltd.

[11] Golos K.M., 1996, Multiaxial fatigue criterion with mean stress effect, Int. J pressure vessels and piping, pp 803-811.

[12] Wheelhouse K., 2001, Fatigue Damage Accumulation Under Torsion and Non-Proportional Push-Pull Interruption Loading, Ph.D. thesis, SHU.

[13] Jayantha Das, Srinivasan M. and Sivakumar, 2000, Multiaxial Fatigue Life Prediction of a High Temperature Steam Turbine Rotor Using a Critical Plane Approach, Eng. failure analysis, Vol. 7, pp 348-358.

[14] Morel F., 2000, A Critical Plane Approach for Life Prediction of High Cycle Fatigue Under Multiaxial Variable Amplitude Loading, Int. J fatigue, Vol. 22, pp 101-104.

[15] Miller K.J. and Brown M.W., 1985, Multiaxial fatigue, A symposium sponsored by ASTM Committees E-9 on Fatigue and E-24 on Fracture Testing San Fransisco, CA, pp12.

[16] Tipton and Nelson, 2000, Multiaxial Fatigue Life Prediction, Int. J fatigue, Vol. 24, pp 533-534.

[17] Steven M. Tipton, Drew V. and Nelson, 1996, Advances in Multiaxial Fatigue Life Prediction for Components with Stress Concentrations, Int. J fatigue, Vol. 19, pp 648.

[18] Fuches H.O. and Stephens R.I., 1980, Metal Fatigue in Engineering, Wiley – Inter science Publication, pp 105-217.

[19] Andrzej BUCZYNSKI and Grzegorz Glinka, 1997, Elastic-Plastic Stress-Strain Analysis of notches under non-proportional loading, Proceeding of the 5th international conference on Biaxial/Multiaxial Fatigue and Fracture Cracow'97, Poland, pp 461-479.

[20] De-Guang Shang, De-Jun Wang and Wei-Xing Yao, 1999, A simple Approach to the Description of Multiaxial Cyclic stress-strain relationship, Int. J fatigue, Vol. 22, pp 251-256.

[21] Kussumaul K.F., McDiarmid D.L. and Socie D.F., 1991, Fatigue under Biaxial and Multiaxial Loading, ESIS Publication 10, pp 46.

[22] Dimitar S. Tchankov, Akihito Ohta, Naoyuki Suzuki and Yoshio Maeda, 1999, Random Loading Fatigue Life Assessments for Notched Plates, Int. J fatigue, Vol. 23, pp 942-946.

[23] Qylafku G., Azari Z., Kadi N., Gjonaj M. and Pluvinage G., 1999, Application of a New Model Proposal for Fatigue Life Prediction on Notches and Key-seats, Int. J fatigue, Vol. 21, pp 753-760.

[24] Dabayeh A.A., Xu R.X., Du B.P. and Topper T.H., 1995, Fatigue of Cast Aluminium Alloys under Constant and Variable-Amplitude Loading, Int. J fatigue, Vol. 18, pp 95-104.

[25] Sandor B.I., 1972, Fundamentals of Cyclic Stress and Strain, The University of Wisconsin Press, pp69.

[26] www.fourmilab.ch/autofile/www/subsection2

[27] www.engineering.com/mechanical/software/p00327/prodover.htm

[28] www.solidworks.com

[29] www.caddpromer.com/cad-software.htm

[30] Habbit,Karlsson&Sorensen,Inc.(ABAQUShomepage):http://abaqus.com

[31] www.engr.utk.edu/ecc/sw/eng/htm

[32] www.mscsoftware.com

[33] Peter Blackmore, 1991, nCode International Ltd.

[34] Mayer H.R., Sawaki y. and Huhner M., 1995, Influence of Transformation-Induced Crack Closure on Slow Fatigue Crack Growth under Variable Amplitude Loading, Fatigue Fract.Eng.Mater,Struct., pp 478

[35] McMahon C, Browne J, 1993, CADCAM fro principal to Practice, Addison-Wesley Publishing Company, pp13

[36] Pavlou D.G., 2000, Prediction of Fatigue Crack Growth under Real Stress Histories, Engineering structures, Vol. 22, pp 1708-1713

[37] Forsyth P.J.E, 1969, The physical basis of metal fatigue, Royal aircraft establishment, Farnborough, Int. J fatigue, Vol. 17, pp 40

[38] Peterson R.E, 1974, Stress Concentration factors, New York: Wiley

Appendix-1

Input-programmes for ABAQUS package

Elastic analysis

For Torsion

```
*HEADING
Bar with a notch under torsion
**DATA CHECK
*PRE PRINT,MODEL=YES,HISTORY=YES,ECHO=YES
*NODE
1,0.,0
4101,0.,35.0
4511,0.,38.0
5331,0.,46.5
6151,0.,55.0
6561,0.,58.0
10661,0.,93.0
41,12.5,0
4141,12.5,40.0
4551,9.0,43.5
5371,7.5,46.5
6191,9.0,49.5
6601,12.5,53.0
10701,12.5,93.0
50000,12.5,46.5
*NGEN,NSET=A0
1,41,1
*NGEN,NSET=A13
10661,10701,1
*NGEN,NSET=A1
1,4101,41
*NGEN,NSET=A2
4101,4511,41
*NGEN,NSET=A3
4511,5331,41
*NGEN,NSET=A4
5331,6151,41
```

```
*NGEN,NSET=A5
6151,6561,41
*NGEN,LINE=C,NSET=A7
4551,5371,41,50000
*NGEN,NSET=A6
6561,10661,41
*NGEN,LINE=C,NSET=A8
5371,6191,41,50000
*NGEN,NSET=A9
41,4141,41
*NGEN,NSET=A10
4141,4551,41
*NGEN,NSET=A11
6191,6601,41
*NGEN,NSET=A12
6601,10701,41
*NGEN,NSET=CNODE
1,10661,41
*NFILL
A1,A9,40,1
A2,A10,40,1
A3,A7,40,1
A4,A8,40,1
A5,A11,40,1
A6,A12,40,1
*ELEMENT,TYPE=CGAX8
1,1,3,85,83,2,44,84,42
1001,4101,4103,4185,4183,4102,4144,4184,4142
1101,4511,4513,4595,4593,4512,4554,4594,4552
1301,5331,5333,5415,5413,5332,5374,5414,5372
1501,6151,6153,6235,6233,6152,6194,6234,6192
1601,6561,6563,6645,6643,6562,6604,6644,6602
*ELGEN,ELSET=ALLEL
1,20,2,1,50,82,20
1001,20,2,1,5,82,20
1101,20,2,1,10,82,20
1301,20,2,1,10,82,20
1501,20,2,1,5,82,20
1601,20,2,1,50,82,20
```

```
*ELSET,ELSET=C
1280,1300,1320
*SOLID SECTION,ELSET=ALLEL,MATERIAL=MS
*MATERIAL,NAME=MS
*ELASTIC
2.08E5,0.3
*BOUNDARY
A0,2
A0,5
CNODE,1
*RESTART,WRITE,FREQ=1
*STEP,INC=20
*STATIC,DIRECT
0.05,1.0
*BOUNDARY
A13,5,5,0.04
*EL PRINT,ELSET=C,POSITION=AVERAGED AT NODES,FREQ=2
S23,E23
*NODE PRINT,NSET=A0,TOTAL=YES,FREQ=2
U1,U2,RF
*END STEP
```

For Tension

```
*SOLID SECTION,ELSET=ALLEL,MATERIAL=MS
*MATERIAL,NAME=MS
*ELASTIC
2.08E5,0.3
*BOUNDARY
A0,2
A0,5
CNODE,1
*RESTART,WRITE,FREQ=1
*STEP,INC=20
*STATIC,DIRECT
0.05,1.0
*BOUNDARY
A13,5,5,0.04
*EL PRINT,ELSET=C,POSITION=AVERAGED AT NODES,FREQ=2
```

```
S23,E23
*NODE PRINT,NSET=A0,TOTAL=YES,FREQ=2
U1,U2,RF
*END STEP
```

Elastic-plastic analysis

For Torsion

```
*SOLID SECTION,ELSET=ALLEL,MATERIAL=MS
*MATERIAL,NAME=MS
*ELASTIC
2.08E5,0.3
*PLASTIC
320.,0.0000
370.,0.0026
420.,0.0050
470.,0.0091
520.,0.0155
570.,0.0264
620.,0.0379
670.,0.0546
720.,0.0886
770.,0.1274
*BOUNDARY
A0,2
A0,5
CNODE,1
*RESTART,WRITE,FREQ=1
*STEP,INC=20
*STATIC,DIRECT
0.05,1.0
*BOUNDARY
A13,5,5,0.04
*EL PRINT,ELSET=C,POSITION=AVERAGED AT NODES,FREQ=2
S23,e23
*NODE PRINT,NSET=A0,TOTAL=YES,FREQ=2
U1,U2,RF
*END STEP
```

For Tension

```
*SOLID SECTION,ELSET=ALLEL,MATERIAL=MS
*MATERIAL,NAME=MS
*ELASTIC
2.08E5,0.3
*PLASTIC
320.,0.0000
370.,0.0026
420.,0.0050
470.,0.0091
520.,0.0155
570.,0.0264
620.,0.0379
670.,0.0546
720.,0.0886
770.,0.1274
*BOUNDARY
A0,2
A0,5
CNODE,1
*RESTART,WRITE,FREQ=1
*STEP,INC=20
*STATIC,DIRECT
0.05,1.0
*BOUNDARY
A13,5,5,0.04
*EL PRINT,ELSET=C,POSITION=AVERAGED AT NODES,FREQ=2
S23,e23
*NODE PRINT,NSET=A0,TOTAL=YES,FREQ=2
U1,U2,RF
*END STEP
```

For cyclic loading

Tension

```
*SOLID SECTION,ELSET=ALLEL,MATERIAL=MS
*MATERIAL,NAME=MS
*ELASTIC
2.08E5,0.3
*PLASTIC
320.,0.0000
370.,0.0026
420.,0.0050
470.,0.0091
520.,0.0155
570.,0.0264
620.,0.0379
670.,0.0546
720.,0.0886
770.,0.1274
**AMPLITUDE DEFINITION
*AMPLITUDE,DEFINITION=PERIODIC,NAME=SINE
1,31.4159265359,0,0
0,1,0,0,0,0,0,0
*BOUNDARY
A0,2
A0,5
CNODE,1
*RESTART,WRITE,FREQ=1
*STEP,INC=200
*STATIC
0.001,1.0,0.0001,0.01
*BOUNDARY,AMP=SINE
A13,2,2,0.05
*EL PRINT,ELSET=C,POSITION=AVERAGED AT NODES
S22,E22
*NODE PRINT,NSET=A0,TOTAL=YES
U1,U2,RF
*END STEP
```

For cyclic torsion

```
*SOLID SECTION,ELSET=ALLEL,MATERIAL=MS
*MATERIAL,NAME=MS
*ELASTIC
2.08E5,0.3
*PLASTIC
320.,0.0000
370.,0.0026
420.,0.0050
470.,0.0091
520.,0.0155
570.,0.0264
620.,0.0379
670.,0.0546
720.,0.0886
770.,0.1274
**AMPLITUDE DEFINITION
*AMPLITUDE,DEFINITION=PERIODIC,NAME=SINE
1,31.4159265359,0,0
0,1,0,0,0,0,0,0
*BOUNDARY
A0,2
A0,5
CNODE,1
*RESTART,WRITE,FREQ=1
*STEP,INC=200
*STATIC
0.001,1.0,0.0001,0.01
*BOUNDARY,AMP=SINE
A13,5,5,0.005
*EL PRINT,ELSET=C,POSITION=AVERAGED AT NODES
S23,E23
*NODE PRINT,NSET=A0,TOTAL=YES
U1,U2,RF
*END STEP
```

For In-phase loading

```
*MATERIAL,NAME=MS
*ELASTIC
2.08E5,0.3
*PLASTIC
320.,0.0000
370.,0.0026
420.,0.0050
470.,0.0091
520.,0.0155
570.,0.0264
620.,0.0379
670.,0.0546
720.,0.0886
770.,0.1274
**AMPLITUDE DEFINITION
*AMPLITUDE,DEFINITION=PERIODIC,NAME=SINE
1,9.4247,0,0
0,1,0,0,0,0,0,0
*BOUNDARY
A0,2
A0,5
CNODE,1
*RESTART,WRITE,FREQ=1
*STEP,INC=200
*STATIC
0.001,1.0,0.0001,0.01
*BOUNDARY,AMP=SINE
A13,5,5,0.005
*BOUNDARY,AMP=SINE
A13,2,2,0.05
*EL PRINT,ELSET=C,POSITION=AVERAGED AT NODES
S23,E23,S22,E22
*EL PRINT,ELSET=D,POSITION=AVERAGED AT NODES
S23,E23,S22,E22
*NODE PRINT,NSET=A0,TOTAL=YES
U1,U2,RF2
*END STEP
```

For non-proportional loading

Path-A

```
*MATERIAL,NAME=MS
*ELASTIC
2.08E5,0.3
*PLASTIC
320.,0.0000
370.,0.0026
420.,0.0050
470.,0.0091
520.,0.0155
570.,0.0264
620.,0.0379
670.,0.0546
720.,0.0886
770.,0.1274
**AMPLITUDE DEFINITION
*AMPLITUDE,DEFINITION=PERIODIC,NAME=SINE1
1,9.424777,0,0
0,1,0,0,0,0,0,0
*AMPLITUDE,DEFINITION=PERIODIC,NAME=SINE2
1,9.424777,0,0
1,0,0,0,0,0,0,0
*BOUNDARY
A0,2
A0,5
CNODE,1
*RESTART,WRITE,FREQ=1
*STEP,INC=200
*STATIC
0.005,1.0,0.0001,0.01
*BOUNDARY,AMP=SINE1
A13,5,5,0.005
*BOUNDARY,AMP=SINE2
A13,2,2,0.05
*EL PRINT,ELSET=C,POSITION=AVERAGED AT NODES
S13,E13,S11,E11
*NODE PRINT,NSET=A0,TOTAL=YES
```

```
U1,U2,RF
*END STEP
```

For Path-B

```
*SOLID SECTION,ELSET=ALLEL,MATERIAL=MS
*MATERIAL,NAME=MS
*ELASTIC
2.08E5,0.3
*PLASTIC
320.,0.0000
370.,0.0026
420.,0.0050
470.,0.0091
520.,0.0155
570.,0.0264
620.,0.0379
670.,0.0546
720.,0.0886
770.,0.1274
*AMPLITUDE,NAME=CYCLE1
0.0,0.0,5.0,0.0,10.0,1.0,15.0,0.0
20.0,-1.0,25.0,0.0,30.0,0.0
*AMPLITUDE,NAME=CYCLE2
0.0,0.0,5.0,1.0,10.0,1.0,15.0,0.0
20.0,-1.0,25.0,-1.0,30.0,0.0
*BOUNDARY
A0,2
A0,5
CNODE,1
*RESTART,WRITE,FREQ=1
*STEP,INC=400
*STATIC
0.005,30.0
*BOUNDARY,AMP=CYCLE1
A13,5,5,0.005
*BOUNDARY,AMP=CYCLE2
A13,2,2,0.05
```

```
*EL PRINT,ELSET=C,POSITION=AVERAGED AT NODES
S23,E23,S22,E22
*NODE PRINT,NSET=A0,TOTAL=YES
U1,U2,RF
*END STEP
```

For Path-C

```
*SOLID SECTION,ELSET=ALLEL,MATERIAL=MS
*MATERIAL,NAME=MS
*ELASTIC
2.08E5,0.3
*PLASTIC
320.,0.0000
370.,0.0026
420.,0.0050
470.,0.0091
520.,0.0155
570.,0.0264
620.,0.0379
670.,0.0546
720.,0.0886
770.,0.1274
*AMPLITUDE,NAME=CYCLE2,DEFINITION=SMOOTH
0.0,0.0,5.0,0.0,10.0,1.0,15.0,0.0
20.0,-1.0,25.0,0.0,30.0,0.0
*AMPLITUDE,NAME=CYCLE1,DEFINITION=SMOOTH
0.0,0.0,5.0,1.0,10.0,1.0,15.0,0.0
20.0,-1.0,25.0,-1.0,30.0,0.0
*BOUNDARY
A0,2
A0,5
CNODE,1
*RESTART,WRITE,FREQ=1
*STEP,INC=400
*STATIC
0.005,30.0
*BOUNDARY,AMP=CYCLE1
A13,5,5,0.005
```

```
*BOUNDARY,AMP=CYCLE2
A13,2,2,0.05
*EL PRINT,ELSET=C,POSITION=AVERAGED AT NODES
S23,E23,S22,E22
*NODE PRINT,NSET=A0,TOTAL=YES
U1,U2,RF
*END STEP
```

For Path-D

```
*SOLID SECTION,ELSET=ALLEL,MATERIAL=MS
*MATERIAL,NAME=MS
*ELASTIC
2.08E5,0.3
*PLASTIC
320.,0.0000
370.,0.0026
420.,0.0050
470.,0.0091
520.,0.0155
570.,0.0264
620.,0.0379
670.,0.0546
720.,0.0886
770.,0.1274
*AMPLITUDE,NAME=CYCLE1,DEFINITION=SMOOTH
0.0,0.0,5.0,0.0,10.0,1.0,15.0,1.0,
20.0,0.0,25.0,-1.0,30.0,-1.0,35.0,0.0,
40.0,0.0
*AMPLITUDE,NAME=CYCLE2,DEFINITION=SMOOTH
0.0,0.0,5.0,1.0,10.0,1.0,15.0,0.0,
20.0,0.0,25.0,0.0,30.0,-1.0,35.0,-1.0,
40.0,0.0
*BOUNDARY
A0,2
A0,5
CNODE,1
*RESTART,WRITE,FREQ=1
*STEP,INC=200
```

```
*STATIC
0.05,40.0
*BOUNDARY,AMP=CYCLE1
A13,5,5,0.005
*BOUNDARY,AMP=CYCLE2
A13,2,2,0.05
*EL PRINT,ELSET=C,POSITION=AVERAGED AT NODES
S23,E23,S22,E22
*NODE PRINT,NSET=A0,TOTAL=YES
U1,U2,RF
*END STEP
```

Appendix – 2

Calculations For Stress Concentration Factor

Elastic stress analysis for axial loading

The resulting stress concentration was calculated as follow

For the modelled specimen theoretical value for K_t =1.6 [41]

Considering the Figure 5.4,

Maximum stress at the notch root = 1840 N/mm^2

Applied displacement for the specimen = 0.2 mm

Relevant load for that displacement = 179.54 kN

Diameter of the notch = 15 mm

Nominal stress at the notch σ_{nom} $$= \frac{179.54 \times 10^3}{\pi (7.5)^2}$$

$$=1015.843 \text{ N/mm}^2$$

Maximum stress at the notch root = 1840 N/mm^2

Calculated stress concentration factor K_t $$= \frac{1840}{1015.843}$$

$$= 1.8$$

Elastic stress analysis for torsion loading

The resulting stress concentration was calculated as follow.

For the modelled specimen theoretical value for K_t =1.2[Peterson, 1974]

Considering the Figure 5.5 and Figure 5.6,

Maximum shear stress at the notch root = 1650 N/mm^2

Applied torsion displacement for the specimen = 0.04 radians

Relevant torsion for that displacement =8.366×10Nmm

Diameter of the notch = 15 mm

By using equations, [Peterson, 1974].

$$\tau_{nom} = \frac{T_c}{J} = \frac{16T}{\pi d^3}$$

Nominal shear stress at the notch $\tau_{nom} = \dfrac{0.8366\times10^3\times10^3\times16}{\pi(7.5)^3}$

$= 1262.29\ N/mm^2$

Maximum stress at the notch root $= 1650\ N/mm^2$

Calculated stress concentration factor $K\tau$ $= \dfrac{1650}{1262.3}$

$= 1.3$

Elastic/Plastic stress analysis for axial loading

The resulting stress concentration was calculated as follows.

Using Neuber's equation,

$K_t^2\ Se = \sigma\varepsilon$

Considering the Figure 5.8,

Stress at the notch $= 600\ N/mm^2$

Strain at the notch $= 1.60 \times 10^{-2}$

Applied displacement $= 0.2$ mm

Relevant load $= 115$ kN

Diameter of the notch $=15$ mm

Nominal stress S $= \dfrac{115}{\pi\ (7.5)^2}$

$= 650.7\ N/mm^2$

Considering cyclic stress-strain curve of the material,

strain 'e' relevant to 'S' $= 0.0057$

Substituting to the Neuber's equation,

$K_t^2 = \dfrac{600\times16\times10^{-3}}{650.7\times0.0057}$

Calculated K_t for elastic-plastic analysis,

$K_t = 1.6$